Research & Development
2020

Mechanical Engineering Letters, Szent István University

Contents

4. Doctoral School of Mechanical Engineering

5. Invited Papers

Tensile strength of grid and concentric PET and affection on 3D printing process

Alaeddine OUSSAI[2], László KÁTAI[1], Zoltán BÁRTFAI[2]

[1]Department of Machine Construction, Institute for Mechanics and Machinery,
Faculty of Mechanical Engineering, Szent István University, Páter Károly u. 1., Gödöllő Hungary
[2]Department of Farm and Food Machinery, Institute for Mechanics and Machinery,
Faculty of Mechanical Engineering, Szent István University Páter Károly u. 1., Gödöllő Hungary

Abstract

3D printing technology is the most common Fused Deposition Modelling (FDM). In an additive process an object is created by laying down successive layers of material until the entire object is created so those process with different settings is important. Tensile test specimens of two types of printed Polyethylene terephthalate were created within the frame of our laboratory research in order to examine the mechanical properties. Rigid (PET) and concentric PET were the used materials for this research. Forty test pieces of the two types raw material were evaluated. The differences in stress-strain curves, tensile strength values and elongation at break were compared among the tested samples. The broken specimens after the tensile tests are illustrated, presenting how the printed test pieces having different parameters were fractured. The optimum printing setting is represented at 100% Grid, where the highest tensile strength of 43,15 MPa at Grid PET and the largest elongation of about 2,18 % at 60% grid PET. Test samples were prepared on a Freedee MakerBot, with variations of geometrical structure (grid and concentric). Results of tensile test revealed that the honeycomb structured samples exhibit the highest strength.

Keywords

Plastic waste, recycled materials; 3D printing; filament preparation; mechanical properties

1. Introduction

3D printing or additive manufacturing is a process of making three-dimensional solid objects from a digital file. The creation of a 3D printed object is achieved using additive processes. In an additive process an object is created by laying down successive layers of material until the entire object is created. Each of these layers can be seen as a thinly sliced horizontal cross-section of the eventual object. Today, there are many different additive manufacturing techniques with high accuracy and large choices of materials available on the market. The most

successfully developed technologies are: Stereolithography (SLA), Selective Laser Sintering (SLS), Laminated Object Manufacturing (LOM), Fused Deposition Modeling (FDM), 3D Printing etc. [Pilipovic et al 2011].

PET is the first preference for recycling and used as a reused material. The applied technology consists of the following steps: PET is dried, then extruded followed by drying and shredding then used for extrusion. The plastics are immensely used in the field of fabrication and designing of small plastics like ABS, HDPE or PET that are then shredded and shaped into the pellets. The pellets are then further extruded to form laments that are used for the making of the 3D printers or the injection moulds for making larger parts or the smaller pieces used in the construction material for sheets. These different methods implemented for fabrication by using recycled plastics are the main standards because of their ease of affordability and straight forward processes but despite that there is some left over complexity issued to these processes [Gipson et al 2015].

Extruded PET recycled more than 10 times in one study had minimal degradation in tensile strength or modulus, Polylactic acid is a good example of it.13 Different ratios of virgin to reground injection melded Poly- butylene terephthalate (PBT) and Polypropylene (PE) showed minimal decreases in their mechanical properties. A study where 3D printing PET filament was recycled maximum five times before component fabrication, found no decrease in mechanical properties other than a 10% reduction in elongation at failure.

Studying the literature, there are many studies performed to improve the mechanical properties of the 3D printed objects, particularly the tensile strength, Tymrak et al 2014 studied the characteristics of mechanical properties of 3D printed ABS and PLA. They utilized tensile test samples made using open-source Rep-Rap 3D printers. Pattern orientation and layer thickness are the main slicing variables which were taken in the 3D printing process. They found that tensile strength and the elastic modulus of the parts produced by the above 3D printers are comparable to components printed by common 3D printing technologies. Extra studies about the influence of structure patterns was studied by Galeta et al 2016, and different geometries on the mechanical properties of 3D printed tensile test specimens were studied.

The main reason for choosing as test material for 3D printing is its flexible nature of being recycled and huge variety in Hungarian recycling companies [Oussai et al 2020]. The main aim of this paper is a tensile analysis, shear and hardness features of the specimens samples made from the recycled PET filament in grid format. These results are compared to the samples produced from the PET filament that are under form of concentric.

2. Preparation for tensile measurement

The tensile test specimens were modelled on the Flashforge creator by the replicator G version 0040 with the Makerbot. Its dimensions are listed in Table 1. For the tensile strength measurement, Zwick / Roell Z100 machine was used.

The experiments have been carried out at a speed of 10 mm/min and 20 °C. The specimens were in a room with humidity of 45–50 % for 24 hours prior the tests.

Table 1. Specimen dimensions type 1B, ISO 527-2: 2012 standard [14]

Main dimension	Value(mm)
Overall length	150
Gauge length	80
Cross section thickness (h)	3,8
Cross section width (b_1)	10
Width of the gripping part (b_2)	20

In our experiments we used models derived from standard specimens for tensile tests defined in ISO 527:2012 standard. Two different hollow lattice-shaped structures were considered: grid and concentric (Figure 1). One set of standard compact full-bodied specimens were printed and tested as a control set, analogous to control group in randomized controlled trial.
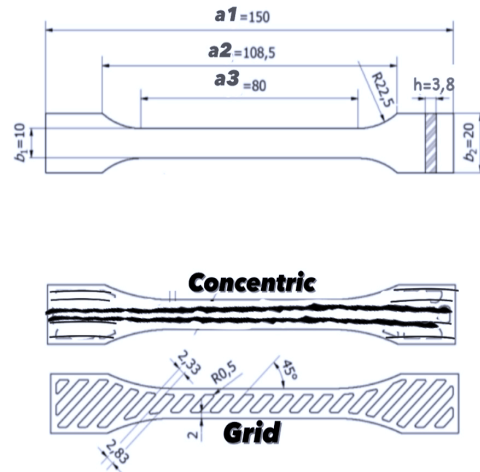
Figure 1. 3D Sample structure types and dimensions (Concentric and grid model)

3. Preparation for tensile measurement

Fig. 3 shows the printed specimens for mechanical measurement. Grid and concentric PET test pieces were heat-treated, as recommended by the manufacturer. In a preheating oven at 80–100 °C, the specimens were heat-treated for 20 minutes and left to cool down slowly. As a result, the polymer structure is arranged in a crystal lattice.

Figure 2. Testing tensile specimens (Testometric)
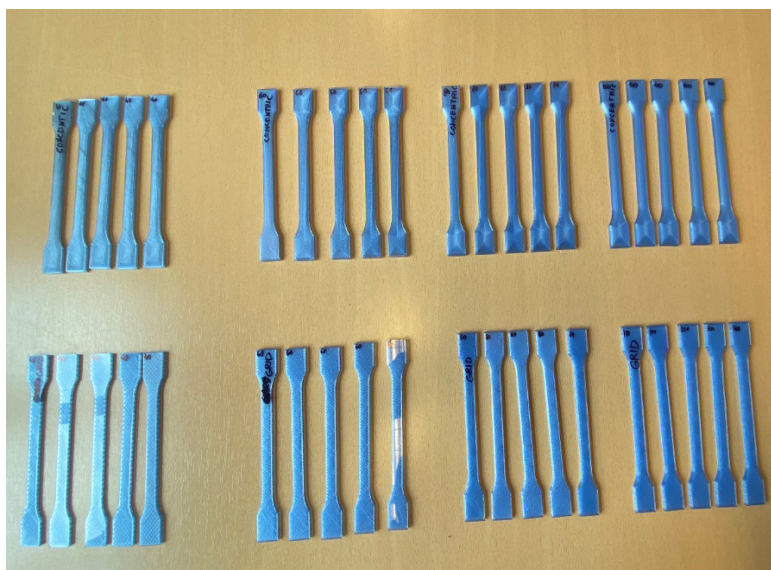
Figure 3. Specimens (top line: Concentric, bottom line: Grid)

For the tensile strength measurement Zwick / Roell Z100 machine was used. The experiments have been carried out at a speed of 10 mm/min and 20 °C, the test was settled as 5 samples of each filling percentage from 40, 60 ,80 and 100% grid and then same percentage as concentric filaments samples and then compare tensile strength and elongation at break.

4. Results and discussion

The tensile testing was performed on Zwick/Roell Z 100 testing machine with a travel speed of 5 mm/min (Fig 2). The load and elongation were failed to be

recorded as well as separate extensometers were not utilized. The shore D digital durometer was used for measuring the hardness of the middle shear specimens. The hardness was measured 4 times and the highest value was recorded to consider the possibility of the needle falling into the small surface depressions.

Table 2. Tensile strength and elongation break of Concentric PET Filament

Grid	Test numbers	Average tensile strength (MPa)	Average elongation at break (%)
100%	5	25,26	2,39
80%	5	21,34	2,61
60%	5	23,92	2,812
40%	5	18,10	3,12

Table 3. Tensile strength and elongation break of Grid PET Filament

Concentric	Test numbers	Average tensile strength (MPa)	Average elongation at break (%)
100%	5	43,15	1,336
80%	5	34,214	1,45
60%	5	37,80	1,64
40%	5	24,33	1,98

Following the initial set of specimens -produced from the virgin PET filament tested and photographed- all other extra specimens built simultaneously with the virgin filament were sent to the Filabot Company, a filament extruder. The specimens there were grounded, and re-extruded into the 1,75 mm 3D printing filament. The extrusion process was done on the Filabot EX2 a bench machine quite commonly used at homes. After receiving the re-extruded filament, the second set of tensile and shear specimens were manufactured using the same equipment and measured in the way as described above.

Table 4. Tensile Properties of Virgin Versus Recycled Polyethylene terephtalate 3D Printed Specimens

	Grid	Concentric
Number of specimens	20	20
Average tensile yield strength (Mpa)	34.871	29.742
Standard deviation	1.593	2.778
Average tensile modulus of elasticity (Mpa)	3670	3346
Standard deviation	224	413

Tensile Testing of Grid PET Specimens   Tensile Testing of Concentric PET
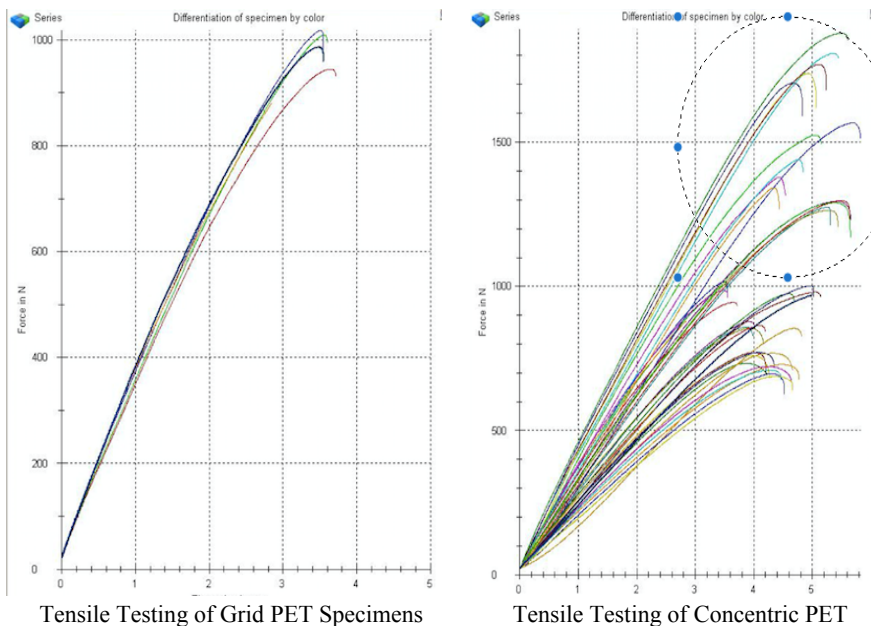
Figure 4. Tensile elongation of virgin and recycled 3D printed PET

Figure 4 presents the average tensile strength of the two tested materials at diverse filling percentage. The specimens achieved the highest tensile strength, including grid PET, with an average value of nearly 34,8 MPa. The minimum tensile strengths were measured at the 40% concentric PET. In the case of Grid PET, the tensile strength is significantly higher compering with the other material. The 40 % filling test specimens have a tensile strength of almost half that of 100 %. The average values of elongation at break are demonstrated in Table 2 and 3, which the Concentric PET shows the highest values.

Conclusion

In this paper, the mechanical properties of the PET 3D printing filament has been examined. Two different types of PET materials, Grid and Concentric pieces were investigated. 40 tensile test specimens were printed with different settings and the values of tensile strength and elongation at break were measured.

Among the tested materials, the highest tensile strength was detected at Grid-PET, while the Concentric PET demonstrated the most substantial elongation. Studying the results we can state that the printing process producing two types of filaments from Polyethylene Terephthalate has a significant effect on the tensile strength and elongation values, the fill of 40 % of Concentric present weakness regarding to the tensile strength, since the strength values are almost halved in opposite with 100 %. Whereas concerning elongation, both Grid and Concentric (40 % and 100 %) are approaching to be the same.
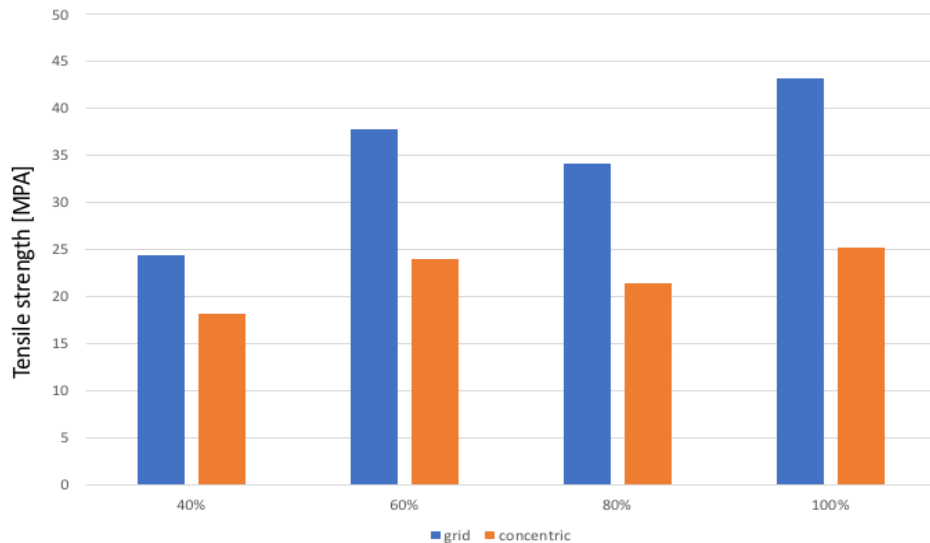
Figure 5. Comparative chart of tensile strengths at various filling percentages

From the tested materials, the best tensile strength was measured while the Concentric filament of PET demonstrated the most substantial elongation then the results show that FDM 3D printing technology and production of two different samples from same material has really anisotropic properties, it can be seen at least in case of Polyethylene terephthalate.

Acknowledgement

References

[1] Tymrak, B. M., KreigerM., Pearce, J. M. (2014), Mechanical properties of components fabricated with open-source 3-D printers under realistic environmental conditions, Materials & Design, 58, pp. 242–246, (English).
[2] Gibson I, Rosen B, Stucker B. (2015) Additive manufacturing technologies: 3D printing, rapid prototyping, and direct digital manufacturing, 2nd Edition. Johnson Matthey Technology Review; 59:193–197 (French)

[3] Galeta, T., Raos, P., Stojšić, J., Pakši, I. (2016) Influence of Structure on Mechanical Properties of 3D Printed Objects, Procedia Engineering, 149, pp. 100–104, 2016. https://doi.org/10.1016/j.proeng.06.644 (translation English)

[4] Oussai, A., Bartfai, Z., Szalkai,I & Katai, L.(2020). Development of 3D printing raw materials from plastic waste. Hungarian Agriculture Engineering Journal, vol. 37, no 37/2020 34-40, DOI: 10.17676/HAE.2020.37.34 (English)

[5] ASTM D638-14, Standard Test Method for Tensile Properties of Plastics, ASTM International, West Conshohocken, PA, 2014, www.astm.org DOI: 10.1520/D0638-14(English)

[6] A. Pilipović, P. Raos, and M. Šercer, (2011) Experimental testing of quality of polymer parts produced by laminated object manufacturing LOM, Tehnički vjesnik - Technical Gazette, vol. 18, no. 2, pp. 253-260, (English).

Developing of knee prosthesis in ADAMS program

Zehouani KHEIREDDINE, Istvan OLDAL

Department of Mechanics, Institute for Mechanics and Machinery,
Faculty of Mechanical Engineering, Szent István University,Gödöllö, Hungary.

Abstract

In the human knee joint, degenerative joint disease may happen with time. The typical treatment of this disease is the total knee replacement through prosthesis implanting. The degenerative wear is the most determining lifetime factor of the current total knee replacements. Therefore the presence of Sliding and rolling cannot be neglected. The reason lies in the fact that this phenomenon causes other material abrasion compared to pure Sliding or rolling alone. This study focuses on developing a knee prosthesis geometry, which fulfils the mechanical and kinematical requirements. To achieve this, a multibody model is proposed using MSC ADAMS software. The MSC ADAMS program is used to describe the rotation of the human knee joint as a function of Flexion, and to investigate how the flexion and rotation movement changes between the condyles of a multibody model of the knee prosthesis as a function of flexion angle (in the functional arc of the knee (20-120º)). Moreover, the multibody model with identical boundary conditions is constituted, and the numerical simulations are carried out using the MSC.ADAMS program system.

Keywords

Biomechanics, knee joint, rotation, Flexion, kinematics,
MSC ADAMS.

1. Introduction

The human knee joint is vital and the most complicated joint of the human body, but it is also very vulnerable. Due to joint disorders (mainly gonarthrosis), installing a prosthesis in the knee joint is necessary. In many cases, they need to be replaced over time due to loosening or worn out prosthesis. To have the prosthesis's kinematic characteristics as close as possible to the healthy knee joint and make it less necessary to exchange them. The kinematic joint needs to be known; in kinematics, knee people are researching the kinematic joint; however, the researchers' methods and evaluations are different from many perspectives, so their results cannot be compared. Accordingly, there is no generally accepted articular kinematic.(Bert, 2005)(Katona et al., 2015)(Kozanek et al., 2009)(Wylde et al., 2007)

Figure 1. Knee joint motion in three dimensions, which is described using six independent variables (Standring, 2008)

The knee is the most extensive and most complicated joint in the human body. The knee is a joint connecting the femur (thigh bone), patella (knee cap) and the tibia (shin bone). (Akalan et al., 2008)(Qian et al., 2006)
For the development of knee prosthesis geometry, we will use the ADAMS program without to use 3D printing or CNC milling. We want to take the easy and fast way without manufacturing and without measuring, so that is why we choose the ADAMS program. And we will compare our results from our new model of the ADAMS program with the results for the prosthesis from the test rig.
We will compare with a test rig results because our results from ADAMS program and the consequences for test rig both of them it is not reality measuring, so at first, we will improve the new model in ADAMS program after that we can use this model to compare with reality knee directly without manufacturing and measuring

2. Materials and methods

Kinematic analyses presented by different authors show a large deviation in the (Figure 2), it is essential to know the movement of the real human knee joint that is we see in (Figure2).

1 Test machine:
The measurement performed on the experimental test machine shown in (figure 2), the Flexion of the knee prosthesis components is performed by a stepper motor.
The rotation-flexion values are recorded by two incremental rotary encoders with a resolution of 180°, Due to the high-stepping restore accuracy of the stepper motor, all measurement we will carry out in the same range flexion.
The test machine is multifunctional, which is suitable for the determination of testing knee prostheses.and in case of a different type of loads and it is also suitable for the knee kinematics and kinetics.
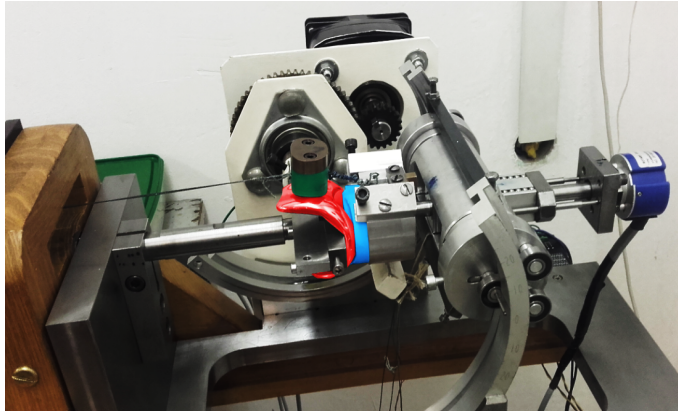
Figure 2. Machine for measurement of the knee prosthesis

Figure 3. 4 types of the knee prosthesis(cadaver)
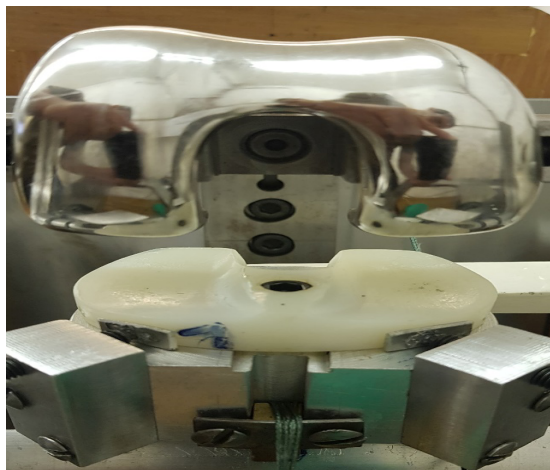
Figure 4. The tibia and the femoral component in the test machine

The knee prosthesis is consisting of two components they are the tibia and the femoral component. The so-called reference function must be achieved with its adequate geometry. In our research, we will begin our investigations based on available knee prosthesis geometry.

For the development of the geometry, we use the ADAMS program, with the use of (ADAMS program) we optimize the tibia joint surfaces.

2. Multibody Model

After creating the geometrical model, multibody model were built with MSC.ADAMS program system. The following boundary conditions were applied on each model (Prosthesis 1, 2, 3, 4, 5) identically:

increased in a certain period of time (STEP (time, 0.0, 0.0, 0.03, -800)) until it reached its maximum value (Figure 5) unbalances could be evaded.
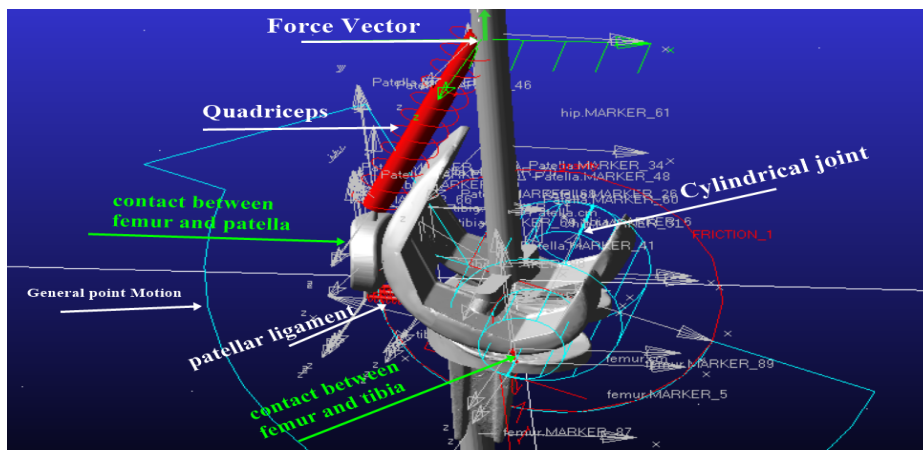
Figure 5. Multibody model in the MSC.ADAMS

3. Results and discussion

In the case of normal Flexion or extension of the human knee joint, the local kinematics of the patellofemoral joint is characterized by partial rolling and Sliding. This particular movement is guided through the connecting femoral-tibial surfaces and the connecting ligaments. The precise ratio of the Sliding and rolling phenomenon throughout the active functional arc of the knee is currently unknown.

The femur rotates about 9º with respect to the tibia while the knee is flexed (bent). It occurs in the tibia as the act of pushing the foot up (dorsiflexion), which causes this bone to rotate internally. It happens due to the crooked hinge phenomenon of the subtalar joint (the joint just below the ankle joint).

The simulations have been carried out on ADAMS model and the following results are derived :

ADAMS model with different position:

– ADAMS model result:

Figure 6. Multibody Model at the position 0 degree.
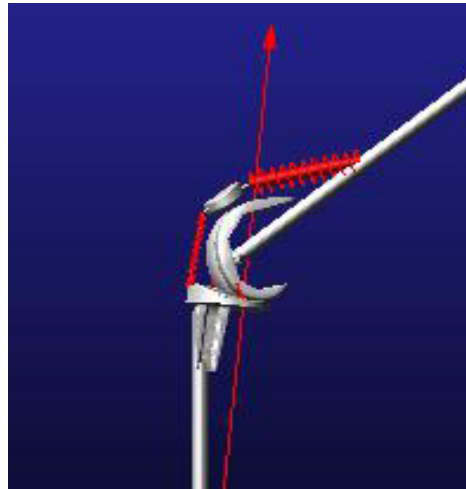
Figure 7. Multibody Model at the position 110 degree.
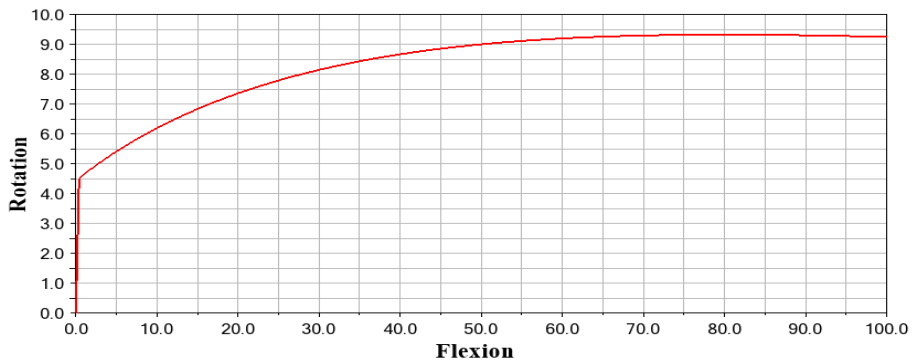
Figure 8. A graph of rotation against Flexion

The pictorial representation at different angle of Flexion is shown in Figures 6 and 7. A graphical relationship between angle of roation with respect to the flexion angle is illustrated in Figure 8. It is observed that the sudden increase in the rotatational angle brings a negotiable change in the flexion angle until 4.5º. A sharp rise in the flexion angle till 35º is seen beyond the rotational angle of 4.5º,

which indicates the onset of sliding between the tibia and the femur in the knee. Similary, the flexion angle in the range of 20°-30˚ makes joint prone to rolling, whereas the stablity in the rotational angle is obtained for flexion angle lies in range of 30° to 110°. The increasing flexion angle indicates that the tendency of Sliding is predominant.

  – comparison between our model and other prosthesis:
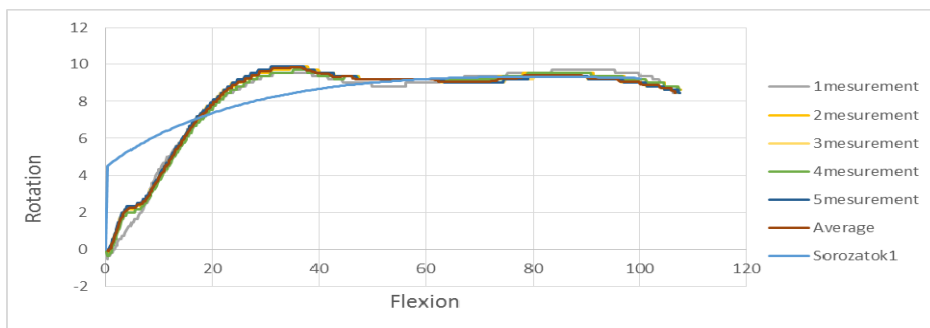
Figure 9. A graph of Rotation against Flexion

To validate the model, it is compared with other prosthetic joints. The rotation as a function of the flexion angle is illustrated in Figure 9. The choosen prothetic joints used for validation are removed from those patients which are looking for the new ones. The average values are plotted together against the proposed model. Having compared the proposed scheme with other prosthesitic joints, it is found that there is a rise in the angle of rotation as the flexion angle varies from 0° to 30° degrees. A good aggrement of value obtained from model with other prosthetic joints is established in the flexion range of 30 to 110°. The slightest deviation between the proposed model and other prosthesis is observed in the interval of 0°–30°. A sliding is relatively high in the proposed model as compare to other prosthetics.

Conclusion

It is concluded that the use of the multibody model reduces time since it does not involve the tibia and the femur as it requires for the knee prosthesis. Moreover, without measuring or by dispensing with a test machine for the knee prosthesis geometry, approximation of the results of our model to a human knee is carried out directly.

The multibody modeling is used to measure the degree of Flexion and rotation of the knee with respect to the position of the knee like extension or Flexion or rotation, as well as inserting a spring between tibia and femur while observing its effects on the perfomance of the knee.

The motion of the knee between 45º and 110º is similar for both the multibody model and the knee prosthesis in the test machine, however, in the beginning from 0º to 40º there are some slight differences between the multibody model and the knee prosthesis in the test machine. This is due to the fact that the initial vibration is experienced at the start of the knee motion in the multibody model.

The pattern obtained by the multibody model provides an insight for future experimental tests related to the rotation and Flexion of the knee joint with respect to the actual normal and friction load.

References

[1] Akalan, N.E., Özkan, M., Temelli, Y., 2008. Three-dimensional knee model: Constrained by isometric ligament bundles and experimentally obtained tibio-femoral contacts. J. Biomech. https://doi.org/10.1016/j.jbiomech.2007.10.021

[2] Bert, J.M., 2005. Unicompartmental knee replacement. Orthop. Clin. North Am. https://doi.org/10.1016/j.ocl.2005.05.001

[3] Katona, G., M. Csizmadia, B., Andrónyi, K., 2015. Determination of reference function to knee prosthesis rating. Biomech. Hungarica. https://doi.org/10.17489/biohun/2013/1/31

[4] Kozanek, M., Hosseini, A., Liu, F., Van de Velde, S.K., Gill, T.J., Rubash, H.E., Li, G., 2009. Tibiofemoral kinematics and condylar motion during the stance phase of gait. J. Biomech.
https://doi.org/10.1016/j.jbiomech.2009.05.003

[5] Qian, S. hua, Ge, S. rong, Wang, Q. liang, 2006. The Frictional Coefficient of Bovine Knee Articular Cartilage. J. Bionic Eng. 3, 79–85. https://doi.org/10.1016/S1672-6529(06)60011-5

[6] Wylde, V., Dieppe, P., Hewlett, S., Learmonth, I.D., 2007. Total knee replacement: Is it really an effective procedure for all? Knee. https://doi.org/10.1016/j.knee.2007.06.001

Study of heat transfer in a cylinder subject to Robin's conditions

Zehouani KHEIREDDINE, Istvan OLDAL

Department of Mechanics, Institute for Mechanics and Machinery,
Faculty of Mechanical Engineering, Szent István University, Gödöllö, Hungary.

Abstract

The conduction of heat in a straight solid cylinder, induced by heat transfer by convection taking place at the side wall, has been studied in the literature and repeatedly in the reference works, clarifying the way to understand the mechanisms of heat transfer without or with generation / destruction (source / then), and especially conduction. This type of heat exchange reveals an importance which does not cease increasing in view of its practical application in several fields of engineering such as: the storage of thermal energy in the form of sensible heat and the design of conductive electric wires. And their cooling. This article is a study of the heat exchange by conduction in a right solid cylinder with arbitrary dimensions. Numerical methods such as finite volumes or finite differences can be used to solve the energy equation (conduction mode) in transient mode. Patterns of isothermal surfaces, heat fluxes and graphs of temperature changes and their gradients with the passage of time will be established from the numerical results of these calculations.

Keywords

Heat transfer, Conduction, cylindrical coordinates, Robin's condition, resolution.

I. Introduction

In industry, the heat exchanger is an essential element of any energy management policy and therefore, consequently, of environmental protection. Much of the thermal energy used in industrial processes pass through a heat exchanger at least once, both in the processes themselves and in the thermal energy recovery systems thereof. They are mainly used in the industrial sectors (chemicals, petrochemicals, iron and steel, agro-food, energy production, etc.), transport (automotive, aeronautics) and the residential and tertiary sector (heating, air conditioning ... etc.). They are, therefore, one of the critical devices of the thermal engineer and are an almost inevitable component in energy control. (Janot, 2012)

This work consists of a general introduction and four chapters:

The first chapter is devoted to bibliographical research on heat transfers by conduction and convection, the coordinate systems used in the study of the

phenomenon and particularly the cylindrical coordinates, the types of the boundary conditions associated with the differential equations governing the problem, notably the Robin boundary condition.

The description of the phenomenon, the mathematical model and its simplifying assumptions, the initial and boundary conditions used are dealt with in the second chapter.

The finite difference method and in particular, the implicit discretization of the equations are exposed in the third chapter. There is also a presentation of the structure of the code written in MATLAB language to solve the problem in question. (Casadevall, 2013)

The different results obtained, as well as comparisons with results obtained elsewhere, comments and discussions are presented in the fourth chapter.

Finally, a general conclusion relating the main results and the choice of the model suitable for this type of geometry is presented, as well as the perspectives envisaged for the continuation of this work. (Pastre, 2002)

I.1 Heat transfer

Heat is a form of energy that flows under the effect of a temperature difference from high to low. Heat, like gravity, penetrates all the substances in the universe and contributes to all of its phenomena. The unit of heat in the international system is the joule (J).

Heat transfer is one of the most common modes of energy exchange. It is a phenomenon that can be found in many sectors of industry and our daily lives. Engineers and technicians are faced with this kind of problem and try to maximize or minimize this phenomenon according to the needs of the industry and to save this expensive energy. As a result, heat transfers have, both in the field of pure sciences and in that of technological applications, an often essential role. This role even becomes decisive when it is at the origin of the techniques used, for example: (heat exchangers, heat engines, thermal insulation, thermal insulation, etc.). The knowledge of the physical laws which govern these modes of heat transfers is an essential and crucial thing because they allow us to control the way and the quality of this flow of heat according to our desire.

Basic knowledge of some vague notions will be cited below, and which are necessary for the understanding and study of this studied phenomenon (Boughali, 2013).

I.1.1 Conduction

We know that the internal energy of a solid, liquid or gaseous body corresponds to the kinetic energy of its constituent elements which are in permanent motion (atoms, molecules, free electrons). Conduction represents the process of heat propagation by direct contact between the particles of a body or between bodies with energy levels. Therefore different temperatures, following the movement of these elementary particles in the case of gases, the thermal transfer conduction is the result of elastic scattering for metals, conduction is determined primarily by

the distribution of free electrons from warmer areas to colder areas, with elastic oscillations of the crystal matrix playing a minor role. In any medium, this mode of heat transfer tends to even out the distribution of kinetic energy of the particles of the substance forming the body mass.

The analytical method of studying conduction considers the bodies which undergo it as continuous media, neglecting the molecular structure of the substance. This hypothesis (or approach) is suitable, given that, in the general case, the bodies under observation are much larger than their elementary particles and the distances which separate them. It should be mentioned that the vast majority of technical applications make use of thermal conduction in solid bodies. (Bianchi, 2004)

I.1.2 Convection
The phenomenon of convection refers to the heat transfer that takes place in moving fluids (liquids or gases). Convection is the process of heat transfer determined by the movement of elementary particles of a fluid (liquid or gas) between zones having different temperatures; this movement causes an intense mixture of fluid particles, which exchange thermal energy (heat) and momentum (impulse) between them. Always taking place in a liquid medium, its fundamental characteristic is that the heat transfer is closely related to the movement of this medium. Convection can occur between layers of fluid having different temperatures or between a streams of liquid flowing along a solid surface having a different temperature than that of the fluid. The mode of conduction always accompanies this phenomenon of convection in the thin film of liquid adhering to the concrete wall, within which the temperature gradient is significant. Taking into account the forces which move the fluid, there are two types of convection: forced and natural or free. In forced convection, the movement of fluid is caused by the action of the external forces of the process (for example, pump, fan, etc.) which implies quite large displacement speeds. Consequently, the intensity of heat transfer by forced convection will be in direct connection with the regime of movement of the fluid. (Diouf, 2010)

I.2 The cylindrical coordinate system
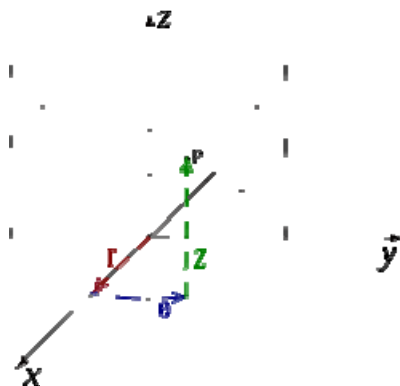
Figure. 1. Cylindrical-coordinate system.

The cylindrical coordinate system is a coordinate system which extends the two-dimensional polar coordinate system by adding a third dimension to it which measures the height of a point concerning the plane identified by the polar coordinates; in the same way that we extend the Cartesian coordinate system from two to three dimensions. The third coordinate is often denoted h or z.

From the Cartesian coordinates (x, y, z)

We can obtain the cylindrical coordinates

(r, θ, z) thanks to the following formulas:

$$r = \sqrt{x^2 + y^2} \tag{1}$$

$$\Theta = \arctan\left(\frac{y}{x}\right) \tag{2}$$

$$z = z \tag{3}$$

II.1 Diagram of the studied geometry:
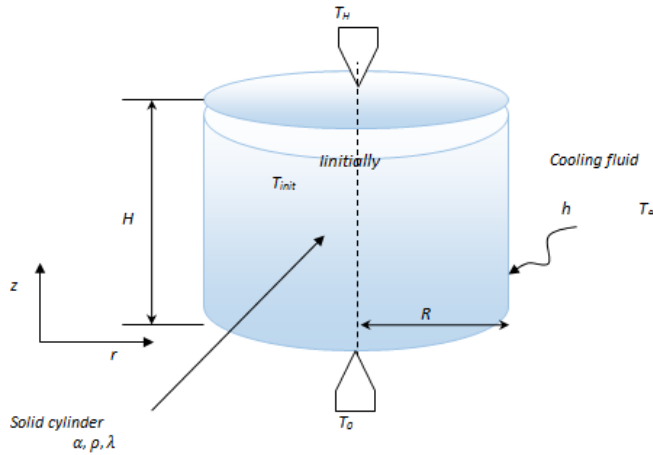
Figure. 2. The geometry of the studied problem.

II.2 Equation of heat and heat flux density

II.2.1 Heat equation
Without a heat source and sink, the heat equation boils down to the following expression:

$$\Delta T = \frac{1}{\alpha}\frac{\partial T}{\partial t} = 0 \tag{4}$$

With $\alpha = \dfrac{\lambda}{\rho \cdot C}$ is the coefficient of thermal diffusivity $(m^2 \cdot s^{-1})$

λ – Is the thermal conductivity (W/m.°C).

ρ – Is the density of the material (kg/m^3).

C is the thermal capacity of the material (J.Kg.°C) .

In cylindrical coordinates with axial symmetry (the temperature T does not depend on the coordinate θ),

The differential equation is written:

$$\frac{\partial^2 T}{\partial^2 r} + \frac{1}{r}\frac{\partial T}{\partial r} + \frac{\partial^2 T}{\partial z^2} - \frac{1}{a}\frac{\partial T}{\partial t} = 0 \qquad (5)$$

Solving equation (4) in dynamic frequency regime, provided with the conditions imposed in Figure 1, and by applying

The method of separating variables leads to the solution given by the following equation:

$$T(r,z,\omega,t) = \sum_{j=1}^{\infty} C_j J_0(u_j \cdot r)\left[A_j \sinh(\beta_j z) + B_j \cosh(\beta_j z)\right]e^{i\omega t} \qquad (6)$$

$J_0(\mu_j r)$ is a Bessel function of the first kind of order 0.

Table 1. Values used in the calculations

Amount	value	Unit (SI)
T_∞	20	°C
h	1500	W/m².°C
T_o	30	°C
T_H	30	°C
T_{init}	55	°C

Table 2. Thermo-physical properties of the materials chosen for the calculations

	The thermal capacity of the material (J/Kg.°C)	The density of the material (kg/m³)	Thermal conductivity (W/m.°C)
Aluminum	888	2700	237
Steel	465	7850	55
Glass	700	2480	0.87

III. Digital solution

III.1 Finite difference method (MDF):

The finite difference method consists in replacing the derivatives appearing in the ongoing problem by divided differences or combinations of point values of the

function in a limited number of discrete points or nodes of the mesh (Boukhari, 2013).

  – Advantages: great ease of writing and low cost of calculation.
  – Disadvantages: the principle of conservation is not assured after the discretization, limitation of the geometry of the fields of computation, difficulties of taking into account of the boundary conditions relating to the derivatives or the gradients of the unknown and in the general absence of error increase results.

III.2 Discretization and mesh:

$$\frac{1}{\alpha} \frac{\partial T}{\partial t} = \frac{\partial^2 t}{\partial r^2} + \frac{1}{r} \frac{\partial T}{\partial r} + \frac{\partial^2 T}{\partial z^2} \tag{7}$$
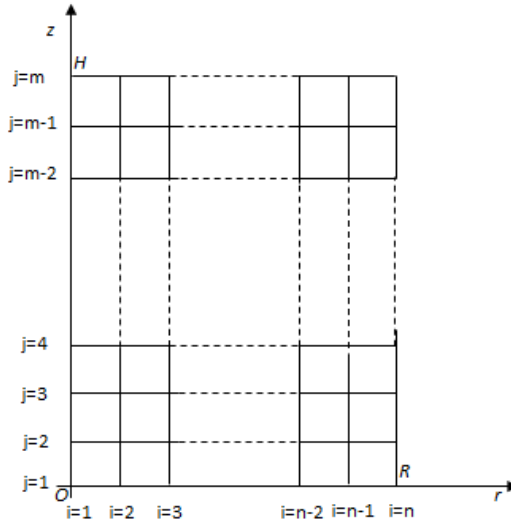
Figure. 3. Mesh of the studied domain.

$$\left. \frac{\partial T}{\partial t} \right|_{i,j}^{k} = \frac{T_{i,j}^{k+1} - T_{i,j}^{k}}{\Delta t} \tag{8}$$

$$\left. \frac{\partial^2 T}{\partial r^2} \right|_{i,j}^{k+1} = \frac{T_{i+1j}^{k+1} - 2T_{i,j}^{k+1} + T_{i-1j}^{k+1}}{\Delta r^2} \tag{9}$$

$$\left. \frac{\partial^2 T}{\partial z^2} \right|_{i,j}^{k+1} = \frac{T_{i,j+1}^{k+1} - 2T_{i,j}^{k+1} + T_{i,j-1}^{k+1}}{\Delta z^2} \tag{10}$$

$$\frac{1}{r}\frac{\partial T}{\partial r}\bigg|_{i,j}^{k+1} = \frac{1}{r_i}\frac{T_{i+1,j}^{k+1} - T_{i-1,j}^{k+1}}{2\Delta r} \qquad r_i = (i-1)\cdot\Delta r \qquad (11)$$
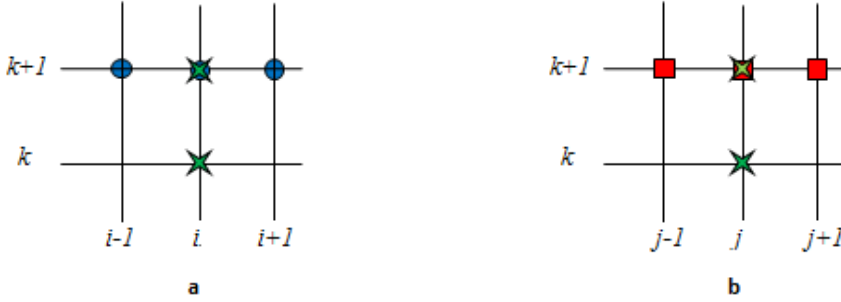
Figure. 4. Implicit pattern in time.

$$\frac{1}{\alpha}\frac{T_{i,j}^{k+1} - T_{i,j}^{k}}{\Delta t} = \frac{T_{i+1,j}^{k+1} - 2T_{i,j}^{k+1} + T_{i-1,j}^{k+1}}{\Delta r^2} + \frac{1}{(i-1)\cdot\Delta r}\frac{T_{i+1,j}^{k+1} - T_{i-1,j}^{k+1}}{2\Delta r} +$$
$$+ \frac{T_{i,j+1}^{k+1} - 2T_{i,j}^{k+1} + T_{i,j-1}^{k+1}}{\Delta z^2} \qquad (12)$$

Or pose: $A = \alpha\dfrac{\Delta t}{\Delta r^2}; B = \alpha\dfrac{\Delta t}{\Delta z^2}$

$$T_{i,j}^{k+1} - T_{i,j}^{k} = A\left(T_{i+1,j}^{k+1} - 2T_{i,j}^{k+1} + T_{i-1,j}^{k+1}\right) +$$
$$+ A\left(\frac{T_{i+1,j}^{k+1} - T_{i-1,j}^{k+1}}{2(i+1)}\right) + B\left(T_{i,j+1}^{k+1} - 2T_{i,j}^{k+1} + T_{i,j-1}^{k+1}\right)$$

After simplification;

$$A\left(1 + \frac{1}{2(i-1)}\right)T_{i+1,j}^{k+1} - (2A + 2B + 1)T_{i,j}^{k+1} + A\left(1 - \frac{1}{2(i-1)}\right)T_{i-1,j}^{k+1} +$$
$$+ B\left(T_{i,j+1}^{k+1} + T_{i,j-1}^{k+1}\right) = -T_{i,j}^{k}$$

We obtain the 5-point formula, valid for $i = 2,...n-1, j = 2,...m-1\,et\,k > 0$

$$A\left(\frac{2i-1}{2(i-1)}\right)T_{i+1,j}^{k+1} - (2A + 2B + 1)T_{i,j}^{k+1} + A\left(\frac{2i-3}{2(i-1)}\right)T_{i-1,j}^{k+1} +$$
$$+ BT_{i,j+1}^{k+1} + BT_{i,j-1}^{k+1} = -T_{i,j}^{k} \qquad (13)$$
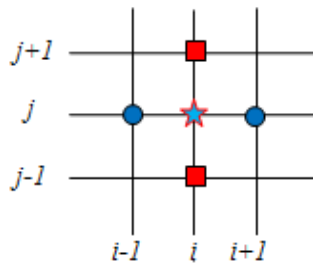
Figure. 5. Five-point formula.

4. Results and discussion

IV.1 Aluminum case: $\lambda = 237$ (W/m.°C), $\alpha = 1.1386 \times 10^{-4}$ (m$^2 \cdot$s^{-1})
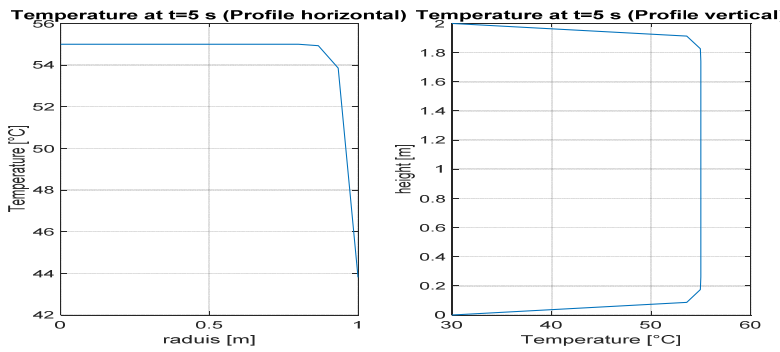
Figure. 6. Temperature profiles along the middle cloths (at t = 5 s)
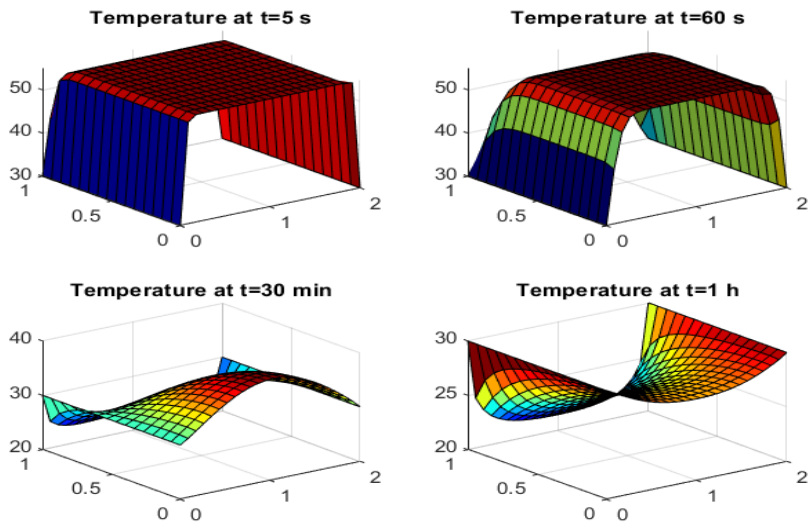
Figure. 7. Temperature distributions at the times indicated

Figs. 6 and 7, for the case of aluminum it can easily be seen that the cooling begins gradually at the side wall of the cylinder where the convection condition is imposed (of the Robin type). However, the two ends of the cylinder also contribute to cooling, but the heat exchange by convection is more intense despite the fact that in this case the conductivity of the material is high. ($\lambda = 237$ W/m.ºC).

IV.2 Steel case: $\lambda = 55$(W/m.ºC), $\alpha = 1.5067 \times 10^{-7}$ (m$^2 \cdot$s^{-1})
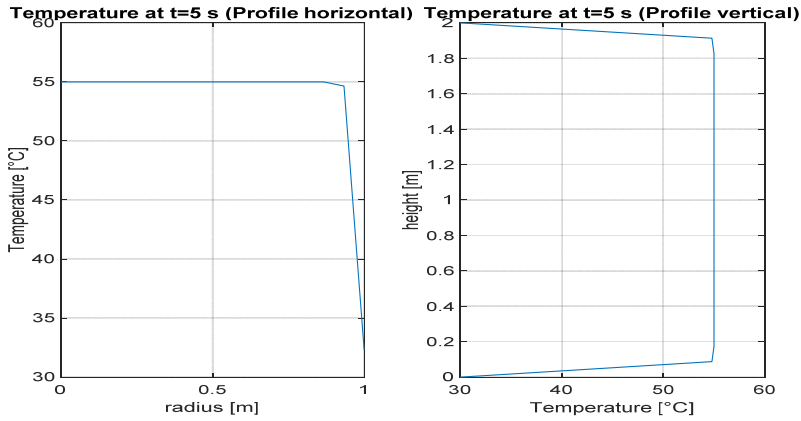
Figure. 8. Temperature profiles along the middle cloths (at t = 5 s)
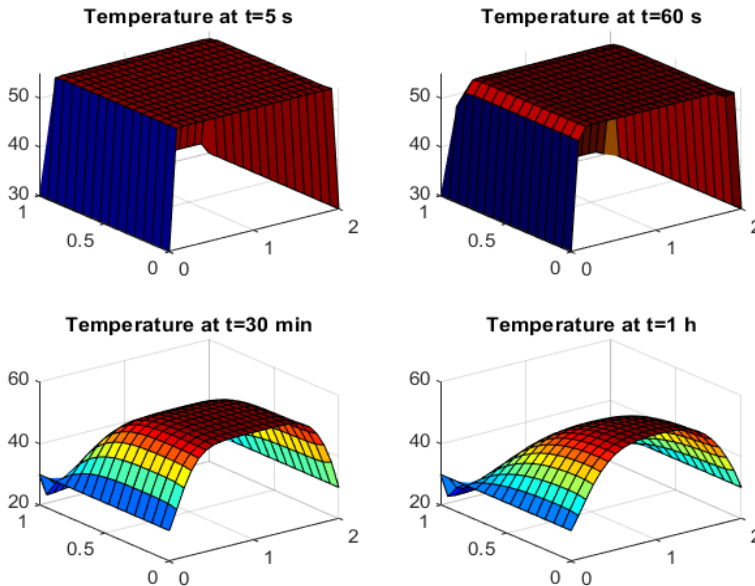
Figure 9. Temperature distributions at the times indicated

We also observe figs. 8 and 9, that in the case of steel, which is less conductive than aluminum, the cooling gradually diffuses within the cylinder, starting from

the three boundaries of at low temperatures. The temperature distribution will reach a uniform state indicating that the cylinder has been cooled over time.

IV.3 Glass case: $\lambda=0.87(W/m.°C)$, $\alpha=5.0115\times10^{-7}$ $(m^2 \cdot s^{-1})$
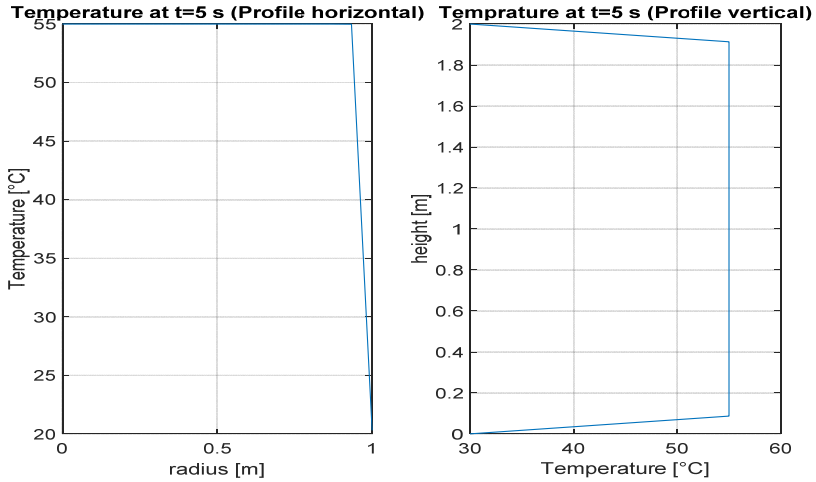
Figure 10. Temperature profiles along the middle cloths (at t = 5 s)
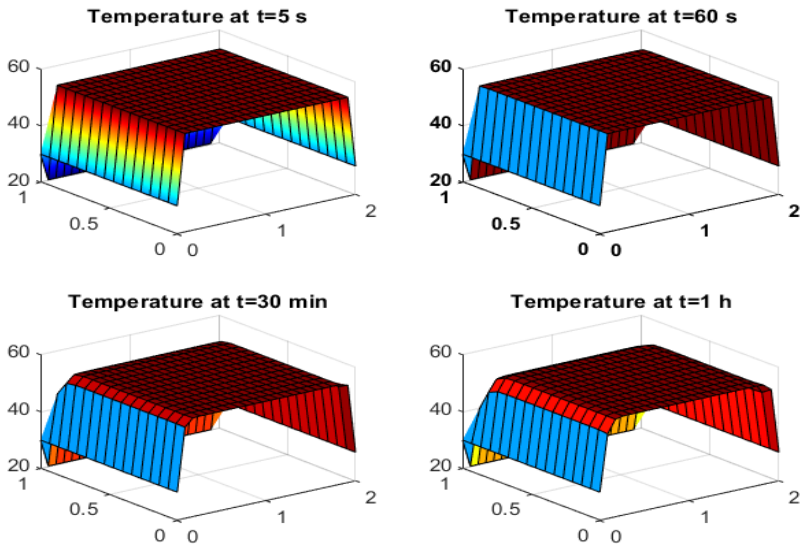
Figure 11. Temperature distributions at the times indicated

In the case of glass, which has low conductivity compared to the two materials already mentioned, the heat diffusion remains moderate despite the heat exchange coefficient by convection being high ($h=1500W/m^2°C$), this which is concluded

from figs. 10 and 11. And the steady state of temperature distribution will be reached after long periods of time.

Conclusion

The issue of minimizing heat transfer times is very important in industry, especially in heat exchangers, which makes it a primary factor in performance.

One can conclude at the end of this numerical study of the transfer of heat in a solid cylinder subjected to the conditions of Robin, that the exchange by convection will be more intense (faster) if the conductivity of the material (and consequently its diffusivity $\alpha = \lambda / \rho C$) is more important. This illuminates the relationship between the two modes of heat transfer in matter (conduction and convection), where the exchange is considered to be effected according to Newton's law of convection.

References

[1] Y. Janot,2012, 'Thermal transfers', École des Mines de Nancy, pp 40-80.
[2] A. J. Casadevall, 2013, 'Introduction to MATLAB', Université Paris Dauphine,pp 422-500.
[3] D. Pastre,2002, 'Methods of Jacobi, Gauss-Seidel, gradiant, conjugate gradient, optimization', René Descartes University, pp 12-300.
[4] S. Boughali, 2013,'Heat transfer by conduction', Kasdi Merbah University,pp1-100 .
[5] A. M. Bianchi,2004, 'Transferts thermiques', Université de la francophonie, pp 200.
[6] A. Diouf,2010, 'Heat transfer in dynamic frequency regime in a cylindrical material', Journal des sciences, pp 33-88.

PCMs in building envelope: characteristics, applications, key parameters and energy contribution

Qudama AL-YASIRI, Márta SZABÓ

Department of Building Services and Environmental Engineering, Institute for Process Engineering, Faculty of Mechanical Engineering, Szent István University, Gödöllő, Hungary.

Abstract

The present paper discusses the main aspects of incorporation phase change materials (PCMs) for building envelope applications. A brief overview of PCM types, properties and desired characteristics for building applications are presented. Besides, the possible incorporation applications in practice are discussed for several building envelope elements and construction materials. The key parameters that affect the thermal performance of PCMs in building applications are presented and discussed. Finally, some state-of-the-art studies reported in the literature are investigated and analysed to highlight the contribution to building efficiency gained by PCMs. It has been shown that PCMs plays an essential role in building envelope and can improve its thermal efficiency significantly. However, more investigations regarding this technology still need to be maintained as presented in the conclusions.

Keywords

PCMs, Building envelope, Energy saving, PCM applications

1. Introduction

Building envelope is a crucial component on building energy efficiency as it adjusts the thermal load and responsible for approximately 50% of heating and cooling loads. In this regard, the International Energy Agency (IEA) reported that in 2018, the building envelope construction activities are responsible for 36% of final global energy used and 39% of CO_2 emissions generated.

Numerous solutions and strategies have been applied to minimise these ratios towards and efficient buildings. Among new technologies, incorporation of phase change materials (PCM) into building elements and components is a viable option for this purpose. PCMs are materials that can store and release the thermal energy through latent heat at an almost constant temperature. Moreover, a considerable amount of heat energy can be maintained by a limited PCM volume, making it in need for today's fast-growing building developments.

PCMs applied to improve building efficiency through different contributions. PCM can shave the temperature entering through the building envelope, which decrease the cooling loads. Besides, incorporation of PCMs in hot locations can

shift the peak load to off-load hours, minimising the reliance on air-conditioning devices. Under cold locations, PCM can work as a heat supplier through storing heat during day hours to utilise it during night hours, or by restricting the escaping heat from indoor towards outdoor.

This paper briefly presents the main aspects of PCM technology in building envelope applications through several sections. Section 1 gives a short overview of PCMs, and their role in the building is given. Section 2 presents the main properties and desired characteristics of PCMs. Section 3 details the possible practical incorporation methods of PCM with building elements and construction materials. Section 4 describes the key parameters that influence PCM's thermal performance. Section 5 investigates some reported PCM contributions to buildings' energy. This paper gives a valuable description of this technology for the researchers and newcomers in this area.

2. Properties of PCMs

PCMs are mainly classified as organic, inorganic and eutectic materials. Organic PCMs are widely used in building applications and further classified as paraffins, fatty acids, alcohols, esters and glycols [Faraj et al., 2020]. Each group has specific thermal and physical properties making it appropriate for a specific building application location. In general, the main properties of each PCM group are tabulated in table1.

Table 1. Advantages and disadvantages of organic, inorganic and eutectic PCMs [Al-Yasiri & Szabó, 2021]

PCM category	Advantages	Disadvantages
Organics	- Available with a wide temperature range - High heat of fusion - Low subcooling - Physically and chemically stable - Compatible with many containers and building materials - Environmentally safe and non-radiative. - stabile after many cycles - Recyclable	- Low thermal conductivity and enthalpy - No sharp melting point - High volumetric change during phase transition - Unstable under high temperatures - Costly for pure materials - Toxic (some types)
Inorganics	- High thermal storage and good thermal conductivity - Available with low cost - Sharp melting temperature - Low vapour pressure	- Considerable volumetric change during phase transition - Show phase segregation and subcooling - Incompatible with metals
Eutectics	- Sharp melting temperatures - High storage capacity	- Costly - Limited in building applications

In building applications, the appropriate PCM candidate must be characterised by several desired characteristics to work effectively. These characteristics are mainly thermophysical, chemical, kinetic, economic and environmental properties, as shown in figure 1.
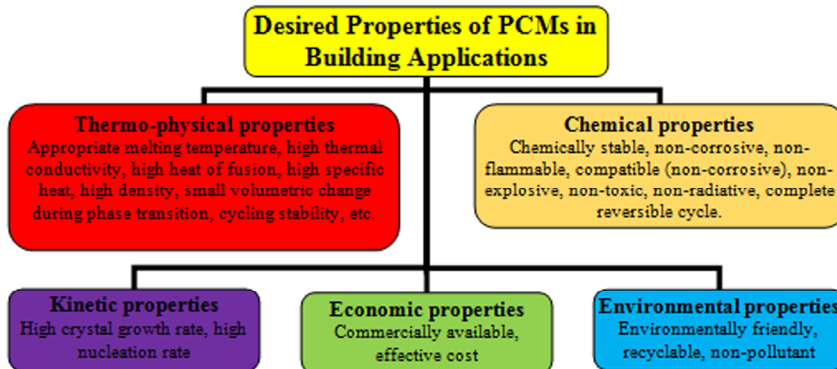
Figure 1. Desired properties of PCMs for building applications.

3. Building envelope applications

PCMs can incorporate with building envelope elements by different methods such as direct mixing, immersing, encapsulation (micro or macro-encapsulation), shape-stabilised and form-stabilised. Accordingly, the PCM can be added directly to the construction materials or inserted independently as a separate component/layer.

Generally, PCM can be integrated with building envelope elements in passive or active strategies. In *passive* strategy, the charging and discharging of heat through the PCM is taken place without any active means. Therefore, the heat would be moved to and from the PCM due to conduction and natural convection. This strategy needs careful selection of PCM type considering the temperature variation throughout the day to satisfy the melting and solidification phases. An external means in an *active* strategy are required to charge or remove the heat from the PCM, such as fans, pumps, thermal collectors, etc. This strategy is more complicated and costly than the passive strategy but utilises the PCM storage capacity efficiently.

Practically, the incorporation of PCM with building elements can be performed in one of the following applications:

Concretes and mortars: The PCM can be combined with the concrete and mortars as a micro-encapsulated form mixed with the raw materials during installation. In such a case, the thermal properties of the mixture would be changed. Therefore, the quantity of PCM microcapsules should be specified to preserve the strengthening of the mixture.

Bricks: PCM either poured inside bricks directly or involved after suitable encapsulation. In the first incorporation form, the brick must be prepared carefully to avoid any possible leakage during the melting phase. Besides, a proper encapsulation container should be used when considering the latter form.

Walls, roofs and floors: PCMs can be a separated layer using panels, sheets or pipes. The effect of element thermal resistance influences the PCM in this application. Therefore, the position of the PCM layer should be adequately studied.

Others: The PCM can be involved in other elements such as slabs and suspended ceilings in the form of sluts, pushes, shelters and packages. In these applications, the PCM is installed as a separate layer utilised actively by blowing a stream of air through the fan. In this case, the PCM is employed as a heat recovery system or a storage medium for heating applications. Some practical applications of PCM are presented in figure 2.

Bricks based PCM   Roof and walls based PCM sheets   Pre-fabricated slab with PCM pipes

Suspended PCM shelters   Roof with PCM shelters   Suspended ceiling with PCM packages   Different PCM metal containers
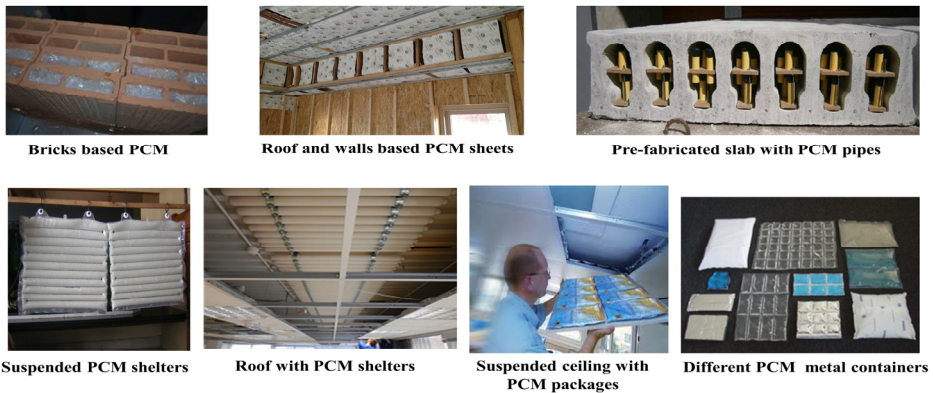
Figure 2. Practical PCM incorporation applications

4. Key parameters of PCM performance in building applications

Several parameters have to be studied when selecting the PCM candidate for a particular building application. These parameters are either related to the PCM itself or the incorporation method used. Generally, these parameters are as follows:

Melting temperature
Melting temperature is the leading thermal property of PCM that should be specified adequately for building applications. PCM melting temperature depends highly on incorporation (heating/cooling) and temperature variation in the studied location. In general, PCMs of melting temperature in the range (~20-30 °C) are suitable for cold locations, whereas higher melting temperature PCMs (~30-50 °C) are effective in hot climates.

Heat storage capacity
This thermo-physical property influences the amount of heat charged into PCM. Therefore, high storage capacity allows more heat to be stored inside the PCM and work efficiently. As mentioned in section 2, the heat storage capacity is varied among PCMs depends on their categories. The total energy storage capacity can be estimated by considering the mass of PCM, PCM enthalpy content, and the number of cycles (daily, each day represent one cycle for melting and solidification).

Effective position
The position of PCM within a building envelope influences the thermal performance of PCM. This parameter has to be studied carefully considering the influence of weather conditions, the thermal resistance of construction materials, incorporation method and mechanical concerns of the building element. It has been reported that the best position of PCM is near the heat source [Al-Absi et al., 2020]. PCM applied in hot locations should be close to the outdoor to restrict the heat from outside and work as insulation. Likewise, PCM should be positioned close to the indoor to trap the heat from inside toward the outside in cold locations. However, PCM optimal position still opens for discussion and should be studied on an annual basis considering weather conditions throughout the year.

Effective quantity (thickness)
This parameter is essential as it links PCM's performance and its effect on envelopes' mechanical properties with economic concerns. Higher quantity should increase the effectiveness of PCM as a result of increased energy storage capacity. However, the extra quantity may not be utilised due to the lack of heat charging/discharging medium. Therefore, building element mechanical strength and incorporation feasibility will be affected.

5. PCM contribution to the building energy

PCMs showed remarkable advancements to the building efficiency in terms of energy-saving, thermal comfort, heating and cooling load reduction, saving of CO_2 emissions, envelope thermal management and peak load delay.

Most of the literature studies were incorporated PCM with building envelope passively. For instance, Hu and Yu [2019] has numerically investigated the performance of PCM board embedded inside wall under five different climate conditions in China. They presented the total energy saving and CO_2 emission reduction, taking into account the PCM type and its position and thickness. The results revealed that incorporating PCM could save energy consumption through building walls by 6% and reduce CO_2 emissions by 1% in the warm locations. They also reported that the PCM position within the building wall is sensitive; thus, placing the PCM layer inside the wall insulation can save 1%–7% more

energy than the PCM layer outside the insulation. Moreover, the increase in PCM thickness can save 2%–6% more energy in severe and hot climate zones. Mohseni and Tang [2021] numerically studied a range of melting temperatures (19 °C -29 °C) with 5 mm and 10 mm thicknesses to specify the optimal case for under Australian climate conditions. Results showed that the best melting temperature depends on the season in which the best melting temperature in summer was 25 °C, whereas the best one in winter is 21 °C. The cooling and heating energy consumption was reduced by 23% and 12%, respectively when the PCM thickness increased from 5 mm to 10 mm. The study concluded that a maximum of 6146 kg/year of CO_2 was saved. Younsi and Naji [2020] investigated the thermal performance of microencapsulated PCM-mortar layer incorporated into the wall. The aim of this study was to improve thermal comfort, downsize heating/cooling systems and shift the peak load. The study considered the mass fraction of PCM within the mortar, the melting temperature, and the wallboard's thickness as effective parameters. Findings showed that the best melting temperature was varied between 24 °C and 28 °C. Moreover, the PCM–mortar layer reduced the interior temperature by 3 °C, and the thermal comfort was improved at PCM mass fraction of 20%–30%. Tunçbilek et al. [2020] numerically studied PCM's thermal performance in conventional bricks on a seasonal and annual basis under the Marmara conditions, Turkey. They studied different PCM melting temperatures range from (18 °C – 26 °C) with different quantities and positions concerning the interior and exterior environment. The results showed that filling brick gaps near the interior environment resulted in better energy conservation and the optimal PCM performance depends highly on the season. However, the best thermal performance was reported for PCM of 18 °C melting temperature. Furthermore, the heating and cooling loads were reduced by 17.6% and 13.2%, respectively, which provided adequate thermal comfort.

For active systems, PCMs were incorporated with solar thermal systems to improve the performance of both technologies. Navarro et al. [2016] experimentally studied the thermal performance of PCMs encapsulated using pipes and inserted inside a prefabricated concrete slab. Two cubicles with active slab (contains PCM) and conventional slab (without PCM) were fabricated to compare the energy saving obtained from the utilisation of PCM under severe and mild winter conditions of Spain. The active slab incorporated with 52 kg of paraffin (RT-21) of 21 °C-22 °C melting temperature and exposure to a hot air stream provided by solar air collector. Findings indicated that the active slab was saved energy by up to 20% during partial melting of the PCM, and 55% at complete melting and solidification cycles compared with the conventional slab. The study further revealed that an energy-saving of 25% and 40% was achieved during the severe and mild winter conditions. Kong et al. [2020] fabricated a hybrid PCM-solar system composed of perlite-based composite PCM wallboard coupled with a solar heating system by capillary pipes. The system was incorporated inside the tested room's wall and compared with other conventional room under winter conditions of Tianjin, China. The results showed that the daily heating energy consumption was reduced by 44.16% for the room provided with the hybrid system compared with the conventional one.

Conclusion

The utilisation of PCMs into building applications is one of the fast-growing technologies adopted in the building industry to improve building efficiency. This paper presented and discussed several aspects of this technology, highlighting the primary key research for future studies. For that, several conclusions and remarks raised from this work are listed, as follows:

- PCMs, despite their types and properties, can efficiently increase the building efficiency. However, the majority of investigated PCMs in the literature are organics and inorganics versus very limited eutectics. The main reason for that is that eutectics have a high range of working temperatures for building applications. New mixtures involving organic and eutectic materials are out of scope.
- Majority of literature studies were investigated the PCM in passive strategies more than active strategies. Although the passive strategy was effective in several locations, many issues such as uncontrolled heat transfer, lack of full PCM utilisation, and lack of heat charging/discharging at specific times. Therefore, adopting new active strategies with minimal operational costs are required.
- Key parameters are essential for the efficient use of PCM in building applications for both the performance and feasibility point of view.
- Most of the published studies were numerical compared with the experimental ones. It is commonly known that numerical studies depend on approximations and forecasting, which make them inaccurate. Therefore, experiments are important to prove the numerical outcomes rely on actual weather conditions and climate effects.

Acknowledgement

References

[1] Al-Absi, Z. A., Mohd Isa, M. H., Ismail, M. (2020): Phase Change Materials (PCMs) and Their Optimum Position in Building Walls. Sustainability, 12(4), 1294. https://doi.org/10.3390/su12041294

[2] Al-Yasiri, Q., Szabó, M. (2021): Incorporation of phase change materials into building envelope for thermal comfort and energy saving: A comperhansive analysis. Journal of Building engineering, 36, 102122, https://doi.org/10.1016/j.jobe.2020.102122

[3] Faraj, K., Khaled, M., Faraj, J., Hachem, F., Castelain, C. (2020): Phase change material thermal energy storage systems for cooling applications in

buildings: a review. Renewable and Sustainable Energy Reviews, 119, 109579, https://doi.org/10.1016/j.rser.2019.109579

[4] Hu, J., Yu, X. (2019): Thermo and light-responsive building envelope: Energy analysis under different climate conditions. Solar Energy, 193, 866-877. https://doi.org/10.1016/j.solener.2019.10.021

[5] IEA, International Energy Agency (2018): The Future of Cooling-Opportinuties for energy-efficient air-conditioning. https://www.iea.org/reports/the-future-of-cooling. (Accessed 15 Jan. 2021)

[6] Kong, X., Wang, L., Li, H., Yuan, G., Yao, C. (2020): Experimental study on a novel hybrid system of active composite PCM wall and solar thermal system for clean heating supply in winter. Solar Energy, 195, 259-270, https://doi.org/10.1016/j.solener.2019.11.081

[7] Mohseni, E., Tang, W. (2021): Parametric analysis and optimisation of energy efficiency of a lightweight building integrated with different configurations and types of PCM. Renewable Energy, 168, 865-877, https://doi.org/10.1016/j.renene.2020.12.112

[8] Navarro, L., de Gracia, A., Castell, A., Cabeza, L. F. (2016): Experimental study of an active slab with PCM coupled to a solar air collector for heating purposes. Energy and buildings, 128, 12-21, https://doi.org/10.1016/j.enbuild.2016.06.069

[9] Tunçbilek, E., Arıcı, M., Bouadila, S., Wonorahardjo, S. (2020): Seasonal and annual performance analysis of PCM-integrated building brick under the climatic conditions of Marmara region. Journal of Thermal Analysis and Calorimetry,141, 613-624. https://doi.org/10.1007/s10973-020-09320-8

[10] Younsi, Z., Naji, H. (2020). Numerical simulation and thermal performance of hybrid brick walls embedding a phase change material for passive building applications. Journal of Thermal Analysis and Calorimetry, 140, 965-978, https://doi.org/10.1007/s10973-019-08950-x

Effect of using the semi-transparent windows on the energetic performance of a typical office building in Hungary

Issam KHELE, Márta SZABÓ

Department of Building Services and Environmental Engineering, Institute for Process Engineering, Faculty of Mechanical Engineering, Szent István University, Gödöllő, Hungary

Abstract

Because buildings' energy consumption plays a key role in the world's consumption of energy it is reasonable to devise solutions to decrease the amount of energy used. Using solar power applications in the sector of buildings is not new, but the emergence of Building Integrated Photovoltaic (BIPV) to integrate the solar panels into the building has become a solution and initiated a new era of solar application in buildings. In this paper, using Semi-transparent windows in a reference office's building in the climate of Hungary was investigated to assess the efficiency of using BIPV through a simulated model using (*EnergyPlus*) software. Three commercial semi-transparent windows with different properties have been chosen to apply a comparative analysis between the performance of these windows with three types of conventional Insulated Glazing Units (IGU) and with the current simple glazing system. The results show that in the continental climate like of Hungary, where the heating loads are the most important comparing to the cooling loads because of the cold winter and warm summer, the thermal conductivity has a major effect on the energetic performance of the semi-transparent windows, even more than the Photovoltaic module efficiency.

Keywords

Semi-transparent windows, BIPV, Photovoltaic windows

1. Introduction:

Energy efficiency is one of the most critical sustainability issues. The energy consumption of buildings must be discussed to solve the various problems caused by global warming, as buildings make up 23–47 percent of all energy consumed. (Tak et al. 2017) The first option is decreasing the building usage of power and this approach is too complex because of the many factors to consider as well as a low estimated potential. However, another way is to use these buildings as power generators. Many solutions have appeared in the light of this concept. Nowadays, this approach became more important and attractive in the

building market because it is more efficient with huge potential and break-even technologies to use. Solar energy has been used for active and passive usage. As for active use, it has been used to generate electricity by photovoltaics, and to produce heat. While passive usage contains mainly the light entering through the transparent surfaces like windows and its effect on heating and daylighting for the buildings.

2. Building Integrated Photovoltaic

The two main categories of applications of photovoltaic technology as an electrical generator are BIPV (Building Integrated PV) and BAPV (Building Attached PV). depending on the way of installing the modules, we can decide about the category of application. Generally, BAPV contains the applications where the modules are attached to the building as an external accessory (for example roof modules) with no direct effect on the structure functions. While BIPV contains solar facades and glazing which replaced the classic materials of the building. BIPV is the most revolutionary idea, where converting any sheet of glass to a photovoltaic panel means a great energy potential. Semi-transparent windows have appeared to be the most vital part of the BIPV systems because the window for the first time doesn't have just the function of letting the daylight in, the semi-transparent window is a multifunctional window that now generating electricity. The estimated potential energy of BIPV was mentioned by (Lai and Hokoi 2015) that BIPV systems in the 27 countries within the European Union (EU) had a technical potential of 951 GWP and could provide 840 TWh of electricity, which has the potential to supply approximately 22% of the total electricity consumption of the 27 countries within the EU in 2030.

A huge variety of types of semi-transparent windows have been studied lately focusing on the energetic performance of the window and its effect on the energetic performance of the building, the visual and thermal comfort. (Lai and Hokoi 2015) reviewed the studies published after 2010 on solar facades. The semi-transparent facades were classified depending on the degree of transparency. They also discussed the optimization of the different types of BIPV facades for lighting and thermal behavior. (Tai and Yan 2017) in their study about emerging semi-transparent solar cells illustrated the new technologies used as electrodes in the recent researches. (Wang et al. 2016) evaluated the performance of a-Si (amorphous-silicone) PV in buildings in Hong-Kong. They developed a model using (*Energyplus*), the research found that Optimized PV IGUs will reduce energy consumption by 25.3 percent and 10.7 percent compared to single clear glass and Low-E glass windows in Hong Kong. Many pieces of research over the last five years, assessed the performance of a huge variety of BIPV systems, using crystalline silicon Photovoltaic material by (Joseph, Kichonge, and Pogrebnaya 2019),(Evola and Margani 2016),(Peng et al. 2019). Amorphous Silicon by (Salameh et al. 2020),(Wang et al. 2016),(Mesloub, Albaqawy, and Kandar 2020), (An et al. 2018), (Martín-Chivelet et al. 2018), (Cuce 2016). Also, (CIGS) and

(CDTE) have been studied by (T. D. Lee and Ebong 2017). while (Sun et al. 2018) reviewed comprehensively the development of using (CDTE) as active material in windows. However, the new active materials have an increased number of researches over the last five years, (DSSC) by (H. M. Lee and Yoon 2018), (Selvaraj et al. 2019), (Chung et al. 2020). Also organic Photovoltaic solar cells (OPVSC) by (Tak et al. 2017).

3. Objectives of the research:

Assess semi-transparent windows performance when integrated into a typical office building in Hungary and compare it to the current performance of regular windows with clear glass, and other common glazing systems.
Validate an index that can be used to evaluate semi-transparent windows performance integrated into existing buildings.
 Measure and evaluate the performance of the semi-transparent windows and the effect on heating loads, and artificial lighting electrical loads in a typical office building in Hungary's climate.
 Compare the performance of several types of commercial semi-transparent windows to optimize the glazing system's energetic performance.

4. Methodology

Most of the experiments on semi-transparent PV windows were carried out either as a virtual model using simulation software like (*ENERGYPLUS*, *TRNSYS*) or as an experimental model using calculation methods, and measuring devices. This study is using the simulation method, and (*EnergyPlus*) software has been used to perform the simulation because it has been validated in many previous studies as a valid software to simulate the window multifunctional role. In his thesis for Ph.D., NG POH KHAI (KHAI 2014) defined a comprehensive parameter to assess the holistic performance of the semi-transparent window, which is NEB (Net Electrical Benefit) As shown in equation(1) it is the sum of the lighting electricity savings and photovoltaic electricity production minus the increase/decrease in electricity consumption required for space conditioning (heating/cooling) as compared to a building with 0% WWR (It means an opaque building).

$$NEB = L_{savings} - C_{elecricity} + PV_{generation} \ [kWh/m^2] \qquad (1)$$

 Where: $L_{savings}$= artificial lighting savings through the utilization of daylight. $C_{elecricity}$ = increase in electricity consumption required for space conditioning due to the transmission of additional solar heat gain. $PV_{generation}$ = photovoltaic window electricity generation output.

If the NEB is positive, it would be reasonable to add the semi-transparent BIPV windows as the energy savings from daylight use and generation are higher than the rise in space conditioning electricity usage. In this way, NEB is a simple index capable of assessing the overall electrical advantage of integrating a semi-transparent BIPV window, relative to a selected reference (solid wall / other glazing systems).

As for the theoretical heating load calculations, it is more convenient and more exact to calculate the heating load referring to 1 m^3 of a building. This value is called specific heating demand, q_{hd}(w/m^2), which can be determined by Equation (2) (Melikyan and Egnatosyan 2014):

$$q_{hd} = \sum qhl + q_v + q_{inf} - q_{int} \qquad (2)$$

Where $\sum qhl$ is total specific heat loss. (w/m^2)

q_v is the specific quantity of heat required for heating the outside fresh air, supplied into the building for ventilation (w/m^2)

q_{inf} is the specific quantity of heat lost for heating outside fresh air, which has penetrated the building through gaps of windows and doors. (w/m^2).

Q_{int} is the specific quantity of heat gain in the building from lighting, electrical devices, and inhabitants. (w/m^2)

5. Simulation

5.1 Simulation process
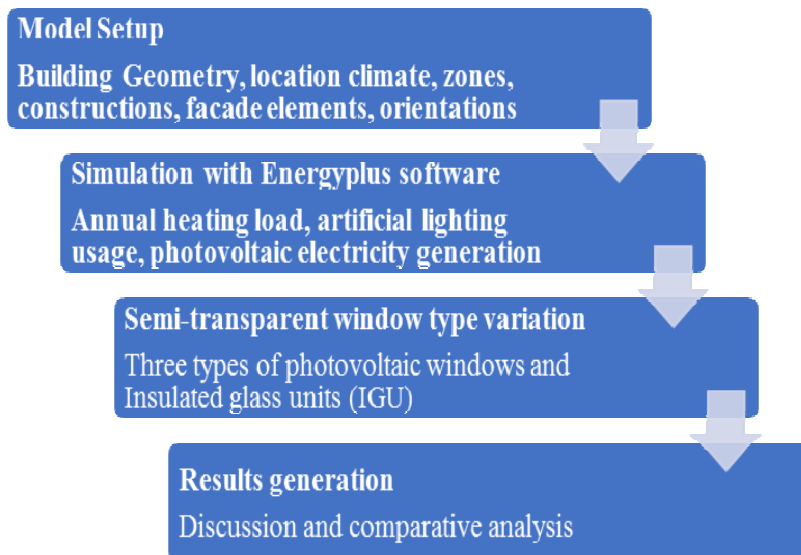
Figure 1. Scheme of the simulation process

5.2 Input Data

Table 1. Reference Building's specifications

Field	Unit	Object
Latitude	deg	47.594332
Longitude	deg	19.3609522
Time zone	hour	1
Elevation	m	219
Floor to ceiling height	m	3.1
Window-to-wall ratio	%	71.20
Illuminance setpoint	lux	500
Infiltration rate		0.1 air change per hour
Gross wall area	m²	2596.6
Above ground wall area	m²	2596.6
Window opening area	m²	1848.64
Gross window-wall ratio	%	71.2
Glazing system		Single pane (6mm of clear glass)

Table 2. Glazing systems' specifications

MODULE	Manu-facturer	Module area (m²)	Maxi-mum Power (W)	Photovoltaic techno-logy	Construction Assem-bly	U value	Solar Heat Gain Coefficient	Visible Transmittance
A	Hanwa Makmax KN-50	0.931	72	a-Si	Single glass laminate	5.076	0.289	0.09165
B	Schott solar (Voltarlux ASI-ISO-E1.2)	0.843	40.4	a-Si	Double glazed unit	1.2	0.1	0.1
C	Spear Alliance (SSM-42S0533Air)	0.931	50	a-Si	Double glazed unit	1.65	0.123	0.0734
E	6mm Clear glass				Single glazed unit	0.9		0.881
F	Normal IGU (2 panels of 6 mm clear glass)				Double glazed unit	0.9		0.881
G	low-e IGU (low-e panel and clear panel)				Double glazed unit	0.9		0.84
H	Low-e tinted IGU (low-e tinted panel)				Double glazed unit	0.9		0.5

The specifications of the commercial windows have been adopted from the manufacturers' catalogs provided and the experiments carried out by Khai. (KHAI 2014). also, from *EnergyPlus v(9-2)* library

Table 3. Structure of the wall, roof, floor, and ceiling

Name	Floor	Exterior wall	Interior wall	Roof	Interior ceiling
Outside layer	Acoustic tile	200 mm heavyweight concrete	19 mm gypsum board	100 mm lightweight concrete	100 mm lightweight concrete
Layer 2	Ceiling air space resistance	50 mm insulation board	Wall air space resistance	Ceiling air space	Ceiling air space
Layer 3	100 mm lightweight concrete	Wall air space resistance	19 mm gypsum board	Acoustic tile	Acoustic tile
Layer 4		19 mm gypsum board			

5.3 Results and Discussion:

Several steps have been carried out to calculate and analyze the performance of each glazing system:

Step 1: Annual heating loads have been calculated for each glazing system.

Step 2: Electrical loads of artificial lighting have been calculated for each one of the suggested systems.

Step 3: The amount of electricity generated by the semi-transparent windows was calculated for each type.

Step 4: After that, the net electrical benefit (NEB) was calculated for each semi-transparent glazing system, clear glass, three types of (IGU), and the results were compared.

Step 5: Discussion and comparison of the results.
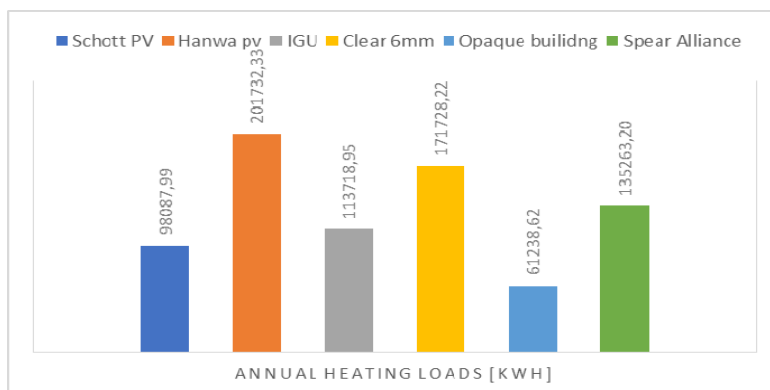
Figure 2. Annual heating loads

Step 1: Figure (2) shows the annual heating loads for each type of glazing system used in the reference Building. Due to its high thermal conductivity, (Hanwa Makmax) didn't achieve decreasing in the demand power for heating, in contrast. The heating loads increase from 171728,22 kWh/year for the current glazing system (clear 6mm glass) to 201732,33 kWh/year for (Hanwa Makmax). While (Schott solar), (Spear Alliance), and (IGU) achieved a good saving percentage due to the relatively low thermal conductivity.
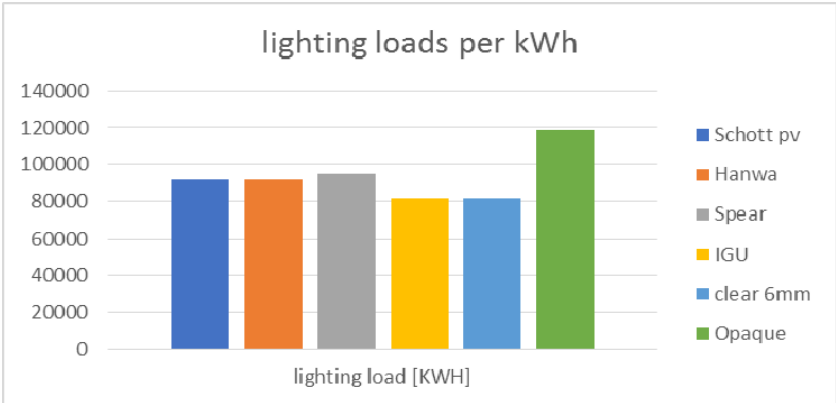
Figure 3. Annual lighting loads
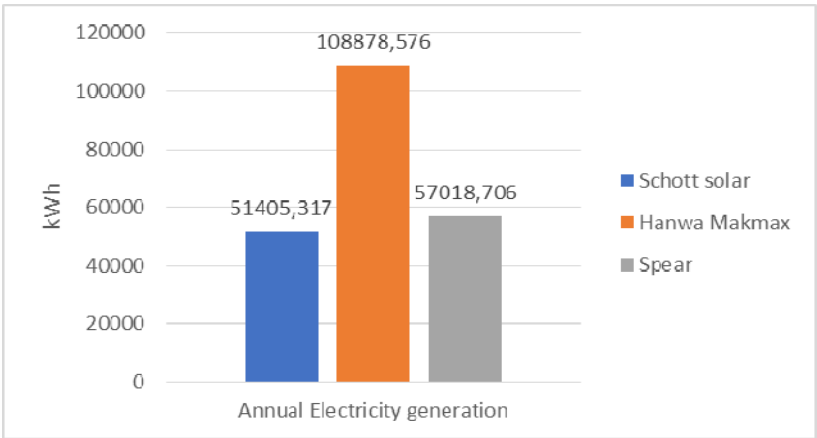
Figure 4. Annual electricity generation

Step 2: The second effective factor in the assessment is lighting electricity consumption, which varies due to the transparency of the translucent windows. Figure (3) illustrates the lighting electrical loads of the building for each glazing system. Artificial lighting is an important part of the building comfort factors, and for power consumption. The opaque building needs 118810.40 kWh/year while

(Schott PV) needs 92179.92 kWh/year. Currently, the building needs approximately 81619.54 kWh/year. Step 3: The third effective factor when assessing the semi-transparent windows is electricity generation. Figure (4) is for comparing the annual electricity generation of each type of semi-transparent windows. The maximum was for (Hanwa Makmax) 108878.576 kWh/year, while the minimum was for (Schott Solar) with 51405.317 kWh/year and slightly better performance for (Spear Alliance) with 57018.706 kWh/year.
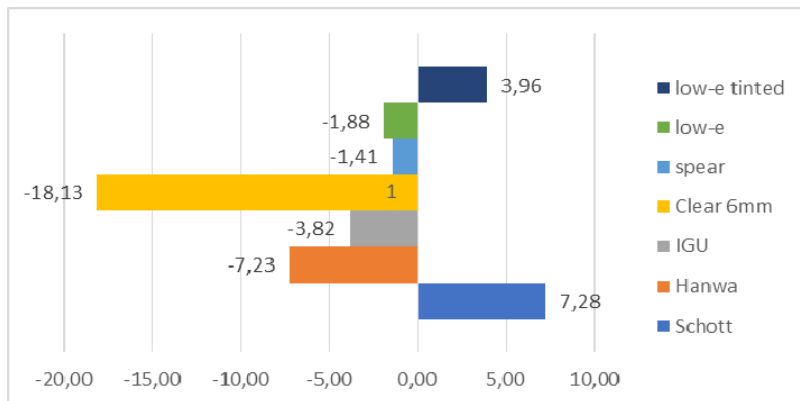
Figure 5. NEB value per kWh/m^2 of each glazing system

Figure (5) summarized the final model of the simulation, The NEB of the examined glazing systems were represented, three types of double clear glass, with three types of semi-transparent PV windows, compared to the current glass system (6mm clear glass). (low-e tinted IGU) achieved NEB of 3.96 kWh, a better result than (low-e IGU) with NEB of -1.88 kWh. This figure shows that the only glazing systems that achieved positive NEB were (low-e tinted IGU) and the semi-transparent window (Schott solar) while the others varied from roughly Neutral performance for (low-e IGU) and (Spear Alliance technology). Even that (Hanwa Makmax) is producing electricity roughly twice as (Schott solar) and (Spear) windows, but the NEB shows that the best saving percentage was for (Schott solar). As mentioned in the discussion of the heating loads variation of each type, even that (IGU) is good at thermal insulation but the new technologies of semi-transparent windows can combine the two features of low thermal conductivity and high transparency in one product. (Schott solar) achieved the Maximum NEB because it has a relatively low thermal conductivity compared to (Hanwa Makmax) and a higher efficiency compared to (Spear Alliance).

Conclusion

1- Six glazing systems were studied and evaluated to have a holistic understanding of each factor and its effect on the performance, single and double

semi-transparent windows with different thermal conductivity, different transparency, and SHGC (Solar Heat Gain Coefficient). It was found that the best performance was for the (Schott solar) semi-transparent window. The results show that in the research climate conditions, low thermal conductivity has a great impact to improve the NEB for the glazing system more than electricity generation. (Schott solar) with thermal transmittance (U=1.2 w/m².k) and maximum power generation of 40 w, has by far better performance than (Hanwa Makmax-42) with (U=5.976) and 72 w maximum generated electricity, because NEB for the first is +7.28 kWh/m², and for the second is -7.23 kWh/m². Besides, improved IGU windows achieved good performance with 3.96 kWh/m² for (low-e tinted IGU) and -1.88 kWh/m² for (low-e IGU). The third semi-transparent window that has been analyzed is (Spear alliance) achieved moderate performance with -1.41 kWh/m².

Generally, the six glazing systems have been analyzed, achieved better performance than the current system (6 mm clear glass), and clearly, using the semi-transparent window in the climate of Hungary has a good potential for better energetic performance in highly glazed buildings (more than 70% WWR), but the main condition affects this performance is the thermal conductivity and the structure of the glazing system itself.

2- The Study showed that lighting loads didn't vary by far between the current glazing system (6mm clear glass) with 81619 kWh/year and the highest demand for lighting loads which is (Schott solar) with 94778 kWh/year, lighting didn't have a big effect on the calculate NEB. This is important for future research because it means that in Hungary's climate, we can be flexible about the transparency of BIPV applications on windows, which will lead to the use of more efficient modules with less care for transparency.

3- The study shows that some types of commercial semi-transparent windows can substitute classical solutions to improve the energetic performance of the building which is using (IGU), this will allow for a bigger application area and a great aid for the environment.

Acknowledgment

References

[1] An, Hyung Jun, Jong Ho Yoon, Young Sub An, and Eunnyeong Heo. 2018. "Heating and Cooling Performance of Office Buildings with A-Si BIPV Windows Considering Operating Conditions in Temperate Climates : The Case of Korea." https://doi.org/10.3390/su10124856.

[2] Chung, Min Hee, Bo Rang Park, Eun Ji Choi, Young Jae Choi, Choonyeob Lee, Jongin Hong, Hye Un Cho, Ji Hyeon Cho, and Jin Woo Moon. 2020. "Performance Level Criteria for Semi-Transparent Photovoltaic Windows Based on Dye-Sensitized Solar Cells." *Solar Energy Materials and Solar Cells* 217 (June): 110683. https://doi.org/10.1016/j.solmat.2020.110683.

[3] Cuce, Erdem. 2016. "Toward Multi-Functional PV Glazing Technologies in Low/Zero Carbon Buildings: Heat Insulation Solar Glass - Latest Developments and Future Prospects." *Renewable and Sustainable Energy Reviews* 60: 1286–1301. https://doi.org/10.1016/j.rser.2016.03.009.

[4] Evola, G., and G. Margani. 2016. "Renovation of Apartment Blocks with BIPV: Energy and Economic Evaluation in Temperate Climate." *Energy and Buildings* 130: 794–810. https://doi.org/10.1016/j.enbuild.2016.08.085.

[5] Joseph, Benedicto, Baraka Kichonge, and Tatiana Pogrebnaya. 2019. "Semi-Transparent Building Integrated Photovoltaic Solar Glazing: Investigations of Electrical and Optical Performances for Window Applications in Tropical Region." *Journal of Energy* 2019: 1–10. https://doi.org/10.1155/2019/6096481.

[6] KHAI, NG POH. 2014. "SEMI-TRANSPARENT BUILDING-INTEGRATED PHOTOVOLTAIC (BIPV) WINDOWS FOR THE TROPICS."

[7] Lai, Chi Ming, and Shuichi Hokoi. 2015. "Solar Façades: A Review." *Building and Environment* 91: 152–65. https://doi.org/10.1016/j.buildenv.2015.01.007.

[8] Lee, Hyo Mun, and Jong Ho Yoon. 2018. "Power Performance Analysis of a Transparent DSSC BIPV Window Based on 2 Year Measurement Data in a Full-Scale Mock-Up." *Applied Energy* 225 (December 2017): 1013–21. https://doi.org/10.1016/j.apenergy.2018.04.086.

[9] Lee, Taesoo D, and Abasifreke U Ebong. 2017. "A Review of Thin Fi Lm Solar Cell Technologies and Challenges." *Renewable and Sustainable Energy Reviews* 70 (September 2015): 1286–97. https://doi.org/10.1016/j.rser.2016.12.028.

[10] Martín-Chivelet, Nuria, Cecilia Guillén, Juan Francisco Trigo, José Herrero, Juan José Pérez, and Faustino Chenlo. 2018. "Comparative Performance of Semi-Transparent PV Modules and Electrochromic Windows for Improving Energy Efficiency in Buildings." *Energies* 11 (6). https://doi.org/10.3390/en11061526.

[11] Melikyan, Zohrab, and Siranush Egnatosyan. 2014. "Residential Buildings: Heating Loads." *Encyclopedia of Energy Engineering and Technology, Second Edition*, no. 4: 1629–36. https://doi.org/10.1081/e-eee2-120051988.

[12] Mesloub, Abdelhakim, Ghazy Abdullah Albaqawy, and Mohd Zin Kandar. 2020. "The Optimum Performance of Building Integrated Photovoltaic (BIPV) Windows Under a Semi-Arid Climate in Algerian O Ffi Ce Buildings."

[13] Peng, Jinqing, Dragan C. Curcija, Anothai Thanachareonkit, Eleanor S. Lee, Howdy Goudey, and Stephen E. Selkowitz. 2019. "Study on the Overall

Energy Performance of a Novel C-Si Based Semitransparent Solar Photovoltaic Window." *Applied Energy* 242 (August 2018): 854–72. https://doi.org/10.1016/j.apenergy.2019.03.107.

[14] Salameh, Tareq, Mamdouh El, Haj Assad, Muhammad Tawalbeh, Chaouki Ghenai, Adel Merabet, and Hakan F Öztop. 2020. "Analysis of Cooling Load on Commercial Building in UAE Climate Using Building Integrated Photovoltaic Façade System." *Solar Energy* 199 (March 2018): 617–29. https://doi.org/10.1016/j.solener.2020.02.062.

[15] Selvaraj, Prabhakaran, Aritra Ghosh, Tapas K Mallick, and Senthilarasu Sundaram. 2019. "Investigation of Semi-Transparent Dye-Sensitized Solar Cells for Fenestration Integration." *Renewable Energy* 141: 516–25. https://doi.org/10.1016/j.renene.2019.03.146.

[16] Sun, Yanyi, Katie Shanks, Hasan Baig, Wei Zhang, Xia Hao, Yongxue Li, Bo He, et al. 2018. "Integrated Semi-Transparent Cadmium Telluride Photovoltaic Glazing into Windows: Energy and Daylight Performance for Different Architecture Designs." *Applied Energy* 231 (June): 972–84. https://doi.org/10.1016/j.apenergy.2018.09.133.

[17] Tai, Qidong, and Feng Yan. 2017. "Emerging Semitransparent Solar Cells: Materials and Device Design." *Advanced Materials* 29 (34): 1–37. https://doi.org/10.1002/adma.201700192.

[18] Tak, Sehyun, Soomin Woo, Jiyoung Park, and Sungjin Park. 2017. "Effect of the Changeable Organic Semi-Transparent Solar Cellwindow on Building Energy Efficiency and User Comfort." *Sustainability (Switzerland)* 9 (6). https://doi.org/10.3390/su9060950.

[19] Wang, Meng, Jinqing Peng, Nianping Li, Lin Lu, Tao Ma, and Hongxing Yang. 2016. "Assessment of Energy Performance of Semi-Transparent PV Insulating Glass Units Using a Validated Simulation Model." *Energy* 112: 538–48. https://doi.org/10.1016/j.energy.2016.06.120.

Reducing nitrogen oxides in ICE R&D laboratory environment

Norbert BÍRÓ[1], György PILLINGER[1], Péter KISS[1], Dániel SZŐLLŐSI[2], Akihiro OHIRA[2]

[1]Department of Vehicle Technology, Institute for Process Engineering, Faculty of Mechanical Engineering, Szent István University;
[2]IBIDEN Hungary Kft

Abstract

In order to meet increasingly stringent emission reduction standards, ICE (Internal Combustion Engine) producers are under constant pressure of evolving R&D (Research and Development). For this reason, development responsibilities also appear on the supplier side. This paper describes the design, development, and testing process of an SCR (Selectiv Catalytic Reduction) dispenser, which suitable for testing internal combustion engine's exhaust gas treatment system. The created equipment opens up modelling opportunities for exhaust gas management system development engineers in order to design tractors and vehicles with less pollutant emission.

Keywords

vehicle exhaust aftertreatment system, SCR, NOx (Nitrogen Oxides), Emission directives, DPF (Diesel Particulate Filter), R&D

1. Introduction

Emission technology is one of the most developing sectors of the engine and automotive industry since the millennium. Tightening emission standards and restrictions, both at European and global level, provide the basis for the development of newer and more modern exhaust gas management systems. The "skillfulness" of the manufacturers has also attracted the attention of the public to keep emissions to an appropriate level.

Among internal combustion engines, diesel engines with the best thermodynamic efficiencies produce a number of pollutants during operation, which modern diesel exhaust treatment systems contain an oxidation catalyst (DOC), a particulate filter (DPF) and a NOx reducing catalyst (SCR) to neutralize. These are treated as one system, scaled and designed as they have a direct impact on each other's operation.

An SCR (eg. AdBlue) system is effective in neutralizing nitrogen oxides, but its use can degrade certain engine performance under certain load conditions and adversely affect the operating parameters of the exhaust gas management system.

For example, it can cause higher soot formation during combustion, which puts an additional load on the DPF. Furthermore, the SCR catalyst has a direct effect on the passive regeneration efficiency of the diesel particulate filter. During passive regeneration, the catalytic material on the DPF surface removes oxygen from the NO_2 content of the exhaust gas while oxidizing soot particles at low temperatures (t = 250-300 °C) . When SCR is used, the exhaust gas NO_2 ratio decreases, thus reducing the amount of oxygen released on the DPF surface, thus reducing the amount of soot burned. Avoiding such phenomena requires further research and development effort on the part of automakers and related automotive suppliers.

In order to explore the deeper connections between the development goals and the system, it is necessary to create a widely programmable SCR (in this case: AdBlue) injection equipment suitable for test purposes, as an injection test system with such properties is not available on the market. It can be used to simulate events such as AdBlue additive overdose or deficiency, leakage, and other system failures or operating conditions that result in measurable emission values.

2. Application in dynamometer equipped engine test cell

The exhaust gas management system is tested under engine bench dynamometer with laboratory conditions, the main units located in the room (Figure 1):
- the exhaust gas treatment system to be tested with the associated diesel engine,
- soot particle number counter,
- exhaust gas concentration measuring equipment,
- the AdBlue injection unit,
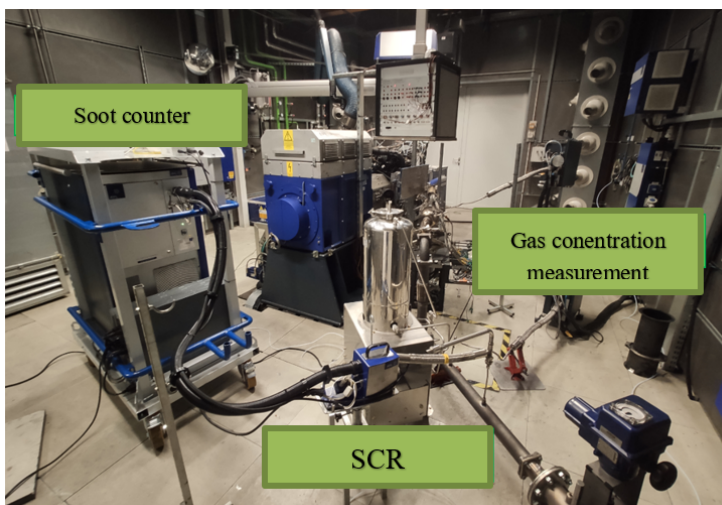- and other sensors (eg. temperature sensor).

Figure 1. Location of exhaust gas treatment system test equipment; Source: Norbert Bíró

The AVL LD (Light Duty) 220 kW dynamometer is equipped with a PSA DW10c , EURO 5 compliant diesel engine, the exhaust side of which is equipped with an exhaust gas management system widely used by the PSA Group for passenger car engines (Fig. 2.). The AdBlue additive injector is located in front of the SCR catalyst and is connected to the exhaust pipe through a 1/8 inch connector. The injection takes place perpendicular to the inlet surface of the SCR catalyst, so that mixing and chemical transformations can be performed optimally.
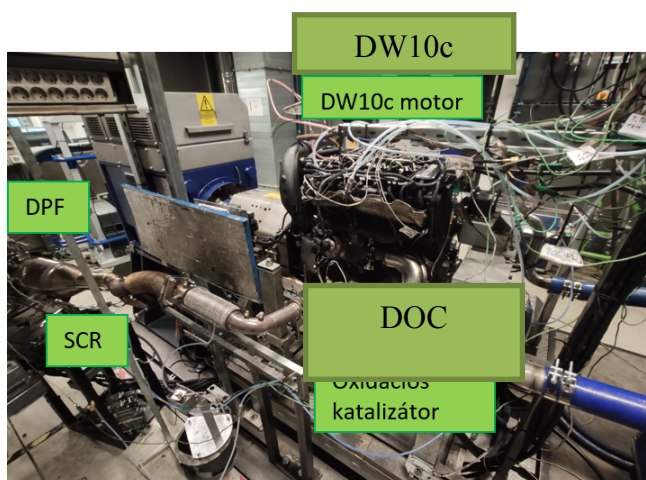
Figure 2. Engine and exhaust system under test; Source: Norbert Bíró

The gas concentration is measured with an AVL AMA i60 wide-range analyzer, which is suitable for the detection of THC, CH_4, NO / NO_2 / NOX, CO, CO_2, N_2O, O_2 and SO_2 gases, as well as for the analysis of both diluted and raw exhaust gases. The meter has official measurement cycles certified by EPA and ECE authorities.
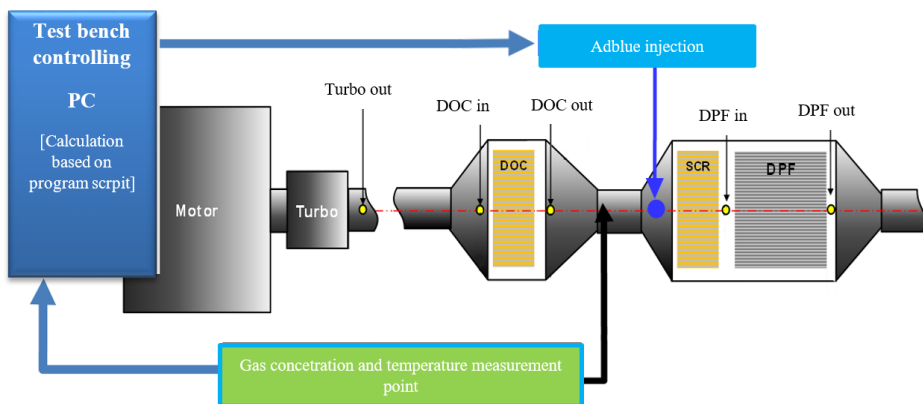
Figure 3. Schematic diagram of a test system; Source: Norbert Bíró

When the test equipment is used in automatic mode, the gas concentration analyzer measures the concentration of the gases in the exhaust gas in real time and transmits them in real time to the dynamometer control computer. From the measured NO_x (NO, NO_2) concentration, the amount of AdBlue additive required for neutralization is determined, as well as the electrical signal for the valve opening time, which is sent to the AdBlue additive injector at an analog output.

The schematic diagram illustrates the structure of the exhaust gas treatment system, together with the measurement and intervention points.

AdBlue dosing unit design
The main component of the dosing unit is a stainless steel tank (X3CrNiMo17-13-3). The tank has a mean diameter of 300 mm, a height of 500 mm and a wall thickness of 3 mm (Figure 4). With these dimensions, store the liquid at a nominal pressure of 2 bar with a double safety factor. The possibility of filling and refilling the tank can be solved through the roof plate on the top, which can be locked / unlocked with a threaded clamp, thus allowing quick and easy use. After the mains air supply has been shut off, the tank pressure can also be reduced by means of a pressure relief valve on the roof plate for refilling, storage or overpressure. The pressure gauge was also located on the roof plate. To check the level of AdBlue liquid in the tank, a vertical transparent plastic tube has been installed, which is connected to the tank via a 1/8 inch connector.

Figure 4. AdBlue dosing unit; Source: Norbert Bíró

The flow of the various media is controlled by electrically controlled solenoid , normally closed valves. The connectors are made of ¼-inch brass and are resistant

to dissolved ammonia. Figure 5. clearly shows the flow direction of air and Adblue, the traversed path. The reducer-controlled compressed air is split in one "T" passage and provides the supply pressure to the tank on the one hand, and supplies compressed air to the venturi pump of the injection nozzle on the other.
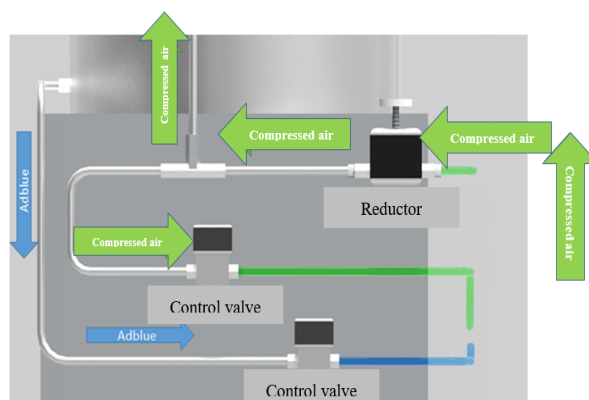
Figure 5. Compressed air and AdBlue pipe lines; Source: Norbert Bíró

Through flexible Teflon tubes that are resistant to dissolved ammonia, both air and AdBlue fluid enter a three-port Nippon control TFA-R4 type solenoid valve. The valve works on the Venturi principle. The compressed air flowing through the upper line creates a negative pressure, so it carries the AdBlue fluid coupled to the lower line. Injection can be stopped by closing the valve, while the injection volume can be controlled by changing the opening time of the valve.

3. Injection control principles

The three 24-volt solenoid valves are powered by a 230V to 24V DC adapter. For commissioning, the toggle switch labeled "POWER" [1.] must be toggled to power the controller (Figure 6). The injector opening frequency can be set with knob [2.] After setting, the injector can be started with the rocker switch [3.] marked "START / STOP". In the start position, the cyclic opening and closing of the injector starts at the set frequency. The process continues until the toggle switch is turned to the "STOP" position. Toggle switch [4.] "EXT / INT" can be used to toggle between internal, ie control as described, and control based on an external analog signal source (AUTOMATIC). When the equipment is used in automatic mode, the gas concentration analyzer measures the concentrations of the gases in the exhaust gas in real time and transmits them to the dynamometer control computer. Based on the control program, the computer determines the amount of AdBlue additive to be injected and the required valve opening frequency.
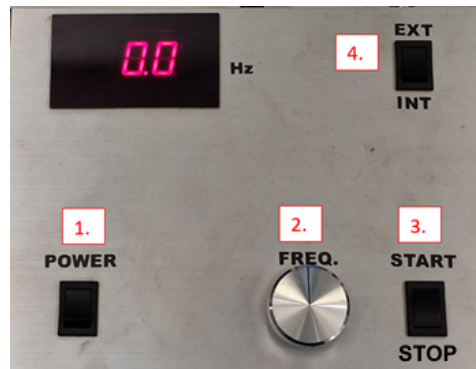
54

Figure 6. Control Panel; Source:Norbert Bíró

Control program script

The control program determines the 24V output frequency of the appropriate frequency to operate the injector based on the gas concentration analyzer data, intake air mass flow rate, hourly fuel consumption, and exhaust gas temperature. The program had to ensure that no injection was performed below the minimum gas temperature of 180 °C required to convert AdBlue to ammonia. Prohibiting injection is especially important at low temperatures, as AdBlue does not contain pure ammonia. When ammonia is injected, it is formed from AdBlue by a hydrolysis / thermolysis reaction. Because both pure ammonia and AdBlue pollutants cannot escape to the ambient air from the exhaust system.

4. Verifying and evaluating the device test result

To test the AdBlue dosing device, the engine placed on the dynamometer implemented the driving cycle shown in Figure 7, so that the operation of the dosing device could be tested at several operating points. The engine and exhaust system are warmed up in two stages. In the first step, run for 10 minutes at 1500 rpm with a load of 50 Nm. This was followed by the second stage with a 12-minute run at 3000 rpm and a load of 180 Nm. The warm-up phase was followed by three load phases with flight times of 2.5, 1.7, and 1.3 minutes. The speed values varied negligibly for the load sections, and the torque values were 220 Nm, 260 Nm, and 295 Nm, respectively. The last load phase was followed by a 10-minute cooling phase running at 1500 rpm and a load of 50 Nm.

Figure 8 shows the gas concentration before and after the SCR catalyst. It can be stated that NO_x reduction is the most efficient in the low and medium load stages, here it neutralizes up to 99% of the harmful gas.

At high loads, the efficiency drops to 75%, which results in nominal values (max: ~ 370 ppm) under the current regulations of EURO VI. At high loads, fuel consumption increases, proportionally to the amount of intake air, and thus the exhaust gas mass flow.
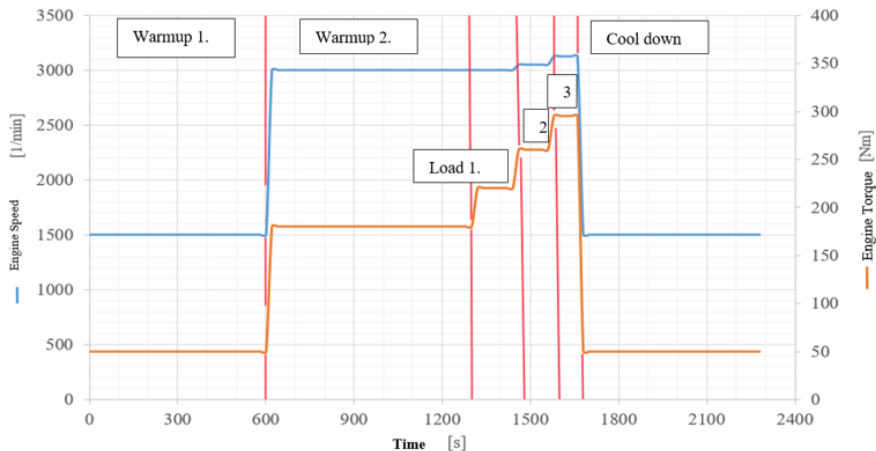
Figure 7. Dosing test cycle; Source: Norbert Bíró

It can be seen that in the case of long-term use at high loads, the amount of AdBlue injected can be increased by increasing the supply pressure of the container and by using a larger diameter injection nozzle.
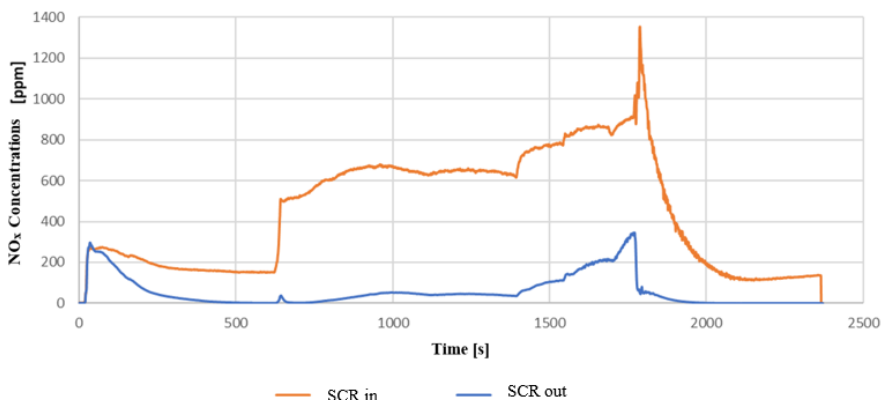
Figure 8. Dosing test cycle; Source: Norbert Bíró

Conclusion

During the preliminary and final tests, the device functioned properly, fulfilled the set goals, and performed the planned functions:

- NO$_x$ neutralization, min. 80% efficiency over the entire test cycle.
- Manual injection setting option, which allows simulating malfunctions in static tests and ExFm (extreme failure mode) tests, thus preventing them.
- Automatic use with ANR (Ammonia Nitrogen Oxide Ratio) 1: 1 settings, which fully corresponds to the operation of NOx reduction systems

(SCR) in standard passenger cars, making it easy to simulate all diesel particulate filters manufactured in accordance with the EURO 6d-temp directives after 09.09.2017.
– No error has occurred since the device was used.

Further development opportunities

Examining the NO_x reduction diagram clearly, it can be seen that in the lower load regions the reduction reaches 99% while in the parts with maximum load the reduction efficiency decreases up to 75%. The output voltage is maximum at these stages, i.e. the solenoid valve operates at the maximum opening frequency, in order to increase the amount of AdBlue injected and thereby increase the reduction efficiency, the following improvements must be made:
– Increase the inside diameter of the injection nozzle or use another nozzle with a larger inside diameter for higher load tests.
– Increase the maximum tank supply pressure from 2 bar to 4 bar, which would not endanger the operation of the appliance. This would increase the amount of Adblue injected, which would increase the reduction efficiency.
These development opportunities would require new tests, but a correspondingly increased AdBlue injection could also open up the possibility of testing more powerful car and truck engines.

Acknowledgement

References

[1] Seher, D., Reichelt, M., and Wickert, S., (2003): Control Strategy for NOx - Emission Reduction with SCR. *SAE Technical Paper 2003-01-3362, https://doi.org/10.4271/2003-01-3362.*
[2] Keuper, A., Unger, H., Huang, J., Bressler, H. et al. (2011): Investigations to Achieve Highest Efficiencies in Exhaust Gas After-Treatment for Commercial Vehicles using an SCR System. *SAE International Journal of Commercial Vehicles.* 145-155.
[3] Kazushige O., (2006): A Study on performance of Performance of Particulate filters Using R-SiC Porous Materials for Diesel Vehicles. *Scientific textbook.* 2.1 – 3.45
[4] Birkhold, F., Meingast, U., Wassermann, P., Deutschmann, O., (2006): Analysis of the Injection of Urea-Water-Solution for Automotive SCR DeNOx-Systems: Modeling of Two-Phase Flow and Spray/Wall-Interaction. *SAE Technical Paper 2006-01-0643, https://doi.org/10.4271/2006-01-0643.*

[5] Akiyoshi, T., Torisaka, H., Yokota, H., Shimizu, T. et al., (2011): Development of Efficient Urea-SCR Systems for EPA 2010-Compliant Medium Duty Diesel Vehicles. *SAE Technical Paper 2011-01-1309*, *https://doi.org/10.4271/2011-01-1309.*

[6] Daimler-Benz Ag. (1996): Process and apparatus for selective catalyzed no-reduction in oxygen-containing exhaust gases. *Patent.*

[7] Daimler-Benz Ag. (1998): Method and device for operating an internal combustion engine with low nitrogen oxide emissions. *Patent.*

[8] Man Nutzfahrzeuge Ag. (1993): Catalytic nitrogen oxide(s) redn. appts. for vehicles - comprises flow mixer urea evaporator hydrolysis catalyst, for exhaust gas treatment. *Patent.*

[9] Jánosi, L., Kiss, P. (1988): Belsőégésű motorok nitrogénoxid kibocsátásának követése más motorjellemzőkből. *MTA-MÉM Agrár-Műszaki Bizottság kutatási és fejlesztési tanácskozás Gödöllő, Magyarország : MÉM Műszaki Intézet,* 34-36.

[10] Ford Global Technologies, Inc. (2002): Method and system for NOx reduction. *US Patent.*

[11] Haldor Topsoe A/S.(2003): Process for the reduction of SCR NOx emissions and apparatus therefor. *Patent.*

[12] Gabrielsson Par L.T. (2004): Process for controlled addition of a reducing agent into nitrogen oxides containing exhaust gas. *Patent.*

[13] Ford Global Technologies, Llc. (2006): Exhaust gas aftertreatment systems. *Patent.*

[14] Robert Bosch Gmbh. (2010): Procedure for checking the functionality of a metering valve of a NOx-reduction system of a combustion engine. *Patent.*

[15] Hilite Germany Gmbh. (2012): SCR exhaust gas aftertreatment device *.Patent.*

[16] Robert Bosch Gmbh. (2015): Vehicle SCR system and its reducing agent supplying device. *Patent.*

[17] Zheng, G., Wang, F., Zhang, S., Zhang, J. et al., Development of Compact SCR Systems with Closely Coupled Injector Configurations. *SAE Technical Paper 2014-01-1546, 2014, https://doi.org/10.4271/2014-01-1546.*

[18] European comission, emission regulation directive https://eur-lex.europa.eu/legal-content/EN/TXT/?uri=CELEX:32016R0646 ; https://eur-lex.europa.eu/legal-content/EN/TXT/?uri=CELEX:32008R0692 ; https://eur-lex.europa.eu/eli/reg/2018/1832/oj

[19] Bíró, N., Pillinger, Gy., (2020): AdBlue-adagoló fejlesztése kipufogógáz-kezelő rendszer optimalizálásához. *Mezőgazdasági Technika 2020. május : LXI. Évfolyam..* 2-5.

[20] Szőllősi, D., Bíró, N., Kiss, P., (2020): A dízel részecskeszűrő (DPF) koromszűrési hatékonyságának megállapítása. *Mezőgazdasági Technika 2020. szeptember : LXI. Évfolyam* 2-5..

Evaluation of the temperature effect on the outputs and efficiency of photovoltaic (PV) cell by using Simulink/MATLAB

Mohammed. H. ALI, Zoltan KURJÁK, János BEKE

Department of Energetics, Institute for Process Engineering
Faculty of Mechanical Engineering, Szent István University

Abstract

As a great potential renewable energy source, solar energy is becoming one of the most important energies in the future. Recently, there has been an enormous increase in the understanding of the operational principle of photovoltaic devices, which led to a rapid increase in the power conversion efficiencies of such devices. Solar cells outputs are varied under temperature changes; the change in temperature will affect the output power from the PV cells and its efficiency. In this paper a relation between output power, efficiency, sun radiation and temperature is evaluated by using Simulink/MATLAB and temperature ambient PV module for a desired efficiency can be obtained.

Keywords

Photovoltaic Cell; PV Solar Efficiency; PV Output Power; Temperature.

1. Introduction

Recently, the massive consumption and exhaustion of fossil fuels has led to an enormous interest in the use of renewable energy sources, such as solar energy. Photovoltaic power is a well-established technology and has recently experienced rapid growth over the last years. A solar cell is basically a p-n semiconductor junction. A DC current is generated when exposed to light. PVs offer several advantages, such as: high reliability, low maintenance costs, no pollution of the environment and no noise. The equivalent PV cell circuit is shown in Figure 1. [Ibrahim *et al* 2017]
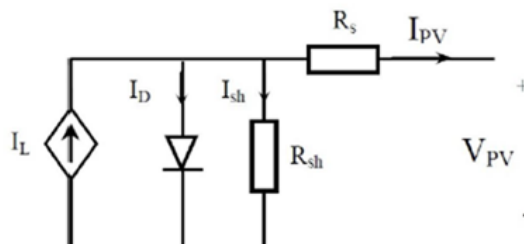

Figure 1. The equivalent PV cell circuit.

PV curves vary with solar insolation and the temperature of the module. Equations (1-5) are used in the description of the characteristics of the PV array.

$$I_{ph} = \left[I_{SCr} + K_i (T - 298) \right] \cdot \lambda / 1000 \tag{1}$$

$$I_{rs} = I_{SCr} / \left[\exp\left(\frac{qV_{OC}}{N_{skAT}} \right) - 1 \right] \tag{2}$$

$$I_o = I_{rs} \left[\frac{T}{T_r} \right]^3 \exp\left[\frac{q \cdot E_{go}}{Bk} \left\{ \frac{1}{T_r} - \frac{1}{T} \right\} \right] \tag{3}$$

$$I_{PV} = N_p \cdot I_{ph} - N_p \cdot I_O \left[\exp\left\{ \frac{q \cdot (V_{PV} + I_{PV} R_s)}{N_S AkT} \right\} - 1 \right] \tag{4}$$

$$P_{pv} = V_{pv} \times I_{pv} \tag{5}$$

Where: I_{ph}: The light generated current in a PV module (A), I_{SCr}: The PV module short-circuit current at 25 ^{o}C and 1000 W/m^2 = 3.6 A, K_i: The short-circuit current temperature co-efficient at I_{SCr} = 0.0017 A/^{o}C, T: The module operating temperature in Kelvin, λ: The PV module illumination (W/m^2) = 1000 W/m^2, I_{rs}: The PV Module reverse saturation current (A), q: Electron charge = 1.6 × 10-19 C, N_s: The number of cells connected in series, k: Boltzman constant = 1.3805 × 10-23 J/K, A = B: an ideality factor = 1.6, I_0: Module saturation current (A), T_r: the reference temperature = 298 K, E_{g0}: the band gap for silicon = 1.1 eV, I_{pv}: Output current of a PV module (A), V_{pv}: Output voltage of a PV module (V), R_s: The series resistance of a PV module, N_p: The number of cells connected in parallel and P_{PV} is the extracted PV power (W). [Azab 2010] [Pandiarajan & Muthu, 2011]

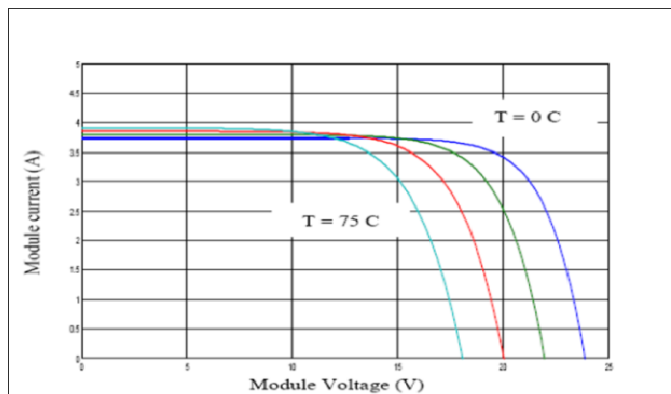## 2. Temperature effect on PV efficiency

Figure 2. Different temperatures with the PV module output I-V characteristics..

PV Solar cells efficiency vary under changes of temperature. The change in temperature will affect the output power of the PV cells and its efficiencies. The voltage is highly temperature-dependent and the temperature increase will reduce the voltage and vice versa. Figure 2 shows the effect of temperature on I-V characteristic of PV module at constant radiation with decreasing temperature, PV current decrease slightly but PV voltage increase clearly. As figure 3 indicates, output power of photovoltaic module increases with decreasing temperature. [Dhinesh *et al* 2020]
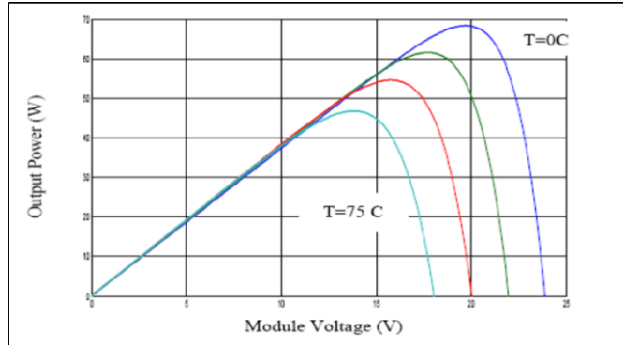

Figure 3. Different temperatures with the PV module output P-V characteristics..

2.1. Efficiency of the PV Module as a function of cell temperature

The solar cell power conversion efficiency can be given as show in equation (6). Where I_{max} and V_{max} are the current and voltage for maximum power, corresponding to solar intensity G and A_{Cell} is Area of solar cell. [Karthikeyan *et al* 2020] The correlations expressing the PV cell temperature (T_{Cell}) as a function of weather variables such as the ambient temperature (T_a), solar radiation G, etc., in this section, it will be discussed. The influence of temperature on the electrical efficiency of the PV cell/module can be achieved by applying basic equations. The effect essentially leads to a relationship in the equation (7): [Risdiyanto *et al* 2014]

$$\eta_{module} = \frac{I_{max} \times V_{max}}{G \times A_{module}} = \frac{Output\ Power\ (P_{max})}{Input\ Power\ (P_{in})} \qquad (6)$$

$$\eta_{module} = \eta_{T-ref} \left[1 - \beta_{ref} \left(T_{cell} - T_{ref} \right) + \gamma \log_{10} G \right] \qquad (7)$$

In which $\eta_{T\text{-}ref}$ is the electrical efficiency of the module at the reference temperature, T_{ref}, and at solar radiation of 1000W/m^2. The temperature coefficient, β_{ref}, and the solar radiation coefficient, γ, are mainly material properties, having values of about 0.0045K and 0.12, respectively for crystalline silicon modules. [Notton *et al*., 2005] The quantities η_{Tref} and β_{ref} are normally given by the PV manufacturer. However, they can be obtained from flash tests in which the

61

module's electrical output is measured at two different temperatures for a given solar radiation flux. [Hart and Raghuraman 1982] In particular, the actual value of the temperature coefficient depends not only on the PV material, but also on T_{ref}. The ratio is given as following equation (8):

$$\beta_{ref} = 1 \Big/ \left(T_o - T_{ref} \right) \tag{8}$$

In which T_0 is the (high) temperature at which the PV module's electrical efficiency drops to zero. For crystalline silicon solar cells this temperature is 270°C. [Farahani 2020] The steady-state power balance determines cell temperature: the input is the absorbed luminous power, which is partially converted into useful electrical output and the rest is dissipated into the surroundings. Convection is the main mechanism for heat dissipation in terrestrial, flat plate applications, and radiation is the second non-negligible mechanism of heat dissipation. A common simplification assumption is made that the drop in the cell-environment temperature increases linearly with irradiance. The coefficient depends on the installation of the module, wind speed, ambient humidity and so on, although a single value is used to characterize the type of module. This information is contained in the Nominal Operating Cell Temperature (NOCT) which is defined as the cell temperature measured under the open-circuit when the ambient temperature is 20 C, the irradiance is 0.8 kW/m2 and the wind speed is 1 m/s. T_{NOCT} is usually around 45 °C.

For variations in ambient temperature and irradiance, the cell temperature (in °C) can be estimated fairly precisely with a linear approximation as in equation (9). [Ali *et al* 2018]

$$T_{cell} = T_a + \left[\frac{T_{NOCT} - 20}{0.8 \, Kw/m^2} \right] \times G \tag{9}$$

If we substitute the equation (9) in the equation (7), we shall obtain the important equation (10):

$$\eta_{module} =$$
$$= \eta_{ref} \left[1 - \beta_{ref} \times \left[T_a - T_{ref} + \left(T_{NOCT} - 20 \right) \times \frac{G}{G_{NOCT}} \right] + \gamma \log_{10} G \right] \times 100 \tag{10}$$

Researchers usually consider T_{ref} =25°C, average η_{ref} = 12% and average βref = 0.0045K.

2.2. Simulation of PV module by MATLAB and the results
The PV solar module is simulated by using MATLAB. The final model is shown in Figure 4. The workspace is added to measure Ipv, Vpv, Ppv in this model.

The time tout is stored in the workspace with scope model can be used to plot graph. The simulated characteristic shows the change in output power as variation in temperature with certain irradiation. The output VI characteristic for 1000 W/m² solar irradiation and various temperatures (5, 25, 45 and 65 °C) with the same irradiation are shown in figures 5 and 6. The simulated characteristic shows the change in power as variable temperature with the same irradiation.
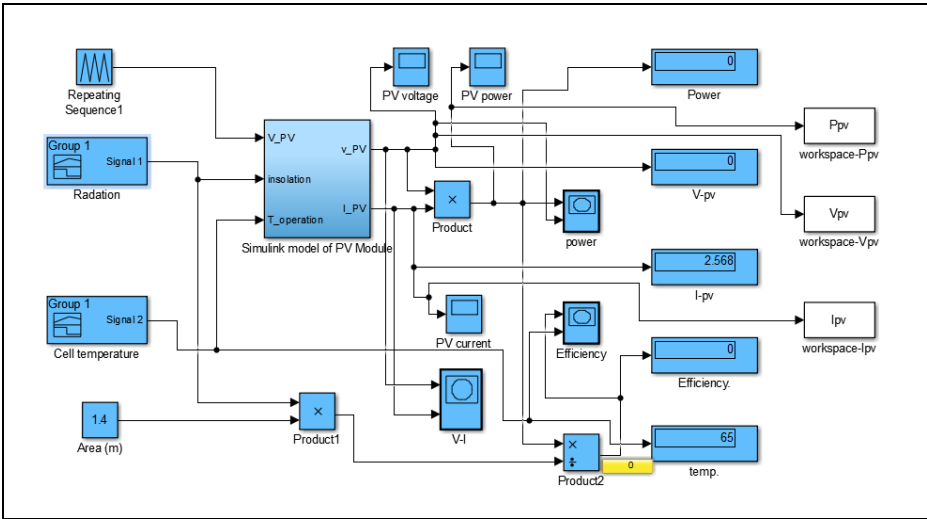
Figure 4. The final Simulink model of PV module.
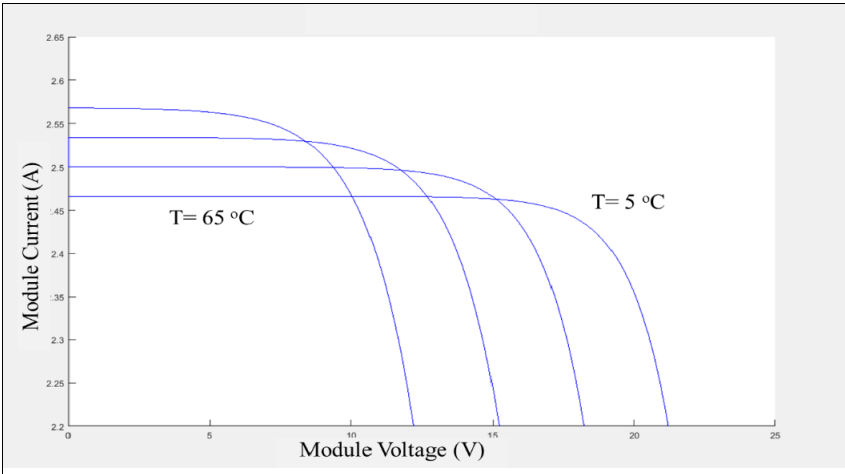
Figure 5. Output – P-V characteristics with varying temperature.

It is evident from this, that the output power decreases significantly when the temperature of the PV module increases and is inversely proportional to it, while

when the PV module temperature is at the reference temperature or less than that, we notice an increase in the value of the output power, and this means that keeping the temperature of the PV module at its proportional temperature, the design or close to it, the output power will be greater and consequently it will be energy saving in addition to reducing investment costs from it due to the absence of other systems as well as operational costs. From that, a higher amount of output power leads to a higher amount of module efficiency (see figure 7) and vice versa. variation of efficiency with temperature at solar radiation of $1000W/m^2$. There is a linear relation between ambition temperature and module efficiency. Decreasing temperature results more electrical efficiency. So for a desired efficiency of a photovoltaic module we can determine what temperature ambient of module is needed, so by changing temperature around PV module we can develop efficiency.

Figure 6. The P-V output characteristics of PV module with varying temperature at constant irradiation.

Figure 7. The efficiency variation with versus output power at different temperature.

Conclusion

In this paper the effects of temperature on the output power and efficiency of photovoltaic modules investigated and by using basic equation a relation between efficiency, sun radiation and temperature is evaluated by using Simulink/MATLAB. The effect of tempe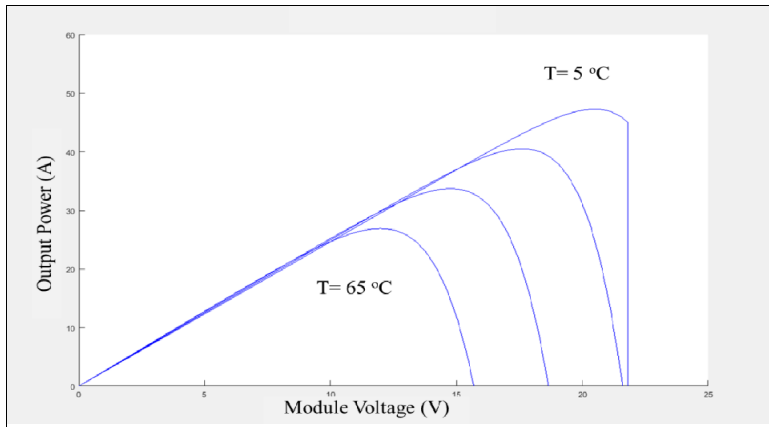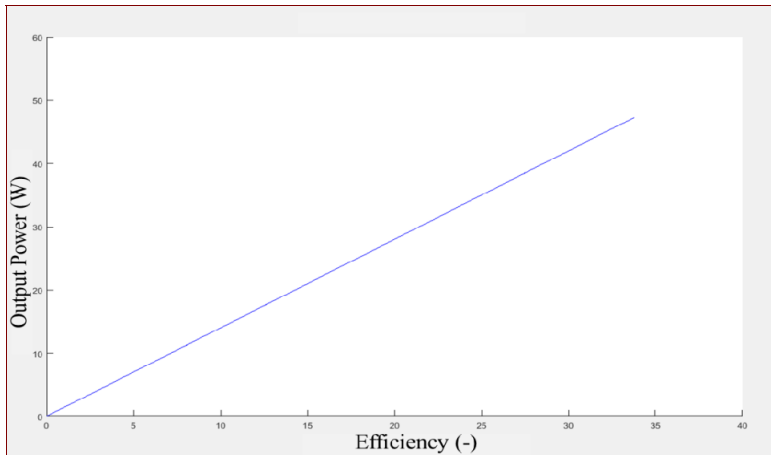rature on the output power of photovoltaic module in cold and hot climates indicated. The present work clearly indicates a decrease in the efficiency of the PV module with increase in temperature, that is due to decrease in PV module voltage greater than the increase of the PV module current all that lead to decrees in the output power and PV module efficiency. For a particular PV module we can find out for a desired efficiency what temperature ambient PV module is needed. So, Decreasing temperature results more efficiency. For a desired efficiency of a photovoltaic module we can determine what ambient temperature of module is needed, so by changing temperature around PV module we can develop efficiency.

References

[1] Ali, A. H., Hamad, H. S., & Abdulrazzaq, A. A. (2018). Performance investigation of grid connected photovoltaic system modelling based on MATLAB simulation. International Journal of Electrical and Computer Engineering, 8(6), 4847.

[2] Azab, M. (2010, July). Optimal power point tracking for stand-alone PV system using particle swarm optimization. In 2010 IEEE International Symposium on Industrial Electronics (pp. 969-973). IEEE.

[3] Dhinesh, V., Vijayakumar, D. G., & Saravanan, D. S. (2020). A Photovoltaic Modeling module with different Converters for Grid Operations. *International Journal of Innovative Research in Technology*, *6*(8), 89-95.

[4] Farahani, G. (2020). Effects of PV Modules Temperature Variations on the Characteristic of PV Array. In ICPES 2019 (pp. 15-30). Springer, Singapore.

[5] Hart. G.W and Raghuraman. P, (1982). Simulation of thermal aspects of residential photovoltaic systems, MIT Report, DOE/ET/20279-202.

[6] Ibrahim, H., & Anani, N. (2017). Variations of PV module parameters with irradiance and temperature. Energy Procedia, 134, 276-285.

[7] Karthikeyan, V., Sirisamphanwong, C., Sukchai, S., Sahoo, S. K., & Wongwuttanasatian, T. (2020). Reducing PV module temperature with radiation based PV module incorporating composite phase change material. Journal of Energy Storage, 29, 101346.

[8] Notton, G., Cristofari, C., Mattei, M., & Poggi, P. (2005). Modelling of a double-glass photovoltaic module using finite differences. Applied thermal engineering, 25(17-18), 2854-2877.

[9] Pandiarajan, N., & Muthu, R. (2011, January). Mathematical modeling of photovoltaic module with Simulink. In 2011 1st International Conference on Electrical Energy Systems (pp. 258-263). IEEE.

[10] Risdiyanto, A., Kristi, A. A., Susanto, B., Rachman, N. A., Junaedi, A., & Mukti, E. W. (2020, November). Implementation of Photovoltaic Water Spray Cooling System and Its Feasibility Analysis. In 2020 International Conference on Sustainable Energy Engineering and Application (ICSEEA) (pp. 88-93). IEEE.

Evaluation of particulate matter low-cost sensors: laboratory case study

Achraf QOR-EL-AINE[1], József BENÉCS[1], András BÉRES[2], Gábor GÉCZI[1]

[1]Department of Environmental and Building Engineering, Institute of Process Engineering
[2] Institute of Environmental Science
[1,2] Szent István University, Páter K. u. 1., Gödöllő, H-2100 Hungary

Abstract

One of the harmful air contaminants that can cause damage to humans and the environment is atmospheric aerosol or Particulate Matter (PM).

Due to their low cost and ability to provide high spatial and temporal resolution PM information, particulate matter low-cost sensors are becoming more commonly accessible and are being increasingly used in ambient and indoor environments. Under laboratory and environmental conditions, researchers have started to test some of these sensors. In this case study, two Particulate matter low-cost sensors were evaluated in a laboratory room, the first one is the BQ20 and the second is the IMRe PM2.5 sensor.

The results showed that the BQ20 is more stable and efficient than the IMRe PM2.5 sensor even though the BQ20 needs to be manually operated and the IMRe is autonomously operated. And the results given by the IMRe could be improved by a calibration of the digital system of the sensor.

Keywords

PM2.5, Indoor air pollution, Particulate Matter low-cost sensors

1. Introduction

Since the industrial revolution, the atmospheric concentration of many substances has increased dramatically because of the massive emission. Thus, it led to the air pollution problem that causes many environmental effects, and human diseases and mortalities. According to the World Health Organization (WHO) 8 million people die every year due to air pollution where nearly 4 million people die prematurely from disease due to indoor air pollution from improper cooking methods using polluting stoves combined with solid fuels and kerosene, and around 91% of the people in the world live in areas where the air quality limits suggested by the WHO are not respected (WHO 2020).

Particulate Matter (PM) is a dangerous substance especially to the human body, it is a complex combination of tiny particles of solid and liquid substances and consists of numerous components such as nitrates, sulfates, organic chemicals, metals, soil, or dust particles (Querol et al. 2013).

Particulate matter (PM) has different sizes, depending on the aerodynamic diameter of the particle. Two main sizes are measured and have crucial limits values in all the air quality standards. First is the PM10 which are particles that have a diameter of 10μm, and are respirable and capable of reaching the upper section of the lung (Querol et al. 2013). Second is the PM2.5, particles with a diameter of 2.5 μm, respirable and can cross the lung barriers and penetrate to the blood system which increases the probability of developing lung and heart diseases, cancer and exposure to a high concentration of PM2.5 can lead to premature death (VALAVANIDIS et al. 2008).

There exist numerous methods that can be used for the measurement of PM2.5 concentration. One of these methods is using Low-cost sensors. As the name indicates the Low-cost sensors are cheap and offer the possibility of gathering massive amounts of high-resolution, air quality data, however, the performance of these sensors need to be evaluated (Kelly et al. 2017), and many case studies were performed to investigate the performance of the Low-costs PM sensors (Austin et al. 2015; Wang et al. 2015).

This paper deals with the changing of the indoor concentration of the PM2.5 pollutant, by investigating the efficiency and the sensitivity of low-cost sensors used during the experiment, and the changing of the PM2.5 concentration with the different conditions applied in each case of the experiment.

2. Materials and methods

In this case study, five experiments were performed in the Building Service and Environmental Engineering Laboratory of Szent Istvan University.

The pieces of equipment used are the following:
- Agricultural diesel engine as a source of pollution
- BQ20 device
- Imre-PM2.5 Sensor

Figure 1. Agricultural diesel engine

Agricultural diesel engine

The engine is used in Agricultural areas to provide electricity for necessary machines that need to be used. The power of the engine is 3.85kw and provides two plugs of AC ˜230V.

BQ20 device

BQ20 (Figure 2) is a mini particle measuring device developed by the Trotec group, it is an Optical particle measuring device for the quantitative determination of the concentration of dust. The BQ20 simultaneously captures quantitative amounts of respirable dust particles (PM10 and PM2.5) with a direct display of the particle masses concentration. The mix of detectable environmental parameters specific to this class of equipment commends the BQ20 as an important help for rapid air quality monitoring at the office, in public facilities, or at home.

Figure 2. BQ20 device   *Figure 6.* Imre-PM2.5 Sensor
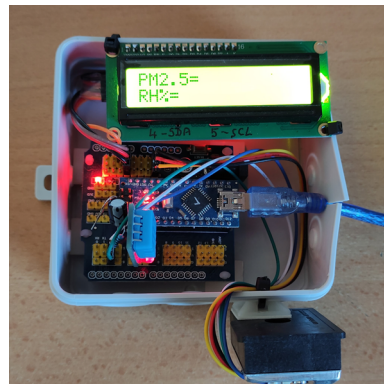
IMRe-PM2.5 Sensor

IMRe (Intelligent Measuring System, in hungarian **I**ntelligens **M**érő **Re**ndszer) (Figure 3) includes a digital signal measurement processor and is associated with a low-cost PM2.5 sensor.

The experiment was carried in one of the rooms in the laboratory (Figure 4), where 3 cases were examined.

The 1st case is without using the ventilation system that exists in the room as shown in Figure 4, and measure the effectiveness of the agricultural diesel engine on the PM2.5 level in the room by turning on the engine for one minute. The 2nd case, the same scenario as the 1st case with the addition of the bottom output of the ventilation system on. The 3rd case is also the same scenario as the 1st case with the top output of the ventilation system on as sketched in Figure 5.

The sensors were placed on a table 5.5m away from the engine, under the top output of the ventilation system, and 6m away from the bottom output of the

ventilation system. Also, the engine was placed near the bottom output of the ventilation system. The purpose was to examine and to analyze the changing of the PM2.5 concentration in the room with the different conditions and sensors.

Figure 7. Hosting room of the experiment
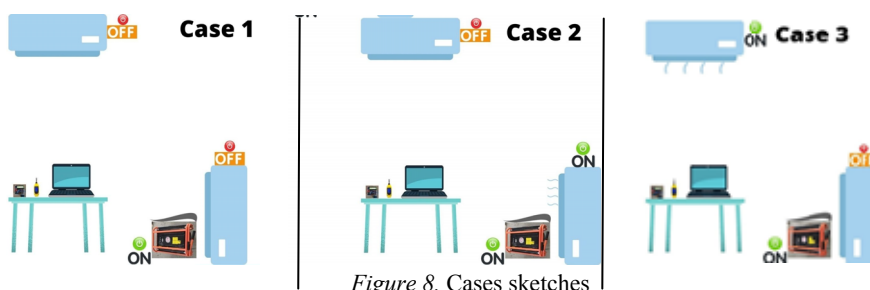
Figure 8. Cases sketches

Results

The results for the two sensors in the three cases had the same diagram shape with a difference in numbers. In the 1st case (Figure 6) where there is no ventilation, IMRe sensor always gives numbers higher than the BQ20. When the Engine was on for 1 minute the concentration of the PM2.5 rise instantaneously and took more than 60 minutes to back to a normal concentration that was before the starting of the engine, while the IMRe continue to register a higher concentration than the BQ20.

For the 2nd case (Figure 7) with bottom ventilation on, the IMRe still register a bigger concentration than the BQ20, as soon as the engine was on the concentration of the PM2.5 rise instantaneously but at a lower level than the 1st case, but decreases faster than the 1st case to stabilize at a certain level.
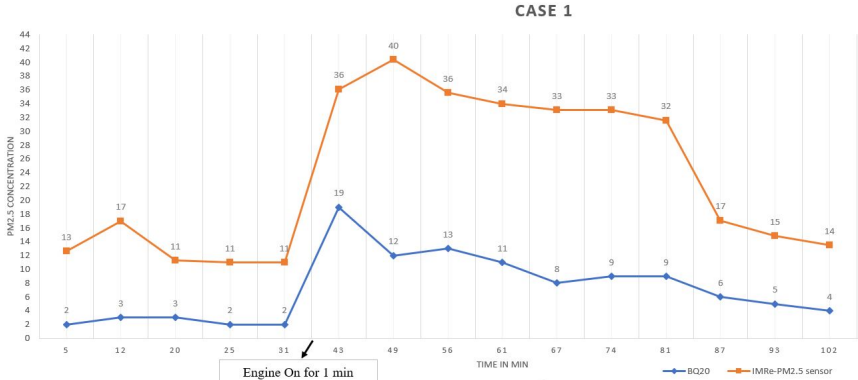
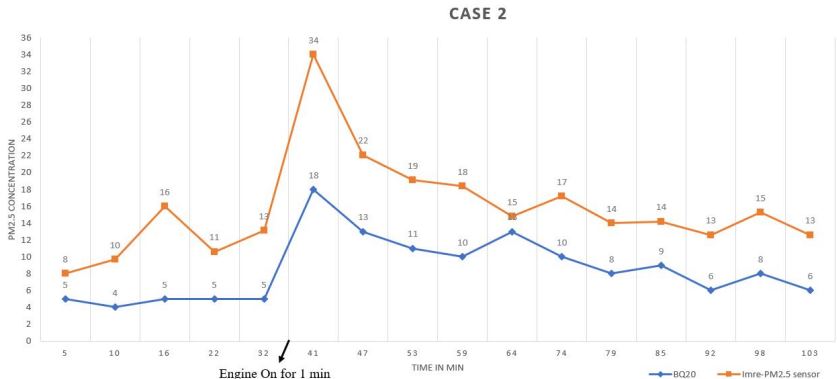*Figure 6.* Sensors measurements in Case 1

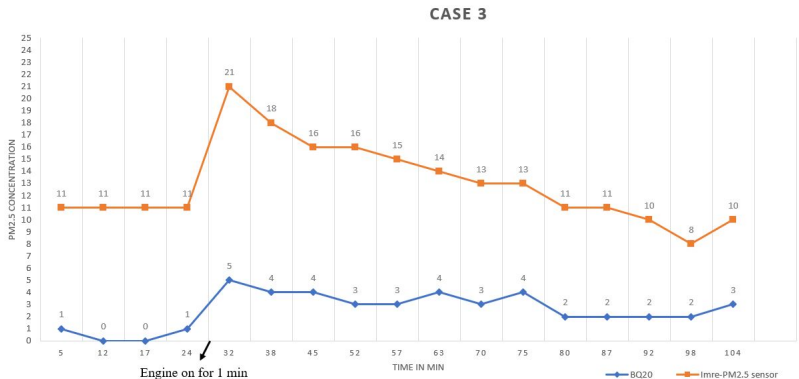*Figure 7.* Sensors measurements in Case 2

Figure 8. Sensors measurements in Case 3

In the 3rd case (Figure 8) with top ventilation on, the IMRe continue to register higher concentration than the BQ20, and when the engine was on it was seen that

the concentration of PM2.5 increased, but it was back to almost the same level as before the engine was on faster than the 1st and 2nd case.

Conclusion

The Particulate Matter low-cost sensors represent a good solution for the monitoring of the Indoor and Outdoor effects of the PM. However, they need to be evaluated to validate the measurements given by those sensors.

In this paper two Particulate Matter low-cost that measure the PM2.5 were evaluated in a laboratory room. The results showed that the IMRe sensor always registers higher concentrations than the BQ20 and it is clear that the number given by the IMRe sensor is not stable and still needs to be calibrated but based on a proven and validated method of the measurement of the PM2.5. Besides, The BQ20 proved to be stable in the measurements, but it can't be automated since it needs human intervention and it is a manually operated device and has a limited memory to register the taken measurements.

References

[1] Austin, E. et al. 2015. Laboratory Evaluation of the Shinyei PPD42NS Low-Cost Particulate Matter Sensor. *PLOS ONE* 10(9), p. e0137789. doi: 10.1371/journal.pone.0137789.

[2] Kelly, K.E. et al. 2017. Ambient and laboratory evaluation of a low-cost particulate matter sensor. *Environmental Pollution* 221, pp. 491–500. doi: 10.1016/j.envpol.2016.12.039.

[3] Querol, X. et al. 2013. *Particulate Matter: Environmental Monitoring and Mitigation*. London: Future Science Group.

[4] VALAVANIDIS, A. et al. 2008. Airborne Particulate Matter and Human Health: Toxicological Assessment and Importance of Size and Composition of Particles for Oxidative Damage and Carcinogenic Mechanisms. *Journal of Environmental Science and Health, Part C* 26(4), 339–362. doi:10.1080/10590500802494538.

[5] Wang, Y. et al. 2015. Laboratory Evaluation and Calibration of Three Low-Cost Particle Sensors for Particulate Matter Measurement. *Aerosol Science and Technology* 49(11), pp. 1063–1077.
doi: 10.1080/02786826.2015.1100710.

[6] WHO 2020. Air pollution. Available at:
https://www.who.int/westernpacific/health-topics/air-pollution.

The use of solar thermal systems in piglet nurseries

Viktor ERDÉLYI, János BUZÁS, László FÖLDI

Department of Mechatronics, Institute for Mechanical Engineering Technology,
Faculty of Mechanical Engineering, Szent István University

Abstract

In this paper the current status of an ongoing research is shown. A previous research is focused on the establishment of a mathematical model of solar thermal system, in which we created the model of a solar collector, heat storage and a displacement pump. Now I search for suitable methods to use this model, and small-scale system to achieve precise surface temperature control of a piglet heater. The main aim of this paper to show the possible directions for research and the measurement and model creating procedure to set up a black box model of a centrifugal pump, which will be used in the user circuit.

Keywords

model, black-box, centrifugal pump

1. Introduction

The number of researchers exploring the possibilities of using renewable energy sources has increased significantly in recent decades, due to the growing demand for energy, the finite amount of fossil fuels and the environmentally conscious way of thinking. Environmentally conscious thinking can be observed more and more in agriculture as well, so the use of solar energy is also more and more typical in the case of livestock farms. In the case of pig farms, this is often used to supplement existing fossil fuel-based or electric heating systems with varying efficiencies.
According to literature sources, solar energy is now increasingly used for heating purposes in both industry and agriculture (Xie et al., 2019).

In my experience, solar thermal floor heating systems used in pig farms are often unable to maintain the expected temperatures because they are systems with a large time constant (Kull et al., 2019) and have a lot of parameters (Lu et al., 2020). Therefore, farmers are choosing more expensive to use electric underfloor heating instead of systems that use the sun's energy directly.

Both the Hungarian and international literature discusses the sub-field of control technology, which aims at the optimal utilization of renewable resources and solar systems in detail. Nowadays, this is an cutting edge and evolving research sector. A little researched area, however, is the thermal utilization of solar energy in temperature-sensitive areas such as the contact heating pads in piglet nurseries,

where piglet comfort is the highest priority to avoid stress (Johnson et al., 2018), which adversely affects animal development.

2. Aims

The aim of the research is to investigate control algorithms that can provide adequate temperature control for systems with large time constants, as well as to further develop methods in this field and to determine the limits of applicability. My goal is to build a small scale model of a solar thermal energy utilization device with the possibility to test:

- different control algorithms (On-Off, PID, model-based, adaptive model-based, artificial neural network)
- various actuators (pump, throttle)

I validate the small sample model on the experimental laboratory of the Department of Physics and Process Control of the Institute of Mechanical Engineering Technology.

3. Methods

Construction of a small-scale model of an agricultural solar energy utilization system.

Mathematical modelling and creation of the consumer-side parts of agricultural solar energy utilization systems after the heat storage tank in a simulation environment, validation of the models on a small scale model. Checking the small scale model on a real system. Comparison based on the quality characteristics of different control algorithms on the validated model.

Control algorithms to be compared: On-Off, PID, model-based, adaptive model-based, artificial neural network. Based on the results of the most appropriate controlling method, teaching of an artificial intelligence, applying it to a small scale model.

Using the small scale model, I validate simulation models that allow rapid comparison of multiple control algorithms.

To achieve this, I use the following methods:

- development of models suitable for describing the time-varying heat and mass flow processes of the consumer-side equipment of a solar energy system (heating elements used in pig farms and the related equipment),
- development of a computer controlled data acquisition and monitoring system which is suitable for the energetic measurement of solar thermal energy utilization systems; and putting them into practice on a microcomputer,
- development and comparison of control algorithms,
- evaluation of different control strategies based on a validated model.

During the elaboration of the task, by examining the quality indicators of the control circuits of the floor heating systems used in pig farming, I plan to achieve a control method that serves the maximum comfort of the animals. The objective

function used to set the control system also considers the settling time, the overshoot, the number of possible oscillations and the degree of stabilized error, as well as the energy demand of the control.

Another important goal is that the knowledge gained in this way can be generalized to larger, robust systems, where dead time compensation is especially important. I consider complex, model-based control procedures and the application of artificial intelligence for the development of such systems to be suitable.

Two different type of system architecture will be tested. These are the central control method, where the user side pump's power is controlled to perform a variable volumetric flow rate, and thus controlling the circuit overall heat transfer, with the use of temperature sensors on all the heating pads. The heating pads individual flow rate cannot be modified by the control system itself, but we must set the throttle valves on each beforehand, to achieve a uniform flow rate on them.

The block diagram of the central control setup is on Figure 1. to be seen.

Figure 1. Block diagram of the central control method

Figure 2. Block diagram of the decentralized control method

Another type which I consider examining is the decentralised method, in which the pump is controlled to maintain a static pressure difference between the suction and

pressure lines, and the throttle valves on each of the heating elements are also controlled to alter the flow rate in order to maintain a static temperature on the surface.

The block diagram of the decentralized control setup is on Figure 2 to be seen.

Since the model of the collector and heat storage unit is already constructed and validated by Tóth et al. (2019). The next step is to measure the working parameters of the used centrifugal pump in the user circuit and build an input-output model based upon the measured data.

The block diagram of the experimental setup is on Figure 3. to be seen.
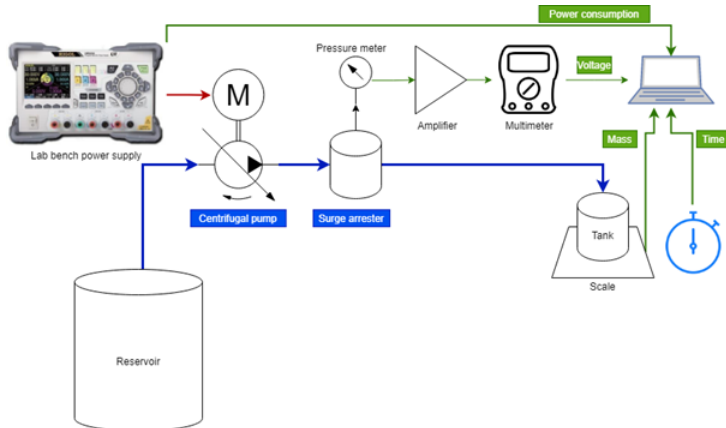
Figure 3. Block diagram of the experimental setup
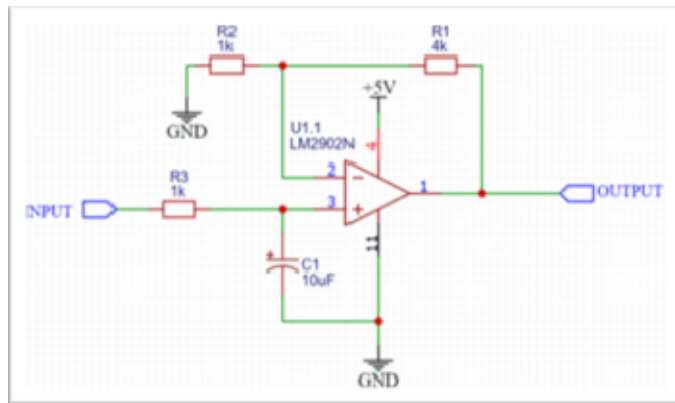
Figure 4. Schematics of the non-inverting amplifier in conjunction of the low pass filter

The pump is sucking water from a reservoir below it, and pumps through a pipeline to a container. The pressure side's pressure is measured by a My1220 type pressure sensor with a measurement range of 0-10 bar and an output voltage range of 0.5-4.5 V. The measurement was done with a Maxwell MX-25 328 USB

enabled multimeter with a precision of 1 mV. To be able to measure low pressures a non-inverting operational amplifier setup in conjunction with a low pass filter with a cutting frequency of 15.9 Hz was utilized. The amplifying factor of the circuit was a factor of 5. Further smoothing was achieved by a pressure surge arrester connected to the pressure line.

The schematics of the amplifier and signal conditioning setup is on Figure 4. to be seen.

The mass flow rate was measured with a precision scale underneath of the container. The change of the mass reading was registered in conjunction with the elapsed time. Knowing the density of water, the volumetric flow rate was calculated. The power consumption of the driving motor of the pump was also logged with the help of a RIGOL DP832 lab bench power supply. The output power of the pump was calculated based on the volumetric flow rate and pressure data. The flow cross section was gradually opened, and the data was collected. The calculated and normalized data is shown in Table1.

Table 1. Measured data

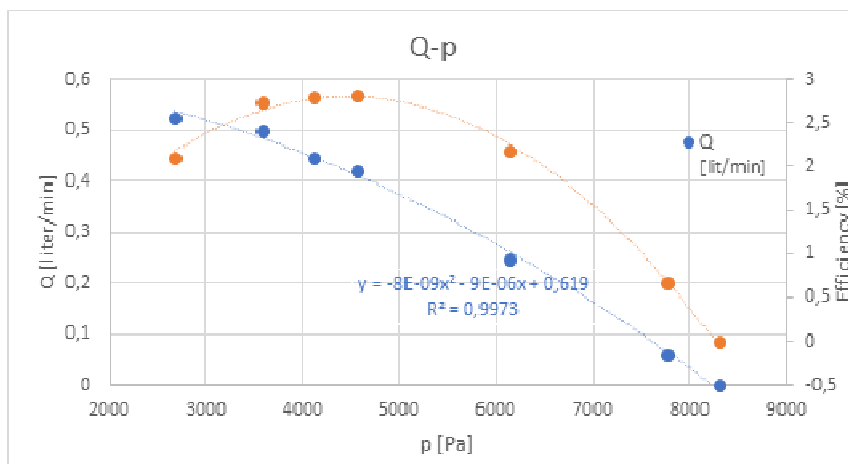|	pressure [Pa]	Q [lit/min]	Pmotor [W]	Pfluid [W]	efficiency [%]
1. stage	8300	0	1,178	0	0
2. stage	7770	0,0597	1,169	0,007731	0,66
3. stage	6136,36	0,25	1,161	0,02522	2,17
4. stage	4566,67	0,420599	1,138	0,032012	2,81
5. stage	4118,75	0,446999	1,131	0,031662	2,8
6. stage	3573,33	0,497999	1,125	0,030685	2,73
7. stage	2675	0,526199	1,119	0,02346	2,1

Figure 5. Diagrams of measured and calculated data in conjunction of the quadratic polynomial trendline of the Q-P characteristic curve of the pump

The quadratic polynomial describes the characteristic curve of the pump satisfactorily since the quadratic regression is 0.9973. This polynomial can be used in simulation software such as MATLAB Simulink to describe the behaviour of the pump. It is important however to note, that the efficiency of the pump is suspiciously low, although the nature of measured data seems to be correct. Therefore, it is necessary to conduct this experiment again with the suction side in level with the pump, and ultimately with the suction side pressure measured as well. In the future more power steps will be also tested, and a 3D lookup table and thus a 3D map will be created.

4. Further expected results

The research will go on to achieve the followings:
- Setting up a more adequate black box model to the pump used in the user circuit, and the comparison of the black box model of a large-scale system pump.
- Designing and modelling of a servo driven throttle valve.
- Comparison of central and local control systems based on quality characteristics and entry and operating costs, where:
  - Central: pump volume flow control,
  - Local: pump differential pressure control, individual volume flow control of heating units with servo driven throttle valves.
- Supporting the selection of an appropriate control algorithm for the control of systems with large time constant.
- Setting up an adaptive model-based controller (measuring the model parameters and taking them into account to minimize the effects of the variable parameters).
- Comparison of HIL (Hardware-In-the-Loop) implementation on a native embedded system with HIL running in a Simulink environment.
- Teaching an artificial neural network based on the developed, validated model to achieve a lower computational demand.

References

[1] Johnson, J.S., Aardsma, M.A., Duttlinger, A.W., & Kpodo, K. R. (2018). Early life thermal stress: impact on future thermotolerance, stress response, behavior, and intestinal morphology in piglets exposed to a heat stress challenge during simulated transport. Journal of Animal Science, 96(5), pp. 1640-1653.
[2] Kull, T. M., Thalfeldt, M., & Kurnitski, J. (2019, november). Estimating time constants for underfloor heating control. In Journal of Physics: Conference Series, Vol. 1343, No. 1, p. 012121. IOP Publishing.
[3] Lu, S., Gao, J., Tong, H., Yin, S., Tang, X., & Jiang, X. (2020). Model establishment and operation optimization of the casing PCM radiant floor heating system. Energy, 193, p. 116814.

[4] Tóth J., Erdélyi V., Jánosi L., Farkas I. (2019). Termikus napenergia-hasznosító rendszer kismintamodelljének identifikációja Magyar Energetika 26: 4 pp. 18-23.

[5] Xie, Q., Ni, J.Q., Bao, J., & Su, Z. (2019). A thermal environmental model for indoor air temperature prediction and energy consumption in pig building. Building and Environment, 161, p. 106238.

Potential of solar energy utilization in Iraq

Maytham H. MACHI[1,3], János BUZÁS[2], István FARKAS[2]

[1]Doctoral School of Mechanical Engineering,

[2]Department of Physics and Process Control, Institute for Mechanical Engineering Technology,

Faculty of Mechanican Engineering, Szent István University, Páter K. u. 1.,

Gödöllő, H-2100 Hungary

[3]Department of Mechanical Engineering, Faculty of Engineering,

University of Kufa, Najaf, Iraq

Abstract

The global energy demand is continuously increasing in connection with population growth and industrial expansion, considering environmental protection, forcing the world community to seek alternative energy sources. This work aims to focus on the importance of solar energy in Iraq as a possibility to solve the shortages of electrical power supply that the people are suffering from for decades. Moreover, it discusses the opportunities and challenges facing the growth of this technology and the benefits of its implementation on the economics of Iraq.

Keywords

1. Introduction

The energy demand is increasing continuously as the population of the world and industrial production increases. Green energy is mainly overgrowing to meets these demands. The environmental concerns pushed the international community to take serious steps towards controlling the pollutants, especially greenhouse gas emissions. Although the energy of fossil fuels will remain available at least in the next future and not disappear soon, the age of abundant, inexpensive energy will not be lasting. For that, searching for alternative energy sources, mostly renewable energy linked to environmental issues, have become crucial (Boukelia and Mecibah, 2013).

The renewable energy sources can produce energy over and over, such as solar, geothermal, biomass, and wind energy, and the new technologies that build on them are considered clean, as it produces about zero emissions of air pollutants and greenhouse gases through optimal use. It will provide an excellent opportunity for facing climate change, which is the problem of the 21st century, by reducing global warming through cutting down the use of fossil fuels as energy sources (Panwar et al., 2011). The utilizing of renewable energy sources will impact solving the problems of supplying energy and water locally and providing a high

employment level for the residence people. Moreover, ensuring sustainable growth of the outlying regions in the mountain and desert zones and reducing migration from rural to urban areas by creating job opportunities (Zakhidov, 2008).

Among the various renewable energy resources, solar energy is more available and accessible in the Middle East region, especially in Iraq (Al-Hamadani, 2020). Solar energy is superabundant, clean, and free, without noise and any harmful pollutants for the environment. The global shortage of energy and the concerns about the environmental impacts should draw attention to adopt the solar energy application as a part of the solution by supporting an intense search for efficient and economical methods to harvest and transform solar energy into usable energy (Mekhilef et al., 2020).

Solar energy can be utilized using two categories of application: solar thermal application, which converts solar radiation into useful heat, and the photovoltaic cell that transforms the solar energy directly to electrical energy. This work presents the possibility of utilizing solar energy technologies to support the power generation in Iraq as it is suffering from the shortage for three decades.

2. Overview on Iraq geography and energy status

Iraq lies in southwest Asia in latitudes 29° 5' and 37° 22' N and longitudes 38° 45' and 48°45' E, with a total area of 438320 km^2. The northern side is bordered by the Republic of Turkey and the Islamic Republic of Iran on the east. The Arabian sea, Saudi Arabia, and Kuwait on the southern border, while Jordan and the Syrian Arab Republic to the west. The north zone consists of mountains, representing the coldest part of Iraq, the middle and the south region almost plain land with clear weather, which makes it one of the maximum solar radiation regions. The Tigris, the Euphrates and some small rivers are flowing through these lands (Abed et al., 2014).

The population of Iraq was 14 million in 1983, increased to 32 million in 2010, and it is expected to be about 64 million in 2050. The growth rate was 2.75% between 1980-1985 and 3.23% between 1995-2000 while it decreased to 2.72% in 2000-2005 and it is expected to reach 1.09% in 2045-2050 (Kazem and Chaichan, 2012).

Iraq is one of the first states that established the Organization of Petroleum Exporting Countries (OPEC), the world's leading oil suppliers. Oil is considered the primary raw material to the Iraqi economy, and the proven crude oil reserves are estimated to be 145.02 Billion barrels based on the OPEC annual statistics, which make him the fifth-largest oil certified reserve (Macneill et al., 2019). The second important raw material to Iraq's economy is natural gas, which unfortunately burned directly during the extraction of the oil. The fixed Iraqi reserve is about 3.6 trillion cubic meters, and this portion puts Iraq in a good position among the countries rich with natural gas. Many other raw materials, such as phosphate, sulfur, and white clay, have less importance to and share the Iraqi economy (BP, 2019).

Although Iraq has a wealth of crude oil and natural gas, it still struggles from the shortage of energy in general and electrical energy. The country passed

through three wars from 1980 till 2003 with international sanctions, which destroyed the country's infrastructure and economy (IEA, 2012). Iraq is buying the fuel necessary to operate gas turbine in the power plant as well as the diesel and petrol fuel due to lack of oil refinery industrials, while its flares off more than 1600 million standard cubic feet per day as useless byproducts of oil extraction, losing billions of dollars of gas (Luay Al-Khatteeb and Harry Istepanian, 2015).

The energy shortage remains one of Iraq's most significant challenges, as the annual electrical consumption growing by average compound growth of 6 to 7 percent since 2003. The peak demand always remains under an exact estimation, but the presumed numbers ranged between 25000 to 30000 MW in summer 2018, while the total generation capacity was around 15000 MW as shown in Fig. 1. The installed generation capacity consists of 478 units spread over the country, with capacity ranging from 1.7 to 300 MW per unit(Istepanian, 2018). The fuel used to operate these units mainly depend on fossil, which forms more than 86.3% of generated electricity, as shown in Fig. 2(Istepanian, 2014). These continuous shortages in fossil fuel and the vast environmental impact struck the bell to search for an alternative energy source with high availability, lower cost, and clean.
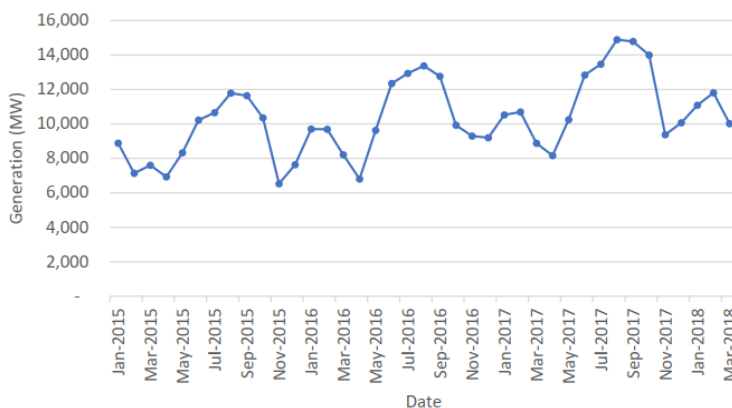

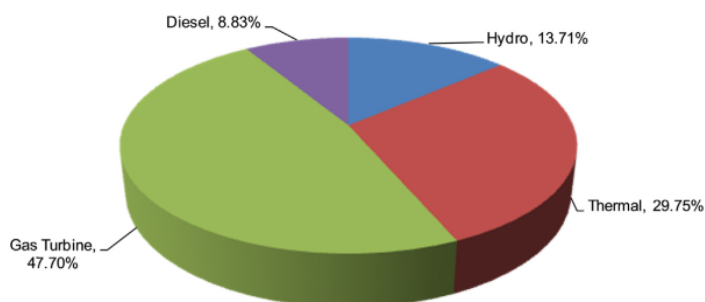*Figure 1.* Iraq's electricity generation (January 2015 – March 2018) (Istepanian, 2018)

Figure 2. Iraq electricity generation profile (Istepanian, 2014)

3. Solar energy in Iraq

Iraq has an excellent possibility of utilizing solar energy because of its high sunbelt location with infinite solar energy potential and numerous sunlight hours. It can be used widely in the southern and western regions, representing two-thirds of Iraq, as the solar radiation duration around 3000 hours/year with a global horizontal irradiation between 5.5 to 6 kWh/m^2 per day as seen in Fig. 3 (Istepanian, 2018).
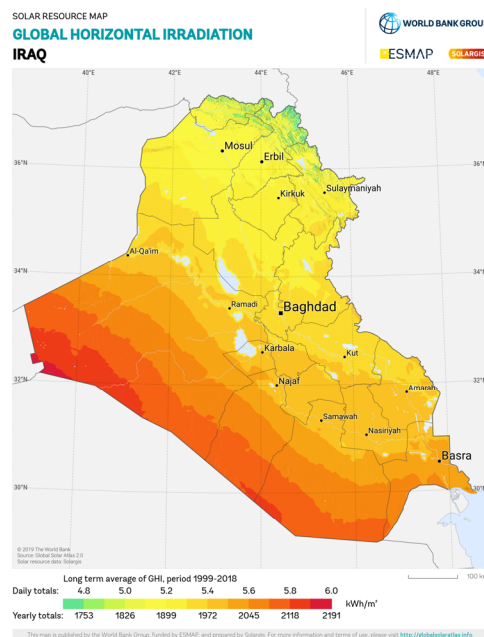

Figure 3. Iraq solar annual horizontal irradiation map

Iraq's climate is described as very hot and generally dry, with plenty of sunshine days. It is mostly desert-like hot, shines in summers, and mild to cold dry in winters. The temperature reaches its maximum during June, July, and August between 43 ℃ to 50 ℃. Moreover, in winter, January's average temperature ranged between 1 ℃ in the southwest desert and the north eastern foothills to 8 ℃ in central part of the country near rivers. Even in Basra south of Iraq, it may reach -4.5 ℃ because of the sea cold water. Also, dust storms are natural and frequent phenomena during the year, especially in June and July, and may last for several days (Kazem et al., 2014).

Many researches have estimated the solar radiation intensity in Iraq. (Akram Al-Khazzar, 2018) conducted experiments to find an average global solar radiation. The measurements conducted in 8 locations were found arbitrarily, which had over one data set in previous literature. The results compared with the data available NASA and Meteonorm sources. The results showed that the

maximum global radiation value was 8.3 kWhr/m^2 in Haditha in July, and the minimum was 1.68 kWhr/m^2 in December in Mosul city. They stated that the satellite data were not reliable and might not be suitable for design consideration.

Based on what researchers have proven the abundance of solar radiation in Iraq through many measurements, it has become crucial to give this topic great importance. The solar energy application can solve the problem of the current shortage of energy, especially in the rural area. Moreover, it has a significant impact on the national economy by reducing fuel costs, providing job opportunities, and reducing environmental problems. Furthermore, that becomes a part of the country's responsibilities towards international agreements to reduce the environmental load, where Iraq was recently signed.

3.1 Solar PV systems

Solar energy can be utilized directly by converting solar radiation into electricity by using photovoltaic cells. The first solar cells in the Middle East were used in Iraq as a rooftop in Baghdad's solar energy research centre in 1986. Iraq set an optimistic plan in 1980 for generating electricity by using solar energy, but the wars that involved and the global sanctions destroy the plan. Moreover, in 2009, the ministry of electricity announced a strategy to install 400 MW of solar and wind power plants by 2016, but the downfall of oil prices and the war against ISIS frustrated this plan. The interest in solar energy returned in November 2017 when the government announced its desire to involve in a public-private partnership project to build about 700 MW of power stations (Table 1) by the end of 2018 (Istepanian, 2018).

Green energy sources are assumed to reach 80% of the electricity demand global growth during the next decade, and it will pass coal by 2025 as the primary source of producing electricity. Moreover, these sources will provide 40% of the electricity supply by 2030. The solar PV has become the new master of electricity supply and will have a massive expansion shortly. Its expected growth rate between 2020 to 2030 by 13% per year represents one-third of electricity demand growth. Furthermore, as the cost reduction during the past decade, solar PV is cheaper than new coal or gas power plants in most countries, and it offers some of the lower electricity prices have ever seen (IEA, 2020).

The electricity cost from Solar PV and CSP (Concentrating solar power) had been reduced by 82% from 2010 to 2019 due to the module's price reduction by 90% and the overall system cost. This lead to a total reduction of PV installation cost by four-fifths over the past decade (see Fig. 4) (IRENA, 2020).

For that, the authorities in Iraq should take a serious step towards adopting these technologies widely by finishing the renewable energy law legislation that contributes a clear vision for the country's energy future. Moreover, reducing bureaucratic procedures to obtain permission to use renewable energy for commercial or domestic purposes, which helps to attract local and foreign investment. Also, encouraging people to use solar panels for household uses by provides easy and long-term loans, increasing awareness of these sources' importance and its impact on improving their economic, environmental, and health conditions.

Table 1. Iraq renewable plan for 2017

Province	Project	Capacity (MW)
Muthana	*Sawa-1*	30
Muthana	*Sawa-2*	50
Muthana	*Khadher*	50
Najaf	*Haydariyah*	100
Anbar	*Remadi*	100
Anbar	*Falluja*	40
Anbar	*Amireya Sumud*	50
Anbar	*Qarma*	50
Babel	*Iskandariya*	225
TOTAL		**695**
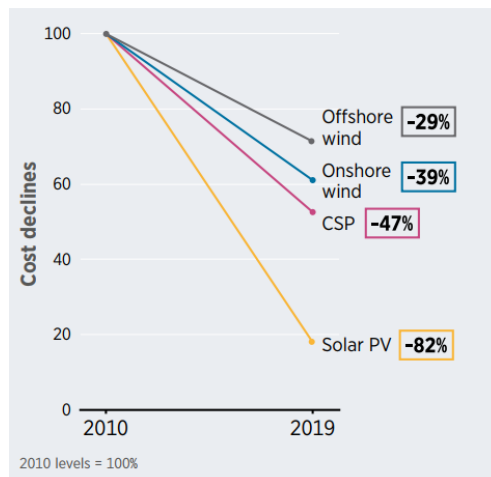
Figure 4. Renewable power technologies cost decreases

Another essential aspect that must be paid attention to is the transformation from conventional to renewable energy sources helps increasing oil revenues by reducing fossil fuels' internal use and decreasing the amounts of imported gas necessary for the operation of power plant leads to increase general economy.

3.2 Solar thermal systems

There are several technologies to collect solar energy and convert it to thermal energy. The simplest one is to use the solar collector to convert the solar irradiation to useful heat, which is transferred through a medium (water, air, oil) used for heating, cooling, drying purposes. The interest of these technologies appeared recently for home use due to the shortage of electricity supply. It would reduce electricity consumption, especially during the day, and reduce electricity bills for citizens.

The upper level is to use concentrated solar power (CSP) plant for producing electricity. Due to the abundance of solar radiation and high weather temperatures, it is expected that this technology will be suitable and encouraging for use in Iraq.

Another interesting technology can be utilized also is solar updraft tower power plant. It is heating the air through a large collector with a chimney in the middle using only solar energy. It operates based on the greenhouse effect principle, updraft effect of the tower, and wind turbines. The air is heated by solar radiation under glass or a transparent roof opened from the sides near the chimney's bottom, where the roof and the ground under it work as the solar collector. The hot air moved from the outside of the solar collector towards its centre, escaping to the atmosphere's upper layers through the solar chimney. The moving air will drive the air turbines, which drove electric generators. One of the advantages of this technology is that it utilizes solar radiation, whether direct or diffuse. Moreover, it does not need water for cooling, unlike some other solar thermal stations, making it suitable for desert climates far from water sources. Furthermore, an important feature is the low maintenance rate, which is limited to wind turbines and generators, as they represent the only moving parts subject to a fixed airflow (Chaichan and Kazem, 2011).

Special attention must pay during the design process of PV and CSP technologies for weather condition in Iraq. As the efficiency my affected by air temperature and dust contamination, which is one of the climate elements.

Conclusion

This study aims to highlight the possibilities of using solar energy in Iraq in various applications, and for that, we would like to draw the following points.

- Solar energy is widely available in all parts of the country, especially in the southern and western regions. The solar radiation duration around 3000 hours/year with global horizontal irradiation around (5.5 to 6 kWh/m^2) representing an excellent opportunity for using solar applications.
- The government's responsible authorities must start completing the legislation of a renewable energy law, which regulates utilizing renewable energy and establishing directions for selling excess energy to the national electrical network. Moreover, providing some facilities such as easy bank loans to encourage people to use solar energy, also offering tax exemptions for importing the devices used in solar systems.
- The use of renewable energy in the agricultural and desert areas has a significant impact on the reclamation of agricultural lands and the establishment of agricultural areas.
- Attention must be paid for weather condition of Iraq during the large-scale power plant design phase especially for the dust contamination.

Acknowledgments

References

[1] Abed, F.M., Al-Douri, Y., Al-Shahery, G.M.Y. (2014): Review on the energy and renewable energy status in Iraq: The outlooks, Renewable and Sustainable Energy Reviews, Vol. 39, pp. 816–827. https://doi.org/10.1016/j.rser.2014.07.026.

[2] Akram Al-Khazzar, A.K. (2018): A Comparative study of the available measured global solar radiation in Iraq, Journal of Renewable Energy and Environment, Vol. 4(2&3), pp. 47-55. Available at www.jree.ir.

[3] Al-Hamadani, S. (2020): Solar energy as a potential contributor to help bridge the gap between electricity supply and growing demand in Iraq: A review, International Journal of Advances in Applied Sciences, Vol. 9(4), pp. 302. https://doi.org/10.11591/ijaas.v9.i4.pp302-312.

[4] Al-Khatteeb, L., Istepanian, H. (2015): Turn a light on: Electricity sector reform in Iraq, Policy Briefing, Brookings Doha Center.

[5] Boukelia, T.E., Mecibah, M.S. (2013): Parabolic trough solar thermal power plant: Potential, and projects development in Algeria, Renewable and Sustainable Energy Reviews, Vol. 21, pp. 288-297. https://doi.org/10.1016/j.rser.2012.11.074.

[6] BP (2019): BP Statistical Review of World Energy, (68th edition).

[7] Chaichan, M.T., Kazem, H.A. (2011): Thermal storage comparison for variable basement kinds of a solar chimney prototype in Baghdad - Iraq Weathers, International Journal of Applied Sciences (IJAS), Vol. 2(2), pp. 1-20.

[8] IEA (2012): Iraq Energy Outlook, World Energy Outlook Special Report.

[9] IEA (2020): World Energy Outlook 2020. Paris. Available at https://www.iea.org/reports/world- energy-outlook-2020.

[10] IRENA (2020): Renewable power generation costs in 2019. Abu Dhabi.

[11] Istepanian, H. (2018): Solar Energy in Iraq: From outset to offset, Iraq Energy Institute, IEI181018 (October), pp. 1-25.

[12] Istepanian, H. (2014): Iraq's electricity crisis, Electricity Journal, Vol. 27(4), pp. 51–69. https://doi.org/10.1016/j.tej.2014.04.006.

[13] Kazem, A.A., Chaichan, M.T. and Kazem, H.A. (2014): Dust effect on photovoltaic utilization in Iraq: Review article, Renewable and Sustainable Energy Reviews, Vol. 37, pp. 734-749.
https://doi.org/10.1016/j.rser.2014.05.073.

[14] Kazem, H.A., Chaichan, M.T. (2012): Status and future prospects of renewable energy in Iraq, Renewable and Sustainable Energy Reviews, Vol. 16(8), pp. 6007–6012. https://doi.org/10.1016/j.rser.2012.03.058.

[15] Macneill, M., Quinn, M., Bayer, C. (2019): OPEC Annual Statistical Bulletin.

[16] Mekhilef, S., Saidur, R., Safari, A. (2020): A review on solar energy use in industries, Renewable and Sustainable Energy Reviews, Vol. 15(4), pp. 1777-1790. https://doi.org/10.1016/j.rser.2010.12.018.

[17] Panwar, N.L., Kaushik, S.C., Kothari, S. (2011): Role of renewable energy sources in environmental protection: A review, Renewable and Sustainable Energy Reviews, Vol. 15(3), pp. 1513-1524.
https://doi.org/10.1016/j.rser.2010.11.037.

[18] Zakhidov, R.A. (2008): Central Asian countries energy system and role of renewable energy sources, Applied Solar Energy, Vol. 44(3), pp. 218-223. https://doi.org/10.3103/S0003701X08030201.

TRNSYS simulation of a flat plate solar system for space heating

Ahmed M. AJEENA[1,3], Piroska VIG[2], István FARKAS[2]

[1]Mechanical Engineering Doctoral School, Szent István University, Hungary

[2]Department of Physics and Process Control, Institute for Mechanical Engineering Technology, Faculty of Mechanican Engineering, Szent István University, Hungary

[3]Mechanical Engineering Department, University of Kufa, Iraq

Abstract

This present study attempted to investigate the possibility of utilising solar energy for space heating in Iraq where the solar radiation is mainly available most time of the year. Heating is a basic need for buildings in cold and overcast climates. The TRNSYS software was used to modelling and simulate of the solar thermal system for space heating by flat plate collectors at a real building. The system operated in Bagdad during the cold season between November and March months. This study shows that the optimized solar thermal system could provide the 57% of space heating by using solar energy. According to the simulations of the developed model in the cold season the auxiliary energy was lowest in March 1364 MJ, the solar fraction was 92%, while the maximum auxiliary energy needs 44477 MJ was required in January, when the solar fraction was 44% for space heating.

Keywords

Solar energy, TRNSYS, space heating, flat plate collector, simulation

1. Introduction

Renewable energy is an environmentally friendly power source that can produce electricity, light, and heat. Solar energy is one of the main types of renewable energy used in many fields these days, such as space heating, pool heating, domestic hot water (DHW) production, cooling, and electrical production without polluting the environment.

The hourly sunlight flux incident on the Earth's surface is greater than the annual energy consumption (Duffie, Beckman & McGowan, 1985), so it gives many provides of opportunity to utilise solar energy.

TRNSYS noun comes from the appellations Transient Systems Simulation software, and it is adaptable transient systems simulation software with a modular structure. TRNSYS is a digital computer program written the language in Fortran. TRNSYS is widely used in solar thermal energy applications. When the time changes to any of the solar thermal system components, the system simulation is defined as a transient simulation (Kalogirou, 2009).

Iraq population increases rapidly and demands for power is increases, as well, population rose by 18 million between 1980 and 2010 and is expected to become 64 million in 2050.

Electric power stations are not able to meet the demand for electricity because of limited production. Iraq is known for its long sunshine hours. In literature, Iraq approximately gets 3000 hours of solar radiance annually, as shown in Figure 1 Iraq receives solar radiation reaching an average of 6.5-7 kWh/m^2 (Kazem & Chaichan, 2012)
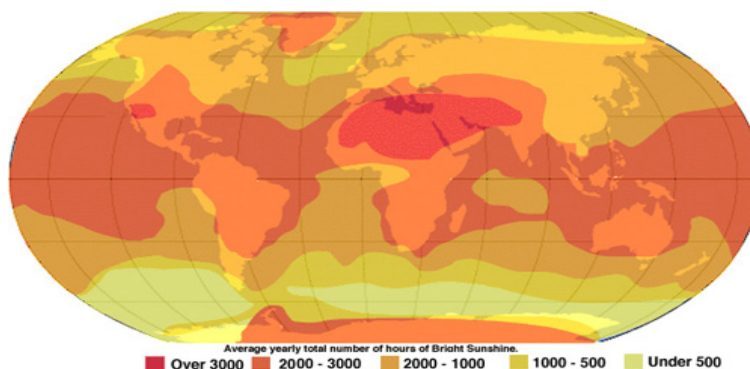

Figure 1. Iraq's position is over 3000 yearly hours of bright sunshine (Alasady, 2011)

Many studies can be found around the solar heating system especially for space heating.

(McLeskey, Terziotti, & Sweet, 2012) studied a flat plate solar heating system, modelled for a 15700 m^2 building student housing in Virginia with used 1930 m^2 of flat plate solar collectors.

(Hazami et al., 2013) introduced an annual energy performance differentiation between the flat plate solar heating system (FPSHS) and evacuated tube solar heating system (ETSHS).

Ayompe et al. (2011) created two TRNSYS models for simulation thermal behaviour of solar heating systems installed in Dublin. The results at flat plate and evacuated tube collector systems were compared with the measured data. The models generated values of collected heats, the collector outlet temperatures give good accuracy with measured data.

Mehdaoui et al. (2014) focused on optimizing the solar system used to heat a 48 m^3 volume hall installed in Borj Cedria. This study using TRNSYS software for to optimize the various solar system parameters as mass flow rate, collector area, the active layer's thickness and the tank volume.

The primary aims of our research are summarized as follows:
  – Create TRNSYS simulation models appropriate for flat plate solar heating systems in Iraq.
  – Predicted monthly and annual auxiliary energy needed by the solar heating system.

    – Investigate the potential of solar energy usage of space heating and the feasibility of achieving greenhouse without the use of fossil fuels to obtain energy in Iraq.

2. Building and TRNSYS model

The building comprises four bedrooms, a reception room, a dining room, two bathrooms, a kitchen, and a machinery room of a typical single-story house in Iraq as it is shown in Figure 2 building arrangements.
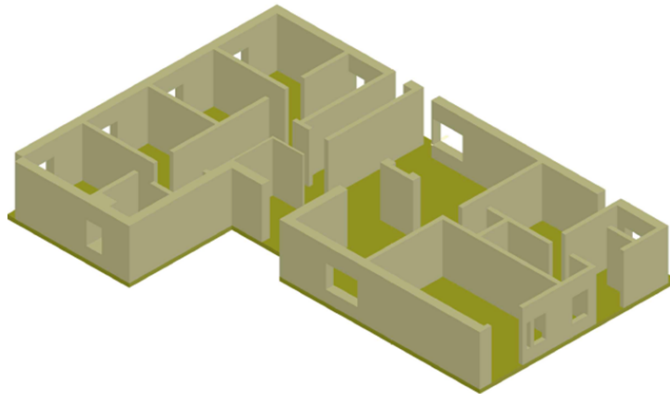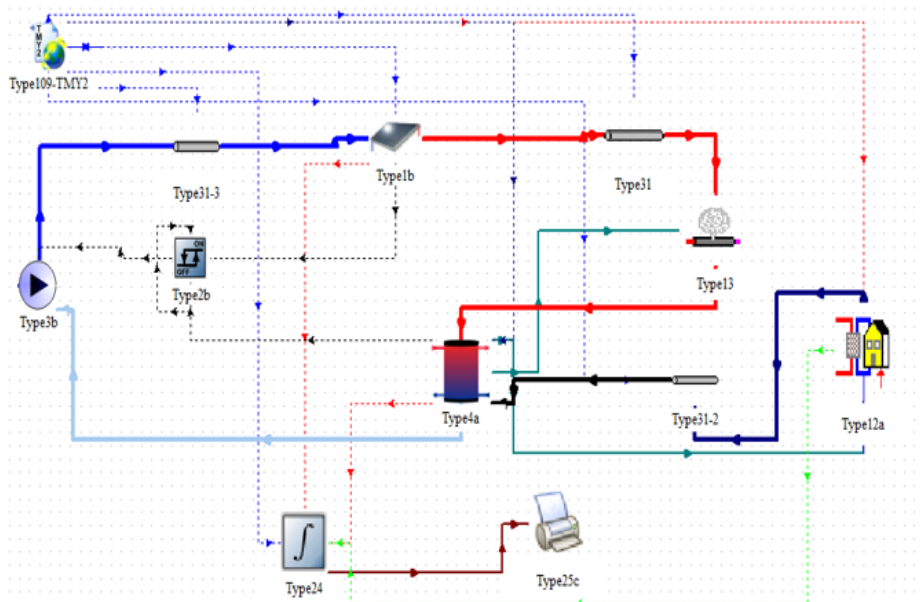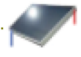

Figure 2. Typical building arrangements

Figure 3. TRNSYS model of solar space heating

Table 1. The values of the leading design and operating parameters

Parameters	Value	Unit
Collector area	50 - 250	m^2
Fluid specific heat	4.190	kJ/kg.K
Intercept efficiency	0.8	
Efficiency slope (Heat transfer coefficient)	13	kJ/(hr.m^2.K)
Collector slope	15 - 80	degrees
azimuth angle	-60 - 60	degrees
Latitude	33.33° N	degrees
Longitude	44.44° E	degrees
Solar constant	4871	kJ/hr.m^2
Storage tank volume	10 - 50	m^3
Fluid density	1000	kg/m^3
Boiling point	100	^{o}C
Mass flow rate	10-80	kg/h

Table 2. Main TRNSYS components for solar water heat system and their symbols

Component Name	Icon	Symbol	Component Name	Icon	Symbol
Flat-Plate Collector		Type 1	Energy / (Degree-Hour)		Type 12
Solar radiation processor		Type 109	Forcing function		Type 13
Thermal storage tank		Type 4	Integration		Type24
Circulation Pump		Type 3	Results		Type 25
Pump Controller		Type 2			
Plotter		Type 65			

The present study used TRNSYS software for modelling the space heating system, as presented in Figure 3.

The model's central element is solar thermal flat plate collector, solar radiation processor, storage tank, pump controller, circulation pump, piping, energy/(degree-hour), printer, quantity integrator, valve. Table 1 presents the leading design and operating parameters values of the solar system components in the TRNSYS model. The main TRNSYS components for the model of the solar heating system are summarized in Table 2.

3. Results and discussions

The created model used to inspect the system's annual performance. The optimum design parameters are directed to by investigated by the simulations. According to the hypothesis, it is required to meet the heating demand. The following design parameters have been obtained from the simulation results:

- Collector slope: 50° from horizontal
- Collector azimuth: 22° East of South
- Collector area: 200 m^2
- Storage tank volume: 15 m^3, built on 80 l/m^2
- Mass flow rate: 50 kg/h.

The results of the simulation are shown in Table 3, which shows the monthly heating load, auxiliary heat used, solar fraction, and efficiency for five months of the cold season. Under these design criteria, the annual solar fraction is 0.57 (57% of the annual heating load) is met by solar, while the auxiliary source supplies the rest.

Table 3. Simulation summary of space heating system

Month	Auxiliary energy (M J)	Load (M J)	Solar fraction	Efficiency
November	5142.91	28595.62	0.82	0.37
December	33944.43	66939.69	0.49	0.44
January	44477.97	79897.14	0.44	0.48
February	16869.92	47059.19	0.64	0.44
March	1364.24	16409.60	0.92	0.44
Total/Average	101799.47	238901.24	0.57	0.43

The Figure 4. shows in the could mounts the efficiency of solar heating system and Figure 5. shows the solar fraction.
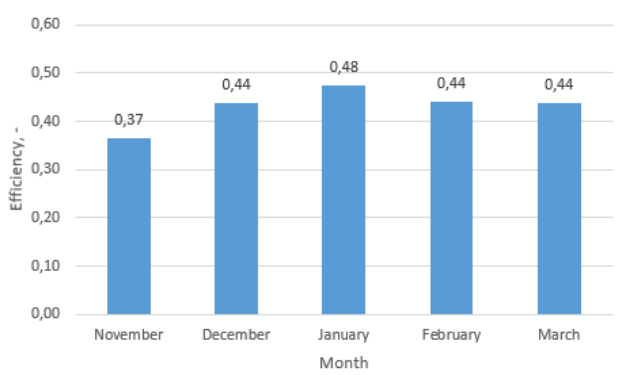

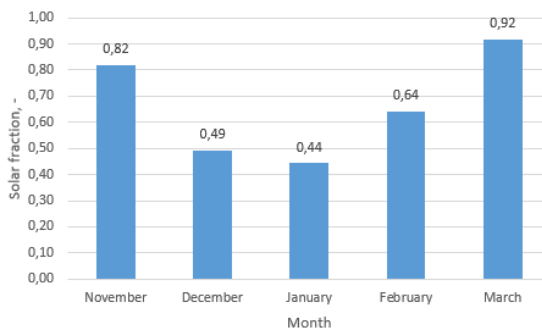*Figure 4.* Efficiency of the solar system

Figure 5. Solar fraction

It is seen from the above results that the solar fraction during November is 0.82. In the peak of the winter season, it reached it is 0.48 in January, when the 44% of the monthly heating load is met by solar. Because the weather in January is colder than November, and then, the heating load is higher. Therefore, the solar system can meet only a part of it. The collector's average efficiency is at its peak in January.

Conclusions

According to the TRNSYS simulation of a solar heating system for Iraq's space heating, the following conclusions are established.
- The predicted extra energy by month required by the solar space heating system in winter is lower during March, while maximum auxiliary energy is required during January.
- The solar fraction of solar space heating systems for the winter season is about 57%. It is higher in March than other winter months for solar space heating.
- The optimum collector flow rate 50 kg/h.
- Iraq's weather has the potential for the use of solar heating systems in winter.

Acknowledgments

References

[1] Alasady, A.M.A. (2011). Solar energy the suitable energy alternative for Iraq beyond oil. 2011 International Conference on Petroleum and Sustainable Development, Vol. 26, pp. 11-15.

[2] Ayompe, L.M., Duffy, A., McCormack, S.J., Conlon, M. (2011). Validated TRNSYS model for forced circulation solar water heating systems with flat plate and heat pipe evacuated tube collectors. Applied Thermal Engineering, Vol. 31 (8-9), pp. 1536-1542.
https://doi.org/10.1016/j.applthermaleng.2011.01.046

[3] Duffie, J.A., Beckman, W.A., McGowan, J. (1985). Solar Engineering of Thermal Processes. American Journal of Physics, Vol. 5.
https://doi.org/10.1119/1.14178

[4] Hazami, M., Kooli, S., Naili, N., Farhat, A. (2013). Long-term performances prediction of an evacuated tube solar water heating system used for single-family households under typical Nord-African climate (Tunisia). Solar Energy, Vol. 94, pp. 283-298. https://doi.org/10.1016/j.solener.2013.05.020

[5] Kalogirou, S.A. (2009). Solar energy engineering: Processes and systems. Solar Energy Engineering. http://dx.doi.org/10.1016

[6] Kazem, H.A., Chaichan, M.T. (2012). Status and future prospects of renewable energy in Iraq. Renewable and Sustainable Energy Reviews, Vol. 16 (8), pp. 6007-6012. https://doi.org/10.1016/j.rser.2012.03.058

[7] McLeskey, J.T., Terziotti, L.T., Sweet, M.L. (2012). Modeling seasonal solar thermal energy storage in a large urban residential building using TRNSYS 16. Energy and Buildings, Vol. 45, pp. 28-31.
https://doi.org/10.1016/j.enbuild.2011.10.023

[8] Mehdaoui, F., Hazami, M., Naili, N., Farhat, A. (2014). Energetic performances of an optimized passive solar heating prototype used for Tunisian buildings air-heating application. Energy Conversion and Management, Vol. 87, pp. 285-296.
https://doi.org/10.1016/j.enconman.2014.07.024

Concept of a solar cell operated hybrid tree

Mensour ALMADHHACHI[1], István FARKAS[2], István SERES[2]

[1]Doctoral School of Mechanical Engineering, Szent István University, Gödöllő, Hungary
[2]Department of Physics and Process Control, Institute for Mechanical Engineering Technology,
Faculty of Mechanican Engineering, Szent István University, Gödöllő, Hungary

Abstract

In the modern cities building, the architectural form is carefully chosen for all the details of the facilities that will be in these cities and also taking care of the energy sources and the number of pollutants that will negatively affect the environment, which negatively affects the health of the people who live in these facilities. One of the best environmental improvements is trees and plants, where they should take a suitable area within modern cities. We will mix the beautiful shape of grape trees to generate appropriate energy according to the available spaces and capabilities in this direction. We can take advantage of the capabilities and reduce the risks to the environment in all the details of the assets in cities and coordinate them so that cities' aesthetic is the standard in designing to produce energy and reduce pollutants. The hybrid tree is the new face of PV technology to generate electricity from an environmentally friendly shape. The grape is one of the world's famous trees. They are characterized by black pillows, which are the colour of the PV cells, and the curved surface increase the active area of the cells compared to the flat ones independently from the seasonal and the daily relative movement of the Sun.

Keywords

hybrid tree, solar energy, optimal shape, solar cell, electricity

1. Introduction

Due to the exponential depletion of traditional fossil fuels, climate change, global warming and ever-increasing energy demand, the search for renewable and clean energy supplies has become one of the greatest problems of our time (Hyder et al., 2018). Compared to fossil fuel energy, renewable energy is comparatively inexpensive, accessible, and eco-friendly (Almadhhachi et al., 2020).

In general, the renewable energy is characterized as energy that comes from resources such as sunlight, wind, rain, tides, waves and geothermal heat, which are continually replenished on a human time scale (Avdic et al., 2013).

The "Solar Tree" is a combination of artistic and technological effort which exists as a form of solar artwork. Within the past several years, artistically inclined inventors have strived to envision new methods to gain utility from solar cell

technology. This relatively new concept was conceived in an attempt to merge new technology, relating to the absorption and use of solar power, and artistic aesthetic.

The first produced polymer: fullerene-based organic solar cells on flexible plastic substrates that have comparable performance using the inverted panel structure to products on rigid glass substrates. Large-area flexible devices with an active device area of 6.5 cm^2 using a steel rule die were produced and cut into palm leaf shapes. 12 leaf-shaped organic solar cells were then assembled to form a prototype "solar palm tree" (Cao et al., 2014). Tree-shaped hybrid Nano-generator (TSHG) is constructed of flexible photovoltaic (PV) and piezoelectric (piezo) film sheets to harness wind and solar energy. The proposed device has been designed to generate electricity if sun, wind or heavy rainfall happens. With an open circuit voltage of 5,071 V, a short-circuit current of 1,282 mA and a maximum power output of 3,42 mW at a loading resistance of 5 kΩ, the TSHG has excellent efficiency (Ahmed et al., 2019).

In this study, it is assumed that trees are better at absorbing solar radiation for two reasons. The first is that the angle of solar radiation is not important because of the spherical shape of the grapes, and the second reason is that the other part of the grape balls will absorb the reflected radiation and thus the efficiency of the solar cells is better.

2. Concept of solar PV tree

The concept of a "Solar PV Tree" is a unique blend of art and technology to form a solar photovoltaic sculpture. Such kind of novel idea was considered as an attempt to use the new technology of solar power and also for artistic aesthetics.

A solar tree is basically a decorative means of producing renewable electricity. Solar tree embodies a steel structure, on top of which solar panels collect Sun's radiant energy to generate electricity, Since PV module are arranged at different angles, a solar PV tree is able to capture incident Sunlight throughout the day irrespective of the position of the Sun. The solar tree's three-dimensional structure can enhance the total surface area of the sunlight acquisition since the sphere adds a feature of the lack of interest in the falling solar angle, and there is also the other part of the ball absorbing the reflected radiation of another ball.
In the cluster of grapes, there will be a slight effect on each other, so the engineering modelling and designing the structure is essential.

The final initiations of a solar tree concept are to improve the public perception of solar PV technology by making it aesthetically pleasing. The objectives of a solar tree concept are:
- Increase the awareness of civilians in the use of renewable energy and solar energy.
- The increase in the forms of trees in residential cities, which messes up the comfort of civilians.

- Increase the efficiency of solar panels as possible.
- Adding aesthetics to cities to create environmentally friendly forms.
- Creating a new form for the surrounding fences for service and entertainment projects such as parks and gardens.

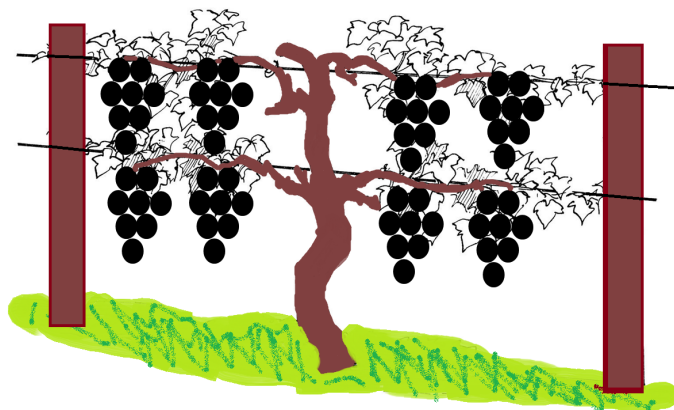The components and general layout of a hybrid solar tree are shown in Fig. 1.

Figure 1. layout of the hybrid solar tree

3. Design parameters of hybrid tree

Trees are one of the basic components of nature and are distinguished by their shapes and colours. This hybrid tree was created based on the black grape tree to harness solar cells to produce electrical energy and convert the shape of the solar panels from classic, traditional form (e.g., on the roofs of buildings) eco-tree. In this case, the electricity was generated from solar energy while adding hybrid trees' aesthetic to the cities.

The tree consists of the stem, branches, and black grape balls (see in Fig. 1) and electrical wires inside the branches and stem and are not visible. The tree has a special inverter that fits with the tree's generating capacity and shape.

For the first time, the black body was integrated with flexible solar cells to form black grape balls to improve solar cell efficiency, and the shape provides bigger useful surface for absorbing solar radiation.The diameter of the grape balls will be 25 cm, and every 7 balls will be one group, so the height of the grape cluster will be approximately 1 m. The grape clusters are distributed according to the application, the location of the trees, the solar radiation and the amount of energy required.

Beside the spherical shape, other shapes (eg. ellipsoid with different axis rate) are analysed for the optimal energy income of the solar radiation.

Solar radiation will be absorbed by the solar cells on the outer layer of the grape balls. The direct solar radiation and the reflected will be absorbed (Verma &

Mazumder, 2014) assumed that the form of sunlight absorption for the tree is in the form of a quadrant spherical, and this theory cannot be applied to hybrid grape trees.

Conclusion

Novel hybrid tree to generate electrical energy to beautify cities in an environmentally friendly way with the incorporation of photovoltaic cells with black body technology for the first time to improve the process of absorbing sunlight and provide the largest possible space to increase the efficiency of solar cells. All these technologies were formed by the black grape tree to generate electrical energy, and the black grape tree is easily distinguished. The external shape was changed by forming an external fence or forming a roof for the buildings' entrances and the corridors between the buildings to decorate the streets.

Acknowledgments

References

[1] Ahmed, R., Kim, Y., Zeeshan, Chun, W. (2019). Development of a tree-shaped hybrid nanogenerator using flexible sheets of photovoltaic and piezoelectric films. *Energies*, *12*(2), 1-10. https://doi.org/10.3390/en12020229

[2] Almadhhachi, M.S., Machi, M.H., Jaber, M.F. (2020). Enhancement of charging system for electrical vehicle using PV panels. *Journal of Mechanical Engineering Research and Developments*, *43*(4), 223-229.

[3] Cao, W., Li, Z., Yang, Y., Zheng, Y., Yu, W., Afzal, R., Xue, J. (2014). Solar tree: Exploring new form factors of organic solar cells. *Renewable Energy*, *72*, 134-139. https://doi.org/10.1016/j.renene.2014.06.045

[4] Hyder, F., Sudhakar, K., Mamat, R. (2018). Solar PV tree design: A review. *Renewable and Sustainable Energy Reviews*, *82* (October 2017), 1079-1096. https://doi.org/10.1016/j.rser.2017.09.025

[5] Avdic, V., Pervan, N., Tasic, P., Zecevic, S., Muminovic, A., (2013). Implementation of the Project "Solar tree" in Sarajevo. *Conference: Green Design Conference, at Sarajevo, Bosnia and Herzegovina, Vol. 2, May 2014*. https://www.researchgate.net/publication/257537153

[6] Verma, N.N., Mazumder, S. (2014). An investigation of solar trees for effective sunlight capture using Monte Carlo simulations of solar radiation transport. *ASME International Mechanical Engineering Congress and Exposition, Proceedings (IMECE)*, *8A*, 1–10. https://doi.org/10.1115/IMECE2014-36085

Transient simulation of a hybrid solar collector system

Ahssan M.A. ALSHIBIL[1,3], Piroska VÍG[2], István FARKAS[2]

[1]Doctoral School of Mechanical Engineering, Szent István University, Gödöllő, Hungary
[2]Department of Physics and Process Control, Institute for Mechanical Engineering Technology,
Faculty of Mechanican Engineering, Szent István University, Gödöllő, Hungary
[3]Department of Mechanical Engineering, College of Engineering, University of Kufa, Iraq

Abstract

The solar thermal collector and photovoltaic systems are mixed for a hybrid solar collector (PV/T). This method takes advantage of the solar light and heat to generate electricity and thermal energy at the same time. This paper reports on the accessibility of models of Photovoltaic thermal hybrid systems. A particular consideration is paid to how the PV/T system in TRNSYS can be modelled and the outcomes of the simulation are collected. It presented the basic model of the PV/T system model and how its outputs appear on the simulation graph to use it for further work.

Keywords

PV/T collector, TRNSYS, solar thermal system, photovoltaics

1. Introduction

Solar systems are considered as one of the energy production alternatives that do not make the contamination or serious wastes and, in this way, reduce the hazard of condition contamination. Utilizing solar energy as an alternative energy source has high reliability, the fact that there is no cost of fuel or any moving mechanical parts. Simply, the sun invests in producing electrical energy by solar photovoltaic cells and thermal energy by solar collectors (Duffie, Beckman, 2013; Kafui et al., 2019).

Between 7% to 16% from solar radiation falls on photovoltaic cells is changed to energy as electricity. In contrast, a part of the residual radiation reflects, and the significant part turns into heat, and this heat increases the solar cell temperature and reduces their efficiency and lifetime (Rodrigues et al., 2011).

The heat absorbed from the solar modules by the solar collector can decrease the PV module's surface temperature. Thus, electricity yield turns out as increasingly ideal, it is possible to use the gathered heat energy in different applications. So, the thermal and electrical energies are extracted by using solar photovoltaic (PV) and thermal (T) collector, or PV/T solar collector. It includes a PV module, and a heat exchanger behind it, the liquid used for cooling distributes in the heat exchanger it can be water, air, or Nano practical (Bődi et al., 2018).

The TRNSYS transient simulation system tool is the usual technique for PV/T modelling and simulation. This technology was explored by many researchers of TRNSYS software.

Elbreki et al. (2016) offered a comprehensive overview of the current development improvements and modelling for PV/T structures that take weather effects into account.

Lämmle et al. (2017) tested the performance of different PV/T collectors in four independent heating systems using TRNSYS. The findings showed that, as unglazed, the PV/T collectors provide better electric power and glazed PV/T achieved high thermal energy.

The simulation model for the uncovered PV/T water collector system was proposed by Aste et al. (2016). For the study, the key parameters that affect the performance of solar cells were considered, such as spectral efficiency, efficiency loss because of temperature raising, real angle of solar radiation incidence, and system thermal inertia. It analysed overall performance and electrical efficiency under three different climatic conditions. In TRNSYS, the mathematical model developed was then implemented and simulation under three meteorological variations was carried out with the same specification. It was noted that the findings were inconsistent with the experimental findings.

In specific, this paper reports on the accessibility of models of Photovoltaic Thermal hybrid systems. Particular consideration is paid to how the PV/T system in TRNSYS can be modelled and the outcomes of the simulation are collected. It presented the basic model of the PV/T system model and how its outputs appear on the simulation graph to use it for further work.

2. Photovoltaic/thermal systems

The whole PV/T system consists of a PVT module, a storage tank to provide hot water for consumption and electrical components, and a cold water delivery pump.

In certain applications, hybrid PV/T systems are considered an alternative to simple PV units. They can be used efficiently to transform the solar radiation consumed into electricity and heat, thus increasing their overall amount of energy (Kalogirou, 2014).

PV/T systems can be seen in many commercial applications, however the most suitable are those that require heat at low temperatures (60-80 °C) and especially at very low temperatures (<50 °C) because both the electrical and thermal performance of the PV/T system can be retained at an appropriate level in these situations. It should be observed that the heat consumption fraction is high at low temperatures, especially in the food industries, and in the paper and textile industries, where up to 80 percent of the overall thermal energy requirement may be accounted for. Water-cooled PV/T systems, for example, might heat water for washing or cleaning processes (Kalogirou, 2014).

The integrated design concept has been presented for water heating in a PV/T, such an integrated system (IPV/TS) is therefore suggested in Figure 1 (Huang et al., 2001).
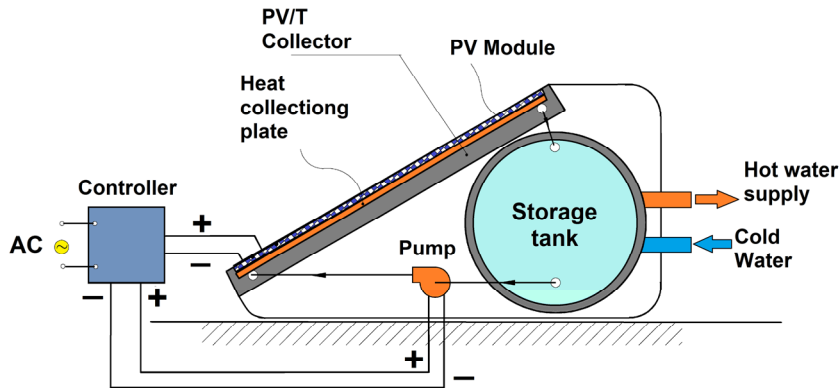
Figure 1. PV/T system (Huang *et al.,* 2001)

3. PV/T components of TRNSYS

The well-known TRNSYS program is a common tool to build a solar system model. This software has been developed by Solar Energy Laboratory participants at the University of Wisconsin (Klein SA et al., 1996).
It is written in Fortran-77, standard ANSII. The software is made up of several subroutines that model components of the subsystem. The mathematical models are expressed as a function of their ordinary differential or algebraic equations for the subsystem components.

Through software such as TRNSYS that can interconnect components of the device in any desired way, resolving differential equations and facilitating the processing of knowledge. By identifying all the components that constitute a certain system, the entire problem of system simulation will reduce.

In the TRNSYS software library, Type50 represents the PV/T collector. It has two groups the first is PV/Thermal collectors - flat plate collectors and the second is PV/Thermal collectors - concentrating collectors. Each group has four different types based on eight operation modes for type 50 of TRNSYS. these modes are as follow (Collins, 2009):

1. Collector loss and cover transmission required.
2. Cover transmission required.
3. Collector loss and angular dependent cover transmission required.
4. Collector loss and cover transmission calculated internally.
5. Concentrating collector. Collector loss and cover transmission required. PV output is free-floating.
6. Concentrating collector. Detailed collector loss and cover transmission required. PV output is free-floating.
7. Concentrating collector. Collector loss and cover transmission required. PV output is set.
8. Concentrating collector. Detailed collector loss and cover transmission required. PV output is set.

PV/T system model in TRNSYS consists of the basic components that make the system to be run. Type50b as PV/T, Type2b as a pump, Type109-TMY2 as a source of weather data, Type4a as thermal storage tank, and Type65a as a plotter of outputs are the main types for system model Figure 2. Each type has outputs linked to the plotter to appear on the final simulation graph.
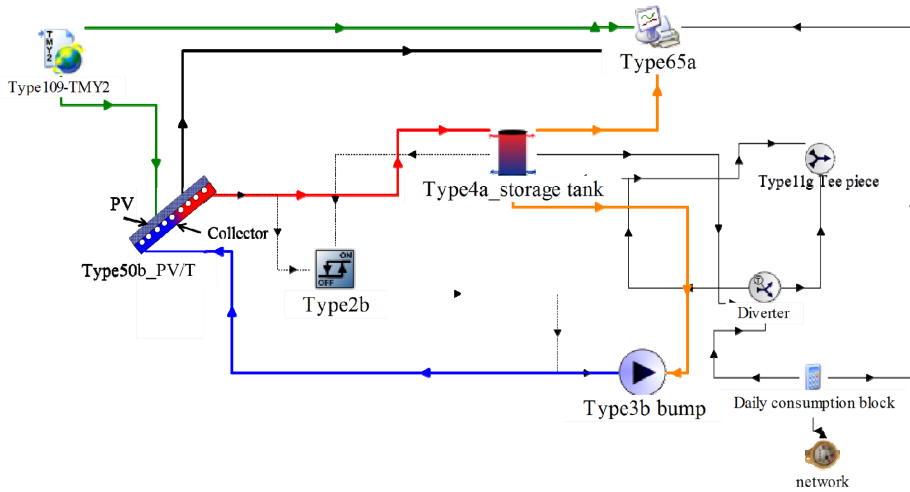

Figure 2. PV/T system model in TRNSYS
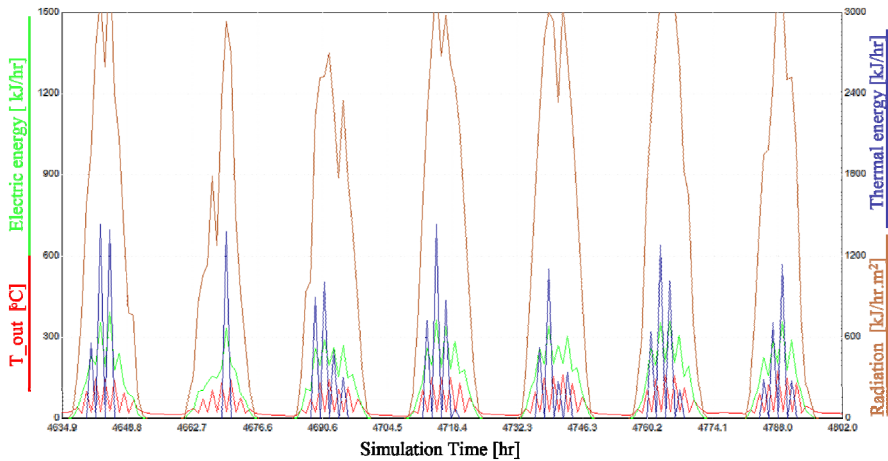
4. Modelling results

Figure 3. A run chart in TRNSYS

The most significant findings relate to the previous PV/T model are electric and thermal energy. The simulation time used in this study for the TRNSYS deck file

is selected randomly, during particular days in July 12 (4634.9 hr) to July 19 (4802 hr) was the period selected for the simulation time, and location was the default on the TRNSYS software. Figure 3. shows the outputs of the PV/T system model, thermal energy from the heat source, electrical energy, output temperature of water in PV/T module, and its relationship with solar radiation during certain simulation time. A comparison between the PV/T and a classical unit of PV module and collector can be tested based on the simulation data.

Conclusions

The PV/T hybrid systems can be used in a range of applications, involving both electrical and thermal energy, especially as the price of solar cells continues to decrease.

The present work reports the hybrid solar collector behaviour as one of the solar energy converters. The simulations carried out in the environment of TRNSYS have made it possible to obtain a thermal and electrical contribution from the PV/T sector to the output of residential buildings.

It provided the basic model of the PV/T system and how its outputs appear for further work on the simulation graph.

In conclusion, TRNSYS software is a promising tool for improving PV/T system performance because of its reliability and flexibility in model making.

Acknowledgments

References

[1] Aste N., Del Pero C., Leonforte F., Manfren M. (2016): Performance nonitoring and modeling of an uncovered photovoltaic-thermal (PVT) water collector, Solar Energy, Vol. 135, pp. 551-568.
[2] Huang B.J., Lin T.H., Hung W.C., Sun F.S. (2001): Performance evaluation of solar photovoltaic/thermal systems, Solar Energy, Vol. 70, pp. 443-448.
[3] Bődi S., Víg P., Farkas I. (2018): Possibilities of improving PV/T system efficiency. Hungarian Agricaltural Engineering, No. 33/2018, pp. 55-58.
[4] Collins M. (2009): A Review of PV, Solar thermal, and PV/Thermal collector models in TRNSYS. IEA SHC - Task 35, p. 78.
[5] Duffie J.A., Beckman W.A. (2013): Solar engineering of thermal processes, Fourth. ed, John Wiley & Sons, Inc., Canada, p. 910.

[6] Elbreki A.M., Alghoul M.A., Al-Shamani A.N., Ammar A.A., Yegani B., Aboghrara A.M., Rusaln M.H., Sopian K. (2016): The role of climatic-design-operational parameters on combined PV/T collector performance: A critical review, Renewable and Sustainable Energy Reviews, 57, pp. 602-647.

[7] Kafui A.D., Seres I., Farkas I. (2019): Efficiency comparison of different photovoltaic modules, Acta Technologica Agriculturae, Vol. 22, No. 1, pp. 5-11.

[8] Kalogirou S.A. (2014): Solar energy engineering processes and systems, 2nd ed, Solar Energy Engineering, Elsevier, p. 816.

[9] Klein S.A. et al. (1996): TRNSYS 14.2. A transient simulation and program. Solar Energy Laboratory, University of Wisconsin, Madison (WI).

[10] Lämmle M., Oliva A., Hermann M., Kramer K., Kramer W. (2017): PVT collector technologies in solar thermal systems: A systematic assessment of electrical and thermal yields with the novel characteristic temperature approach, Solar Energy, Vol. 155, pp. 867-879.

[11] Rodrigues E.M.G., Melício R., Mendes V.M.F., Catalão J.P.S. (2011): Simulation of a solar cell considering single-diode equivalent circuit model, Renewable Energies And Power Quality, pp. 369-373.

Invited Papers

1. Diki Ismail PERMANA, Dani RUSIRAWAN, István FARKAS:
   Organic Rankine cycle analysis based on Tura geothermal power-plant excess steam

The authors' team is research partner of the faculty in the field of energetic research and process modelling.

2. Jozef Rédl, Juraj Maga, Gábor Kalácska, Davood Kalantari:
   Time series data processing of liquid nonlinear flow

The authors' team is research partner of the faculty in the field of farmengineering research and process modelling.

3. Henrik Domanovszky, Zoltán Bártfai:
   Critical safety hazard factors of hydrogen fuel for on-road application

The authors' team is research partner of the faculty in the field of energetic research and vehicles modelling.

Organic Rankine cycle analysis based on Tura geothermal power-plant excess steam

Diki Ismail PERMANA[1,3], Dani RUSIRAWAN[3], István FARKAS[2]

[1]Doctoral School of Mechanical Engineering, Szent Istvan University
[2]Department of Physics and Process Control, Institute for Mechanical Engineering Technology,
Faculty of Mechanican Engineering, Szent Istvan University
[3]Department of Mechanical Engineering, Institut Teknologi Nasional
E-mail: dicky91permana@itenas.ac.id, danir@itenas.ac.id, Farkas.Istvan@szie.hu

Abstract

Renewable energy sources are the key to overcome reducing usage of fossil fuel to generate electricity. Geothermal is one of many renewable energy that be a suitable solution for reducing fossil fuel. Hungary has a potential low-medium temperature geothermal that can be generating electricity. One of them is Tura geothermal plant that already established with 2.7 MW electricity and became the first geothermal power-plant in Hungary. The excess steam from Tura geothermal power-plant is still have a potential energy that can converted to electricity. The objective of this study is to generating electricity from the excess steam of Tura geothermal plant with Organic Rankine cycle application.

Keywords

renewable energy, geothermal, organic Rankine cycle

1. Introduction

Mankind had lived over many decades depending on fossil fuel to fulfil their needs. But, using fossil fuel bring harm to environment and it cannot be replenished (EA, 2016). Renewable Energy sources is the key to overcome reducing usage of fossil fuel to generate electricity. Renewable energy like solar thermal, geothermal, biomass and waste heat sources from industries are capable in decreasing the rate of the consumption of fossil fuels. Unfortunately, most renewable energy sources are dependent on climatic variation and are not suitable for base load operations. Geothermal energy could be a viable solution for reducing the effects of global warming and dependence on fossil fuel, since the availability of geothermal energy is potentially enormous, provides a clean, reliable source of renewable energy and is available in many parts of the world (Sohel, 2011), and including also in Hungary.

Based on Figure 1, which is describe the distribution of renewable energy for the electricity and heating sector from 2010 to 2020 has changed. One of the concerns is management in the geothermal sector has developed quite rapidly from

4.23 PJ in 2010 to 16.43 PJ in 2020, while in the biomass sector it has decreased by 20PJ in the last ten years (Boda, 2016). This confirms that the Hungarian government is very serious about developing geothermal utilization, both for electricity and also for heating applications.
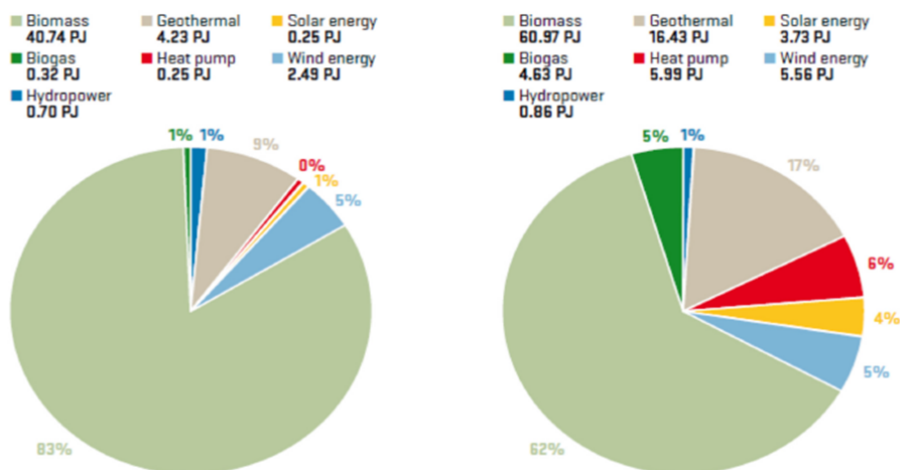

Figure 1. Distribution of renewable energy sources use in the electricity heating and cooling sectors (20210 and 2020) in the NREAP of Hungary (Boda, 2016)

According to Geothermal Finance and Awareness in European Regions (GEOPAR), Hungary has a special geological position which is located astride the Pannonian Basin, where several geothermal potentials that have high enthalpy have been found with an average gradient of about 50 °C/100 m which is an area that has low temperature geothermal energy in Europe. (Kiss et al., 2016).

In Hungary itself, geothermal utilization for electricity generation has been implemented in Tura region (30 km east of Budapest) and it is become the first geothermal plant in Hungary that producing electricity. The design temperature of power plant is about 125 °C with 86 kg/s (outflow rate) with total production capacity is 2.7 MW and the excess hot water of the field is around 75-78 °C (Boda, 2016). The low-medium temperature of excess hot water from the field is still have a high amount of enthalpy that can be utilised for generating electricity. However, these moderate and low-medium temperature heat sources cannot be efficiently converted into electricity through the conventional Steam Rankine Cycle. Organic Rankine Cycle (ORC) has been considered as most feasible cycle to generating electricity while recovering various heat sources. ORC is same as the conventional Steam but uses low boiling temperature of organic fluids or refrigerants instead of water.

ORC has been studied both theoretically and experimentally since the 1970s for small-scale systems with yield efficiency <10%. Commercial ORC applications first appeared in the late 1970s and 1980s for medium-scale power plants

developed to convert geothermal and solar energy. Nowadays, the number of ORC plant is increasingly growing with more than 1800 MW installed worldwide (Jouhara et al., 2018) from various heat sources such as geothermal brine, biomass combine heat and power (CHP) and waste heat recovery (WHR). So, the objective in this study is to determine the optimum conditions for the ORC application that utilise the excess hot water from geothermal field and determine a suitable working fluid.

2. ORC thermodynamic modelling

Figure 2 shows a simple schematic of an ORC consisting of an evaporator, turbine, condenser and pump. The heat source used for the ORC process comes from the heat of the Tura geothermal plant injection with the following conditions. This heat is extracted by a heat exchanger and heat transfer occurs with the working fluid which depends on its thermo-physical properties and usually have a low boiling temperature.
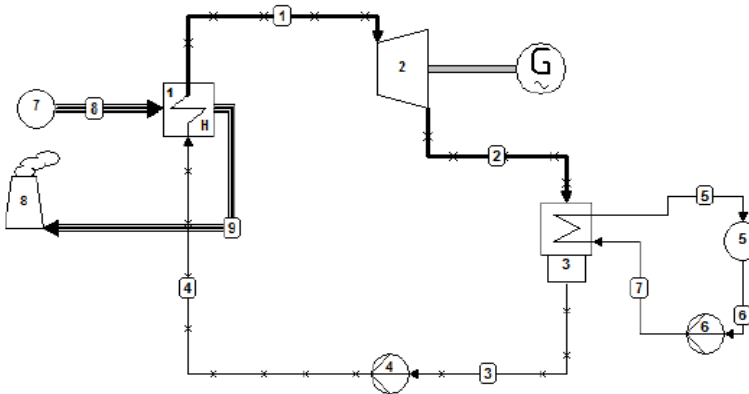

Figure 2. Simply ORC diagram

The first and second laws of thermodynamics can be used to determine the performance of the ORC. The amount of work generated and the heat required by the ORC can be determined by the energy equilibrium equation. The equations in each component are as follows (Moran et al., 2008):

Process 1-2, turbine: $\dot{W}_t = \dot{m}(h_1 - h_2)$,

Process 2-3, condenser: $\dot{Q}_{out} = \dot{m}(h_2 - h_3)$,

Process 3-4, pump: $\dot{W}_p = \dot{m}(h_4 - h_3)$,

Process 4-1, evaporator: $\dot{Q}_{in} = \dot{m}(h_1 - h_4)$,

Net power output:
$$\dot{W}_{net} = \dot{W}_{turbine} - \dot{W}_{pump} = (h_1 - h_2) - (h_4 - h_3),$$

Thermal efficiency:
$$\eta_{thermal} = \frac{\dot{W}_{net}}{\dot{Q}_{in}} = \frac{\dot{W}_{turbine} - \dot{W}_{pump}}{\dot{Q}_{in}}.$$

The above equation is an ideal condition where all losses that occur are ignored. In actual conditions many losses occur including an increasing entropy in the compression and expansion process. In this study, the isentropic efficiency for turbine is set up at 85% and for pump is 90%.

The isentropic efficiency for turbine is defined as:
$$\eta_{turbine} = \frac{h_1 - h_2}{h_1 - h_{2s}}.$$

The isentropic efficiency for pump is defined as:
$$\eta_{pump} = \frac{h_{4s} - h_3}{h_4 - h_3}.$$

Figure 3 shows the type of T-s cycle that depends on the pressure of working fluid in evaporator when the heat is given. If the working fluid pressure is less than the critical pressure ($P_1 < P_{crit}$), during heat transfer in evaporator, the working fluid will evaporate from the liquid phase to the vapor phase by passing through the 2-phase region, this process is called a sub-critical cycle (process cycle: 1-2-3-4-1). While, for the super-critical cycle (process cycle: 1*-2*-3-4-1), the pressure of working fluid is above critical pressure during heat transfer occur, in other words a working fluid does not passed through two phases region but past the critical region directly.
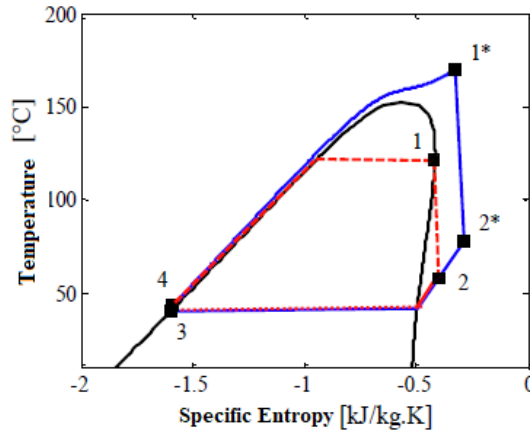

Figure 3. Sub-critical and supercritical for working fluid in T-s diagram

3. Working fluids selection

The working fluid chosen for this analysis is based on critical temperature, but other factors to consider are ODP (Ozone Depleting Potential) and GWP (Global

Warming Potential) where these two factors determine how much the working fluid can affect the environment in this case in terms of ozone and global warming (Permana, 2019). The Table 1 contains information on the working fluids that will be used in this study.

Table 1. Working fluids properties

Working fluids	$T_{critical}$ (°C)	$P_{critical}$ (MPa)	ODP	GWP	Type
R125	66,023	3,6177	0	3450	Super-critical
R143a	72,707	3,761	0	4400	Sub-critical
R32	78,105	5,782	0	670	Sub-critical
R22	96,145	4,99	0,04	1790	Sub-critical
Propane	96,74	4,2512	0	3,3	Sub-critical

After determining the working fluid chosen in this study, the next step is to determine the optimum conditions for each working fluid, where the optimum conditions are very important to maximize the excess heat from the geothermal residual. So in this study the excess steam reinjection is around 68 °C for upper limit temperature and the cooling water temperature is around 10 °C and mass flow rate of ORC's cycle is around 1 kg/s. In this case, the pressure becomes a variable which will be varied to find out the optimum pressure which can produce the highest output power and efficiency. Meanwhile, the tools used to determine the properties of each working fluid are using NIST Refprop and for validating calculations using the Cycle Tempo program.

4. Analysis of parameters

In this study, the pressure losses that occur in the evaporator, pipes and mechanics are neglected. Table 2 shows the default parameters to be used in the ORC simulation calculation using five working fluids in optimum condition. The excess steam temperatures and cooling water temperatures are standard value for cutting edge of medium-enthalpy geothermal applications (Nusiaputra et al., 2015).

The inlet turbine temperature of ORC is kept constant at 68 °C, which is the temperature limit is still below the limit of injection temperature to the reservoir (70 °C) to avoid temperature crossovers in the evaporator and it is not allowed. The turbine inlet pressure is varied to find out how much pressure will produce the highest output power and efficiency. The initial determination for the turbine inlet pressure is adjusted to the inlet temperature where the incoming pressure is constant at a predetermined temperature and it is 68 °C. The next step is varying the pressure inlet by lowering it to form simulated ORC characteristics with each selected working fluid.

Table 2. ORC analysis parameters

ORC process parameters	
Evaporation temperature	68 °C
Condensation temperature	10 °C
Pump efficiency	0,9
Turbine efficiency	0,8
Temperature difference in evaporator	10 °C
Mass flow rate cycle	1 Kg/s
Geothermal fluid parameters	
Excess steam temperature	80 °C
Injection Temperature	70 °C
Pressure	20-30 bar

5. Result

Figure 4 is a graph that shows the results of performance calculations in the form of pressure changes to output power with five different working fluids. It can be seen from the graph that the smaller the pressure that enters the turbine, the smaller power produced. In this case Propane is a working fluid that has the highest work net produce of 41 kW at a pressure of 2.48 MPa, while the R125 has the lowest work net produce of 10.25 kW at the highest pressure of 3.6 MPa. This is because the expansion of the turbine work experienced by propane is greater than the other working fluids.
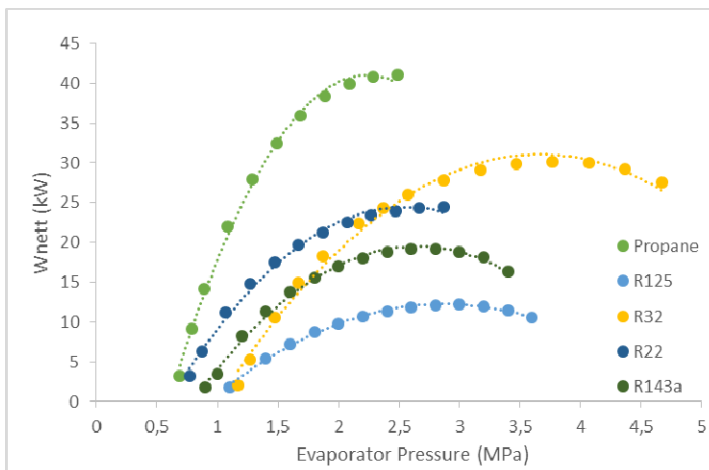

Figure 4. Evaporator pressure vs work net

Figure 5 is a graph that shows the results of performance calculations in the form of pressure changes to thermal efficiencies with five different working fluids.

It can be seen from the graph that the smaller the pressure that enters the turbine, the smaller thermal efficiency that cycle can achieved. In this case R22 is a working fluid that has the highest thermal efficiency of 12.12% at a pressure of 2.97 MPa, while the R125 has the lowest thermal efficiency of 8.17 % at the highest pressure of 3.6 MPa. This is because the heat utilization of the evaporator as a heat provider with amount of 206.7 kJ/kg can be utilised more by R22 compared to other working fluids.
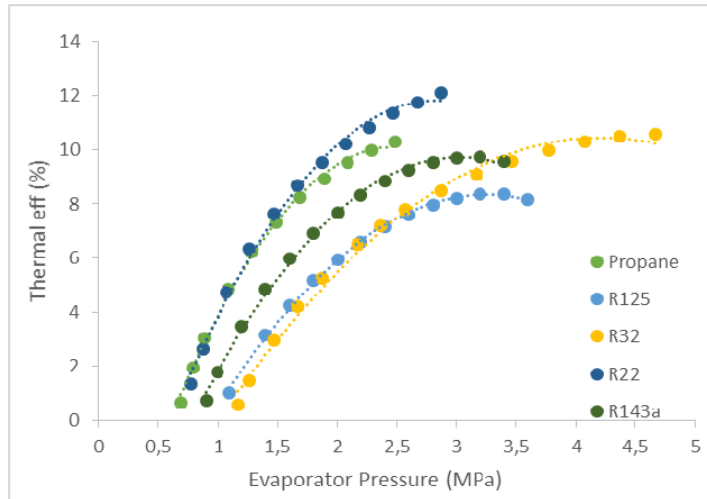

Figure 5. Evaporator pressure vs thermal efficiency

Conclusion

Based on analysis above, it can be concluded that the excess steam from the Tura geothermal power plant with a temperature of 78 °C can be utilised as an ORC heat generator by using five different working fluids. The limitation in this analysis is to lock the turbine inlet temperature at 68°C and the cooling temperature at the condenser at 10 °C by varying the turbine inlet pressure. Another result is it found that the propane working fluid produces the largest output power with a large 41kW with a thermal efficiency of 10.3% at 2.487 MPa. Meanwhile, the working fluid R22 has the greatest thermal efficiency with 12.12% with an output power of 24.45 kW at 2.87 MPa.

Acknowledgements

References

[1] International Energy Agency (2016): Energy and air pollution, World Energy Outlook – Special Report 266.
[2] Sohel, M.I. (2011): Thermodynamic modelling and simulation for high efficiency design and operation of geothermal power plants. *PhD's Dissertation,* Department of mechanical engineering, University of Canterbury, New Zealand.
[3] Boda, K. (2016): Fostering geothermal development in Hungary opportunities and bottlenecks, UNU-GTP Report: Iceland, pp. 26-27.
[4] Kiss M.V., Hetesi, Zs., Kiss, T. (2016): Issues and solution relating to Hungary's electric system, Energy, Vol. 116, 2016, pp. 329-340.
[5] Jouhara, H., Khordehgah, N., Almahmoud, S., Delpech, B., Chauhan, A., Tassou, S.A. (2018): Waste heat recovery technologies and applications, Thermal Science and Engineering Progress, Vol. 6., June 2018, pp. 268-289.
[6] Moran, M.J., Shapiro, H.N. (2008): *Fundamental of engineering thermodynamics 6th edition*, USA: John & Wiley, p. 978.
[7] Permana, D.M., Mohammad, A. (2019): Pemanfaatan panas buang flue gas PLTU dengan aplikasi Siklus Rankine Organik, Barometer, Volume 4, Indonesia, pp. 197-202.
[8] Nusiaputra, Yodha Y, et al., (2015): Empirical correlation for optimal turbine inlet temperature and pressure for geothermal sub-and supercritical Organic Rankine Cyle, Proceedings World Geothermal Congress, April 19-25, 2015, Melbourne, Australia, pp.1-7.

Time series data processing of liquid nonlinear flow

Jozef RÉDL[1], Juraj MAGA[2], Gábor KALÁCSKA[3], Davood KALANTARI[4]

[1]Department of Machine Design, Faculty of Engineering,
Slovak University of Agriculture in Nitra, Slovakia
[2]Department of Machines and Production Biosystems,
Faculty of Engineering,
Slovak University of Agriculture in Nitra, Slovakia
[3]Institute for Mechanical Engineering Technology,
Faculty of Mechanical Engineering,
Szent István University, Gödöllő, Hungary
[4] Department of Farm Machinery, Faculty of Agricultural Engineering,
Sari Agricultural Science and Natural Resource University, Iran

Abstract

The goal of this article is to the application of time series filtering methods for processing nonlinear milk flow in the milking process of dairy cows and detection of the autocorrelation function. We have measured the milk flow from each cow udder teat. The milked milk has been stored in separate vessels (tanks) and been measured their weight in kilograms in the defined time. The Department of Machine Design of the Slovak University of Agriculture developed the measurement unit for the Research Institute for Animal Production Nitra. We were measured the experimental data in the process of software testing in real duty. To normalize the magnitude response of experimental data we were used the Butterworth low pass filter. We designed an algorithm for numerical differentiation of stochastic function to get the volume flow rates. Finally, we were generated the normalized autocorrelation function to detect autocorrelation of volume flow rate for each tanks.

Keywords

low pass filter, liquid flow rate, numerical differentiating, dairy cows milking

1. Introduction

In many, agricultural application has been used the mathematical statistical methods to processing of measured stochastic experimental data. The statistical parameters as autocorrelation function, correlation coefficient, covariance, standard deviation, probability density and distribution, helps the researchers and designers to improve the design process of devices that are used for measurement process. I our case, we were processed the measured data set form milking. The measurement of milk flow was realized on self-produced

equipment defined in [9]. Software for processing and transferring of measured data was developed by [8]. Analyze is based on the review of similar research works. The research of [11] provided the milk flow measurements on 124 cows and were analyzed to determine how they are affected by vacuum level, pulsation rate, pulsation ratio of the milking machine, and the breed, age, stage of lactation, and milk yield of the cow. The many published articles about non-linear flow in the field of farm engineering e.g. [16] deal with research of dynamics of liquid, and some specially with milk production of dairy cows and evaluate the measured data with respect to animal nutrition or analyzed the basic statistical parameters as described in [2,3,10,11,12,15]. The methods of processing of random (stochastic) datasets are described in the publications [1,5,6,7,14].

2. Material and methods

2.1 Measurement of milking process

For measuring, of the milking process we were designed and manufactured the measurement device as described in [8]. The experimental data were processed with software MPM developed by [9]. The milking milk from individual udder treats was stored in separate milk tanks. The strain-gauge weighing scale measured the weight of flowed milk. The measured values were stored in the memory of the computer by software MPM and then saved in table format. The experimental data were obtained in the process of software testing on the sample and random dairy cows in real duty, labeled with numbers 111,160,166. Experimental measurement was realized in the milking parlor located in the Research Institute for Animal Production Nitra. The measured data are depicted in the figures 1,2,3.
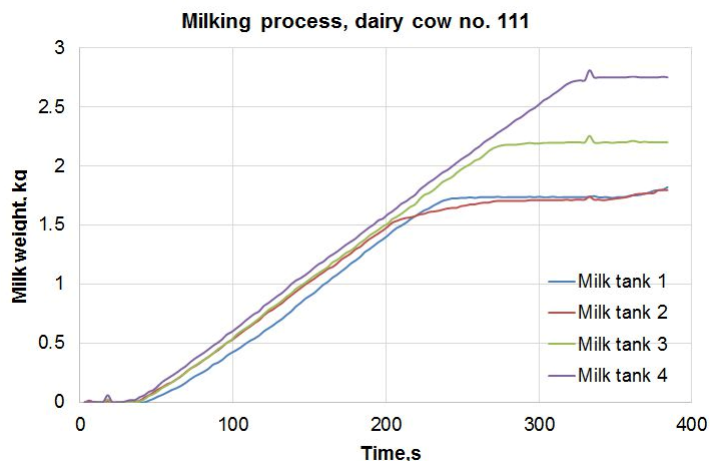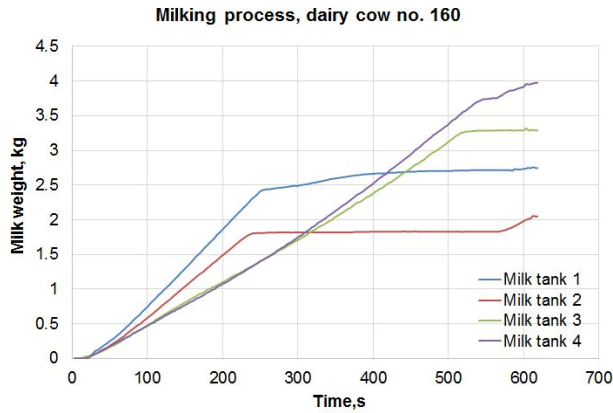

Figure 1. Offtake of milk of cow no.111
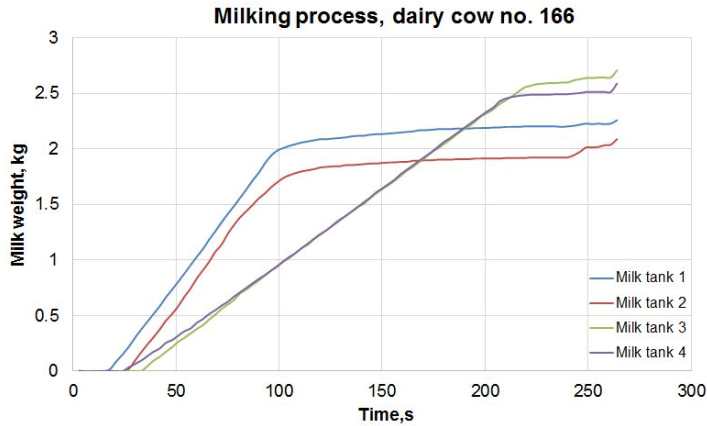
Figure 2. Offtake of milk of cow no.160

Figure 3. Offtake of milk of cow no.166

2.2 Data conversion

The measurement of the milking process based on the measurement of incrementing the weight of the milk tanks. The time step of measurement was chosen for 3 second. To convert the measured data for the next processing we have to find the relevant density of milk. To convert the weight to the volume we were used equation (1).

$$V = \frac{m}{\rho} \tag{1}$$

where:

V – volume in l ,

m – weight in kg ,

ρ – milk density in $\dfrac{kg}{l}$.

As published in [11,12] the specific gravity of milk measured at $15°C - 20°C$ is normally $1,028 - 1,033\dfrac{kg}{l}$. The specific gravity depends on the protein and fat content. For the conversion of the measured weight to real volume, we have changed the equation (1) to the next form:

$$0V_{(i)} = \frac{m_{(i)} - m_{(i-1)}}{\rho} \tag{2}$$

where:

i – incremental index in range $\left(1,n\right\rangle$, where n is total count of readings.

For conversion we were used the density value $1,030\dfrac{kg}{l}$ as published in [2].

Applying the equation (2) we got the raw dataset of milk flow in liters, depicted in figures 4,5,6.
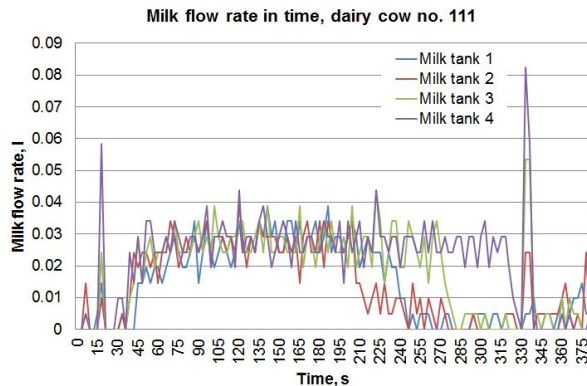

Figure 4. Milk flow rate

As shown in figures 4, 5, 6, the time series of milk flow got a random character, where the graphs got the high pitch peaks and steep parts. These points occurs sometimes when milking vacuum pulsator produced vibrations (noise) that are transferred through the tubes with milking milk until to milk tank. The strain-gauge weighing scale records these signals. To eliminate the unwanted peaks and make the record more usability we were chose to filter the measured data with the Butterworth filter implemented in the Matlab® software. The liquid flow dynamic is defined in [7,13].
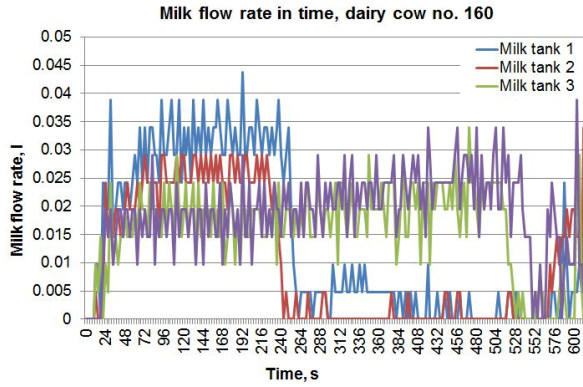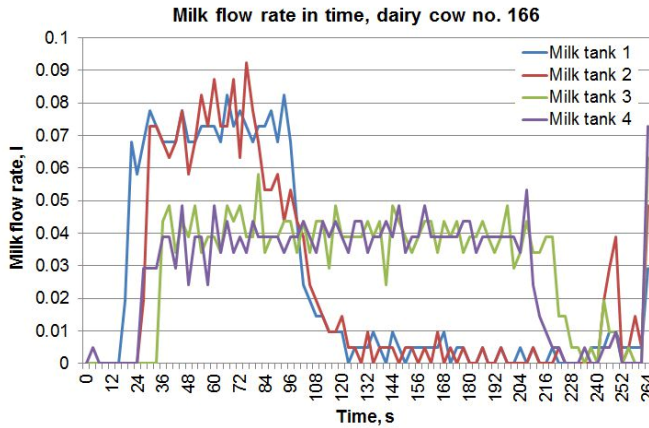
Figure 5. Milk flow rate

Figure 6. Milk flow rate

3. Results and discussion

Butterworth Filter

As defined in [5,6], for processing the measured signal, the low pass analog filter was designed. The impulse response $h_r(t)$ of an ideal analog low pass filter is simply obtained by taking the inverse Fourier transform of its frequency response $H_r(j\Omega)$:

$$H_r(j\Omega) = \begin{cases} T, |\Omega| \leq \Omega_c \\ 0, |\Omega| \rangle \Omega_c \end{cases}, \qquad (3)$$

$$h_r(t) = \frac{1}{2\pi} \int_{-\infty}^{\infty} Hr(j\Omega) \cdot e^{j\Omega t} dt \ . \tag{4}$$

Now the impulse train $g_p(t)$ is given by

$$g_p(t) = \sum_{-\infty}^{\infty} g[n] \cdot \delta(t - nT), \tag{5}$$

Therefore, the output $g_a(t)$ of the ideal low pass filter is given by the convolution of $g_p(t)$ with the impulse response $h_r(t)$ of the analog reconstruction filter :

$$g_a(t) = \sum_{-\infty}^{\infty} g[n] \cdot h_r(t - nT), \tag{6}$$

Substituting $h_r(t)$ into the impulse function we get the transfer function for ideal analog filter. For real application is useful to use the reliable approximations and in the case of low pass analog filter were chosen the Butterworth approximation. Amplitude transfer of Butterworth filter n[th] degree is defined as follows:

$$\left| H_a(j\Omega) \right|^2 = \frac{1}{1 + \left(\dfrac{\Omega}{\Omega_c} \right)^{2N}} , \tag{7}$$

Designed filter is defined with two parameters. The first is degree of filter N and second is cutoff frequency Ω_c. Designed filter is approximate on the maximum flat amplitude with passband 3dB which is clear from the next equation 8.

$$G(\Omega) = 10 \, log_{10} \left| H_a(j\Omega) \right|^2 . \tag{8}$$

Finally, the transfer function could be defined as follows:

$$H_a(s) = \frac{\Omega_c^N}{\displaystyle\prod_{l=1}^{N} (s - p_l)} , \tag{9}$$

where:

$$p_l = \Omega_c \cdot e^{j\left[\pi(N+2l-1)/2N\right]}, l = 1,2,..,N \,, \qquad (10)$$

Finally we get the general form of the filter as described in equation (11) by [6].

$$B_n(s) = \prod_{k=1}^{\frac{n}{2}}\left[s^2 - 2.s.\cos\left(\frac{2k+n-1}{2n}.\pi\right) + 1 \right], n = even$$

$$B_n(s) = (s+1)\prod_{k=1}^{\frac{n-1}{2}}\left[s^2 - 2.s.\cos\left(\frac{2k+n-1}{2n}.\pi\right) + 1 \right], n = odd \,, \qquad (11)$$

where :
n – order of filter .

Matlab code
We were created the algorithm for filtering the milk flow datasets in Matlab® software. The low-pass Butterworth filter was applied. The visualization in Matlab environment of both datasets is on figure 7. The code is based on the source from [5]. Applied source code is below.

Matlab® source code:

```
% Butterworth filter 11-11-2020
% t – time vector loaded from workspace
% x- original vector array loaded from workspace
cof=0.25  % cut-of frequency
n=6        %   filter order
[b,a] = butter(n,cof); %  building the filter
 yy = filter(b,a,x);     % returning the filtered data matrix
createfigure(t,x,t,yy) % data plot function
% end Butterworth filter 11-09-2020


function createfigure(X1, YMatrix1)
%Function for creating plot
%  X1: vector of x data
%  YMATRIX1:  matrix of y data
figure1 = figure; % Create figure
axes1 = axes('Parent',figure1); % Create axes
hold(axes1,'on');
plot1 = plot(X1,YMatrix1); % Create multiple lines using matrix input to plot
set(plot1(1),'DisplayName','Original');
set(plot1(2),'DisplayName','Filter');
ylabel('Flow rate, L'); % Create ylabel
xlabel('Time, s'); % Create xlabel
box(axes1,'on');
```

```
grid(axes1,'on');
legend(axes1,'show'); % Create legend
% End function
```
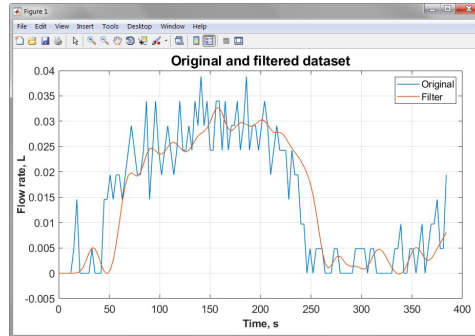

Figure 7. Original and filtered dataset

In Matlab® algorithm of the Butterworth filter, the parameters $[b,a]$ are the transfer function coefficients obtained from the Matlab command "*butter*".
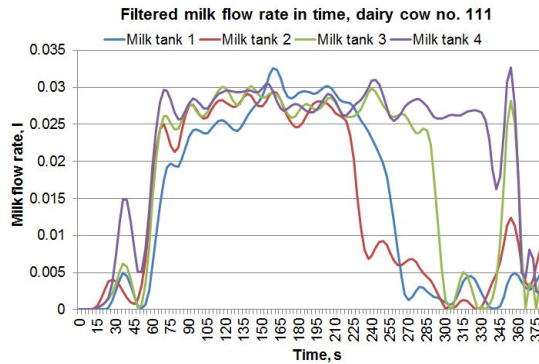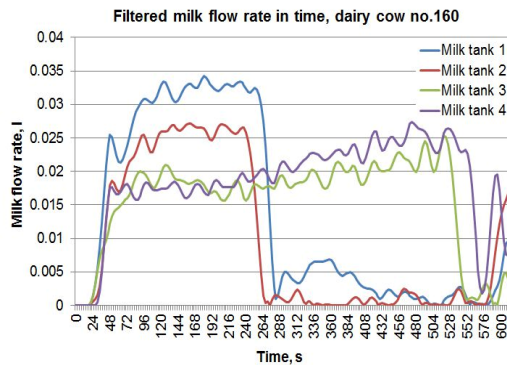

Figure 8. Filtered milk flow
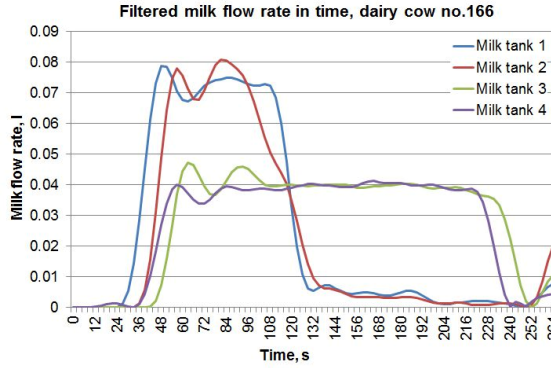

Figure 9. Filtered milk flow

Figure 10. Filtered milk flow

Volume flow rate

As defined in the standard ISO 80000-4 [4], the volume flow rate has the form:

$$q_V = \lim_{\Delta t \to 0} \frac{\Delta V}{\Delta t} = \frac{dV}{dt}, \tag{12}$$

and in the general form:

$$q_V = \frac{dV}{dt}, \tag{13}$$

where:

dV – derivative of volume

dt – derivative of time.

To evaluate the efficiency of the dairy cow's milk production we solved the equation (13), numerically. For this purpose we were create a simple universal software *NummDiff*, and it is written in Visual C# .NET. The application is depicted in the figure 11. The application allows the user differentiating numerically any function, which are given by time series. For the differentiating is needed the time vector also. The application allows the user to using a few differentiating method, which are:

- − forward,
- − backward,
- − midpoint,
- − Lagrange,
- − center 5th points,
- − parametric.

For our dataset we were used the forward method in the next form:

$$df\left(x_i\right) = \frac{f\left(x_{i+1}\right) - f\left(x_i\right)}{h}, \text{ where } h \text{ - time step.} \tag{14}$$
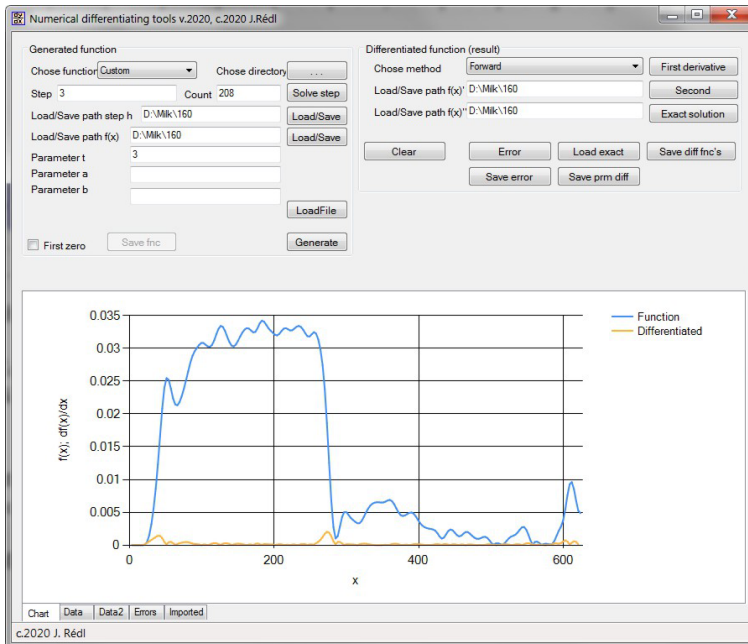
Figure 11.

The main window of differentiating process of one sample is depicted in the figure 11. We were produced the volume flow rate for each measured flow samples and then we made a sum for each four samples in each measurement sets 111,160,166 as is shown on figures 12, 13, 14.

Figure 12. Volume flow rates, sample 111
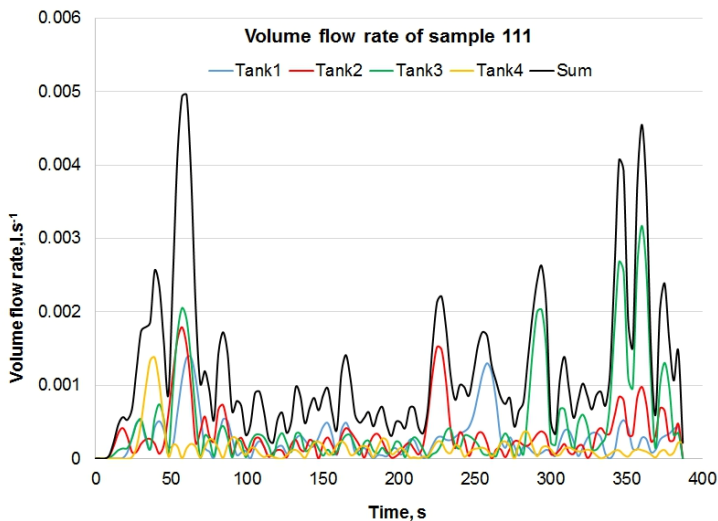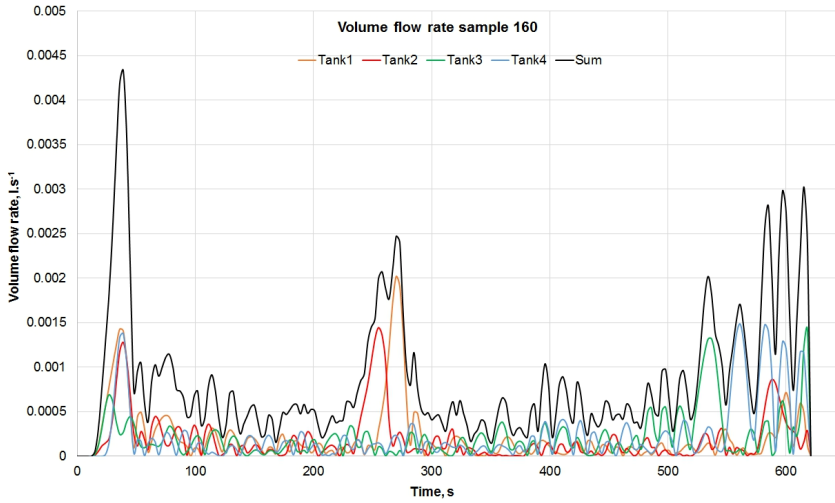
Figure 13. Volume flow rates, sample 160
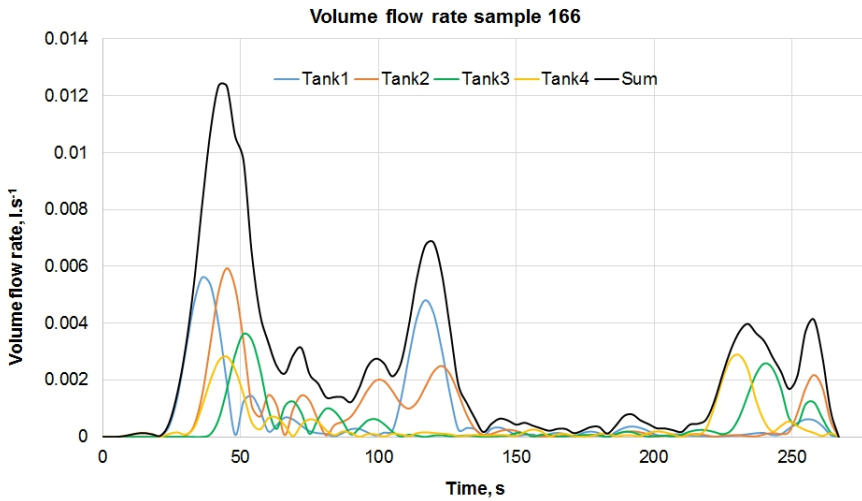
Figure 14. Volume flow rates, sample 166

Finally, we set up the Matlab code for detecting the autocorrelation function for each sum of volume flow rates for each samples. The autocorrelation function is defined by [1,14] as follows:

$$Acf(r) = \frac{1}{N-r} \sum_{i=1}^{N-r} \tilde{x}_i \cdot \tilde{x}_{i+r} \quad , \tag{15}$$

where *r*=0,1,2…*m* define the count of lag.

Applying the equation (15) in the Matlab script editor for each sums of samples with defined lags we get the autocorrelation functions which are depicted in the figures 15,16,17.

Figure 15. Autocorrelation function for sample 111

Figure 16. Autocorrelation function for sample 160

Figure 17. Autocorrelation function for sample 166

Conclusions

In this paper, we are dealing with experimental dataset handling with stochastic data evaluation method. The datasets are obtained from exp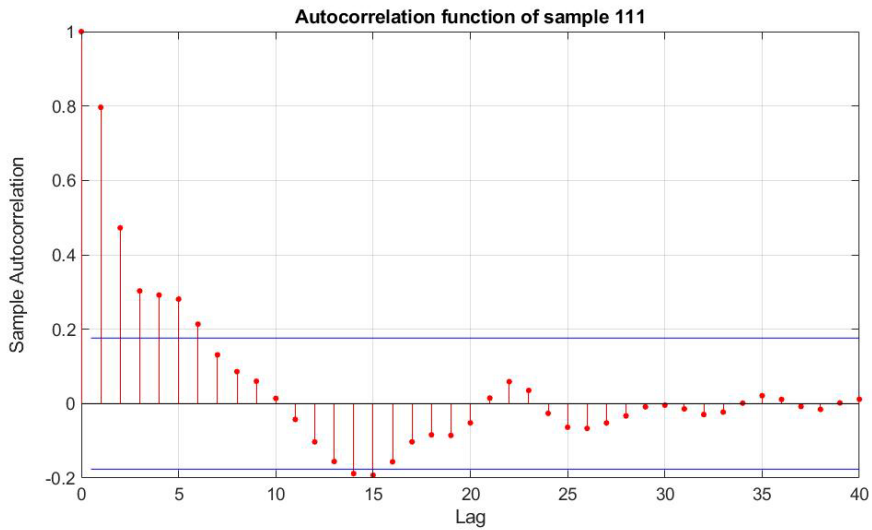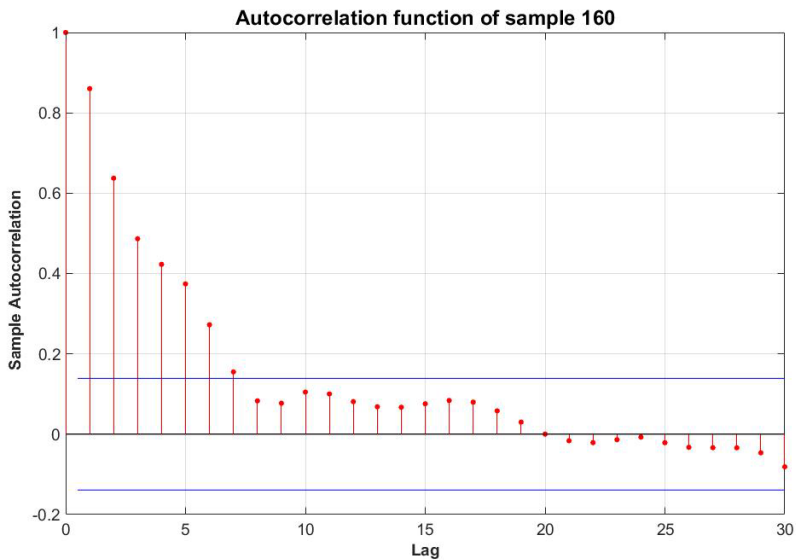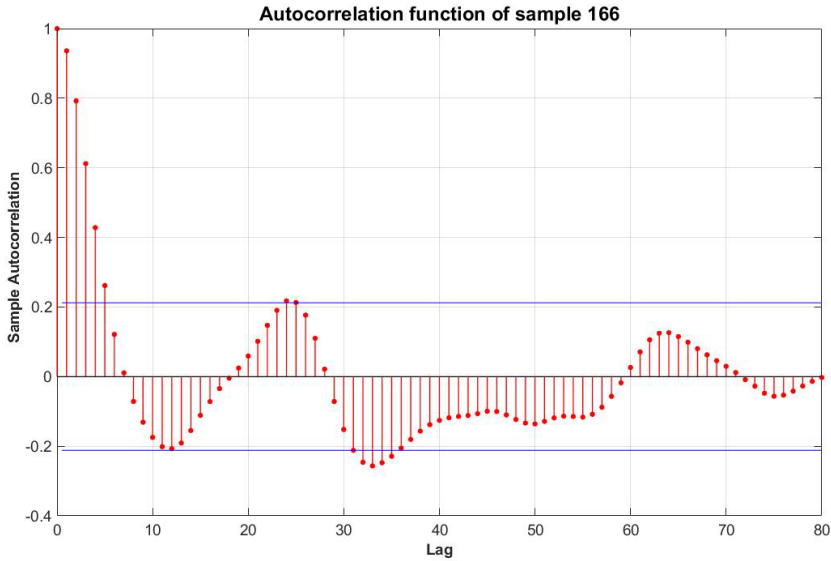erimental measurement from real duty of designed equipment. The measurement data was related to the measurement of milked milk from each dairy cow udders. The amount of milked milk is measured by tensometric gauge mounted on the measurement device. The measured data was transferred through port RS232 to the COM1 port into the PC. Communication software stored measure weight in the MS Excel data format for the next data processing. We transformed the measured weight (in kg) in every three second to the milk flow rate (in liters). From this transformation, we get the stochastic dataset with random noise as results of vacuum pulsator functionality. To eliminate the produced noise we were set up a low pass Butterwort numerical filter in Matlab software environment. This filter were applied on the contaminated dataset with specified cutoff frequencies. After the numerical filtration, we get the normalized dataset. From normalized milk-flow dataset we were solved the volume flow rate with numerical differentiating of stochastic function. For this purpose, we designed the software NummDiff in Visual C# language. The software allows to users utilize a few differentiating methods. We used the forward method. The results of differentiating process are depicted for each tanks and we counting the sum for each tanks of each samples. Reducing the produced charts, we were chosen the application of autocorrelation function analysis only for each sums of samples 11,160,166. The produced autocorrelation functions are depicted on the

128

figures. From applied analysis, we can conclude that the analyzed random dataset is purely stochastic. The autocorrelation function is a part of wide stochastic data analysis. For the limitation of publishing space of this journal, we realized only the autocorrelation calculation where the defined lags for each sum of samples. Number of autocorrelation lags must not exceed the number of observations minus one. The applied methods and results are utilizable in the field of the dairy cow's nutrition research, milking yield support, optimization of milk production process, optimization of welfare processes, optimization of milking equipment design and manufacturing at last.

References

[1]Čačko, J. – Bílý, M. – Bokoveczky,J. (1984) Meranie, vyhodnocovanie a simulácia prevádzkových náhodných procesov. VEDA 1984

[2]Chandan, R. C.- Kilara, A.- Shah, N. P. (2016). Dairy Processing and Quality Assurance (2nd Edition) pp. 77-105. John Wiley & Sons. Retrieved from: https://app.knovel.com/hotlink/pdf/id:kt011NBMQ9/dairy-processing-quality/chemical-c-references

[3]Ferreira,C.F.- Clay,J.S.- De Vries, A. (2020) Distribution of seasonality of calving patterns and milk production in dairy herds across the United States. J. Dairy Sci. 103:8161–8173. https://doi.org/10.3168/jds.2019-18138

[4] ISO 80000-4:2020-04, Quantities and units. Part 4: Mechanics

[5]Martinez, W. L. - Martinez, A, R. (2016). Computational Statistics Handbook with MATLAB®, Third Edition, Taylor & Francis Inc; 3 New edition edition (25 Jan 2016)

[6]Mitra, S.K. (2010). Digital signal processing. MC Graw Hill India

[7] Patience, G. S.(2017). Experimental Methods and Instrumentation for Chemical Engineers. Elsevier; 2nd edition 2017.424 p. ISBN-10 : 044464038X

[8]Rédl, J. (2004). Software for a continual reading and recording of amount of milk from a single quarters. In Nové trendy v konštruovaní a v tvorbe technickej dokumentácie 2004: zborník z medzinárodnej vedeckej konferencie poriadanej počas konania 11. Medzinárodného strojárskeho veľtrhu v Nitre, Nitra, 27. máj 2004. v Nitre : Slovenská poľnohospodárska univerzita. (2004), s. 113-120.

[9]Rédl, J. - Gaduš, J. - Božik, M. (2005). Design and production of equipment for continuous reading of the amount of milk from individual quarters. In Nové trendy v konštruovaní a v tvorbe technickej dokumentácie 2005 : zborník z medzinárodnej vedeckej konferencie poriadanej počas konania 12.

Medzinárodného strojárskeho veľtrhu v Nitre : Nitra, 26. máj 2005. Nitra : Slovenská poľnohospodárska univerzita. (2005), s. 91--97. ISBN 80-8069-517-2.

[10] Sandrucci, A.- Tamburini, A. - Bava,L. – Zucali,M. (2007). Factors Affecting Milk Flow Traits in Dairy Cows: Results of a Field Study. J. Dairy Sci. 90:1159–1167.

[11] Schmidt, G. H. - Van Vleck, L. D. (1968). Measuring Milk Flow of Dairy Cows. Faculty Papers and Publications in Animal Science. Paper 422. University of Nebraska - Lincoln.

[12] Small-Scale Dairy Farming Manual Volume 1. Retrieved from http://www.fao.org/ag/againfo/resources/documents/Dairyman/Dairy/V 1U1p1.htm

[13] Sümer,M.P. - Helvaci,S.F (2008) Solid-Liquid Two Phase Flow. Elsevier Science 2008. 534 p. ISBN-10 : 0444522379

[14] Štulrajter, F. (1990). Odhady v náhodných procesoch. Alfa Bratislava . Nitra

[15] Zezza,A. - Federighib,G. - Kalilouc, A.A. - Hiernauxd, P. (2016) Milking the data: Measuring milk off-take in extensive livestock systems. Experimental evidence from Niger. In: Food Policy vol.59,pp. 174-186. https://doi.org/10.1016/j.foodpol.2016.01.005

[16] Bártfai Z. Török S (2006): New methods for the evaluation of the hydromotors. Hungarian Agricultural Engineering, 18. pp. 1-5. , 5 p. (2006)

Critical safety hazard factors of hydrogen fuel for on-road application

Henrik DOMANOVSZKY, Zoltán BÁRTFAI

Department of Farm and Food Machinery, Faculty of Mechanical Engineering,
Szent István University, Páter K. u. 1., Gödöllő H-2100 Hungary

Abstract

Despite the fact that nowadays Hydrogen is mostly considered a carbon-free energy vector, this tiniest molecule is in its artificially separated status and one of the most difficult and dangerous substances to handle on earth. The engineering community acknowledges this fact and treats hydrogen carefully, using it in the chemical industry with a respectable safety record. However, to distribute hydrogen to millions of untrained customers such as vehicle owners seems a parlous idea. Serious risks can arise due to the mass production, the cost sensitivity of which might has a negative impact on material and production quality. Further risks are posed by imprudent user behaviour, unqualified maintenance and repair, in which the unreliable quality of aftersales parts can increase the possibility of faults and equipment time-wear, may lead to additional risks. Any failure within a H_2-system may incur not only the cost of an unworkable vehicle, but the cost of human lives.

Keywords

Hydrogen fuel, FCEV hydrogen gas powered fuel-cell electric vehicle, compressed hydrogen, composite pressure vessel

1. Introduction

Despite all the surrounding hype, it should be clear that battery technology does not present a useable solution to all transport needs – the almost 100 million vehicles manufactured globally per year cannot rely only on batteries. Political pressure to reduce CO_2 emissions, which was initiated more than a decade ago and which concentrates only on tailpipe emission has not rectified. Car manufacturers are left with no better option but to sell as many locally emission-free vehicles as possible, at the cost of their business interests and partly the expectations of their customers. This problem circle creates another basis for the push towards FCEV development, which is also known as "zero emission", despite the known issues related to local emission and hydrogen production.

2. Infrastructure network

Of course, the fuelling network could grow to a useful scale, if provided that: (a) the price of the hydrogen fuel allows for (b) a positive business case together

with (c) the hydrogen powered vehicle penetration growth – and provided that all of this could be realised within (d) at acceptable industrial risk level within the hydrogen infrastructure network.

This downloadable study is intended to provide a knowledge basis and an overview on the problems we are facing regarding the long term safety related to the (c) hydrogen powered vehicle penetration growth, and (d) the hydrogen infrastructure network, which together include a combination of serious hazards.

3. Status of the risk assessment

Until now, numerous papers have been presented on vehicle safety on topic ranging from pressure equipment through crash worthiness to analysis of the behaviour of the hydrogen, attempting to obtain conclusions from the different parties in the industry and scientific world, as well governmental funding supported experiments. However, the reality of the consumers – vehicle owners, out of brand services, life-long usage behaviours – has not been not analysed or at least no report on results related to this topic has been confirmed. This means that no one really cares what will happen if hydrogen comes out of the laboratory.

4. Hydrogen related known hazard

Hydrogen is used in industry (chemical, and not energy) level, where strict regulations, a serious knowledge basis as well as understood hazard identification are present. However, accidents take place. Furthermore, the non-industrial (societal) environment is unlike the industrial one. For dozens of reason, the risks associated with hydrogen in the non-industrial environment are not controllable and precautions are fruitless. As a first example, while in industrial applications each possible point of hydrogen escalation can be continuously monitored, that is not the case in consumer applications. There is no odour, no colour, which would allow us to recognize hydrogen, is presents, which presents a serious risk as hydrogen is extremely flammable in the presence of air, or even more, oxygen.

The size of the hydrogen atom is extremely small, the radius is 25 pm, or 2.5×10^{-11} m, based on this small size, many of the materials mentioned as gas tight, not sufficiently structured against the hydrogen diffusion, especially in the long term. Hydrogen is not only the lightest atom and molecule, but also the density of its gas form is very low. For this reason hydrogen is often stored and transported in the highly compressed stage as only this way it can be used as fuel for vehicles (for cars the targeted pressure is 700 bar, which can be exceeded by a significant amount). The compression rate causes high physical stress for the materials used.

The flammability range of hydrogen-air mixture is stated to be from 4 % (LEL) to 74.2 % (UEL), however this is the case only at room temperature and the range

widens with the increase of temperature, and at 400°C it is already 1.4 % to 87.6 %, so in fact any mixture is combustible. There are further characteristics, which make hydrogen so special: its gas-air mixture can be ignited with as little energy as 0,017 mJ, about 40-times less than required by gasoline-air mixture to ignite, and as a comparison, one cannot feel an electrostatic shock under 1 mJ. Than, a perfectly burning mixture has a high temperature of 2318 K, what is mostly invisible.
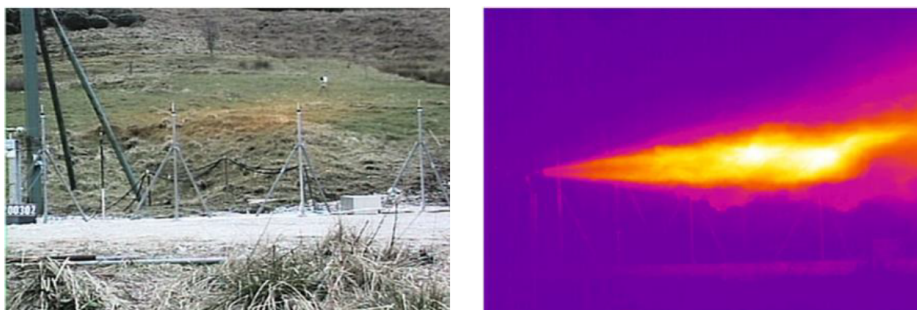

Figure 1. Comparison between the visible flame (left) and the flame extent obtained through thermal imaging (right) (Moonis et al., 2010, taken from [Donatella Maria Chiara Cirrone PhD Thesis – Hazards from catastrophic failure of high-pressure hydrogen storage, 2018])

The seriousness of this phenomenon is increased by the propagation velocity of a flame, which is about 6 times the speed of the frequently used hydrocarbons. One should also be alert that the static electricity forming ignition hazard of hydrogen is also serious. In simple words, an unintended release of hydrogen results in electrostatic discharge originated ignition.

A release of unattended pressurised hydrogen excess to air is accompanied by a jet flow and blast wave and a short living but high temperature "hemispherical cloud" which is like a fireball. *"The speed of detonation wave depends on a composition of hydrogen-air mixture. In stoichiometric mixture it can be as high as 2000 m/s. The safety of hydrogen automotive applications and the related infrastructure, including garages, maintenance workshops, underground parking, and tunnels, is a main area of concern."* [HyTunnel-CS_D1.2 – Report on hydrogen hazards and risks in tunnels and similar confined spaces, 2019].

5. Hazard in the vehicle environment

The Reader can assume that these are the H_2 molecule-related risks, which are well known, and the large -scale automotive industry has had for long the ability to handle them. However, the industry cannot keep everything under control. If someone has doubts about it, they should familiarise themselves with the diesel scandal, which shows how systematic and self-confident on various "solutions" was the fault at most of the OEMs.

Compared to the emission scandal, in the case of it is hydrogen fuelling rather than conformity to the existing regulations that poses the real hazard. This one is far beyond that. It is a careless regulatory issue. Political forces, which believe in carbon-free ruling at the expenses of the citizens, will solve all those problems detected within the last 50 years – which in a naturally way set obstacles in front of technology competitiveness – which even the most polite would call 'naive'.

Let us review some statements, from the last few years declared by respectful knowledge centres:

- The Sandia National Laboratories: "Relatively large amounts of hydrogen often soluble in polymer materials; therefore, exposure to high-pressure hydrogen may cause damage (blistering or swelling) of the polymer materials. This is manifest in high-pressure applications due to depressurization of a system (or rapid temperature changes) as hydrogen expands in free volume and at interfaces within the polymers."

- The HySafe project: „The reasons that cause the embrittlement of materials are still debated in the scientific community. Hydrogen embrittlement detection seems to be one of the most difficult aspects of the problem…. The main knowledge gaps on this matter are concentrated on the reasons that cause the embrittlement of materials…. Currently this phenomenon is not completely understood and hydrogen embrittlement detection, in particular, seems to be one of the most difficult aspects of the problem."

- The HyCOMP project report noted about the safety calculation of the high-pressure fuel tanks: "As a result for the long-term operation, the increase in damage accumulation rate due to the elevation of the temperature could significantly affect the lifetime of the composites. It was calculated that the lifetime for the composites subjected to creep test at 70% of the average failure stress decreased from 2e+27 years to 0.2 year when the ambient temperature changed from the room temperature to 90 °C." Despite of concluding this, suggesting a reduction of the Safety Factor for the different regulations which actually existing for the high-pressure hydrogen storages.

- A tank rupture in fire accident report by Lionel Perrette, Helmut K. Wiedemann is concluded: "This remark underlines that tank fire protection and bus fire safety can not rely only on the performance of isolated protected tank systems." – This can be explained; the safety regulation is way not sufficient.

- Robert Zalosh in life simulating and analysing the vehicle tank incidents: "The results of these tests suggest that the danger zone associated with hydrogen cylinder rupture extends to a radius of roughly 100 m from the hydrogen vehicle."

- The European FP6 & FP7 supported HySafe project was dare enough to enforce the knowledge basis of the hydrogen technology related incidents: "..was to strengthen, integrate and focus fragmented research efforts to provide a basis that will allow removal of safety-related barriers to the implementation of hydrogen as an energy carrier.

Synthesis, integration and harmonization of these efforts aimed at breaking new ground in the field of hydrogen safety and at contributing to the increase of public acceptability of hydrogen technology within Europe by providing a basis for communicating the risks associated with hydrogen. One of the means to achieve those objectives was the development and establishment of the Hydrogen Incident and Accident Database, HIAD"…HIAD is intended to become the up-to-date repository of any accidental event related to hydrogen technology." – Well, this was an excellent initiative. BUT, the collected information database is NOT anymore publicly available for an unknown reason. Someone might have thought that it is better to hide it from the public? As communicated in 2012; they had collected 250 hydrogen related accidental events with 835 people involved. The basis has been growing continuously since.

– The French Ministry's ARIA Database recent publication [Hydrogen and transport: the risks should not be underestimated, 2020] makes it clear: "An analysis of 372 events involving hydrogen (produced or generated accidentally) in the ARIA database is a reminder that hydrogen remains a hazard even for proven industrial processes. For example, 73% of hydrogen incidents involved fires and/or explosions, 27% involved non-burning hydrogen leaks or hydrogen-induced stresses on materials without human consequences, 15% of fires and/or explosions involving hydrogen resulted in the death of at least one person and 43% resulted in injuries." – while they stating it in an earlier publication – "With regard to the origin of accidents involving hydrogen, the analysis shows that in over 70 % of the cases "organisational and human factors" contribute to the deep-rooted causes of the accidents. Constant vigilance must be called for at all hierarchical levels in the facility - management, supervisory staff, technicians, subcontractors – while bearing in mind that there is a permanent risk of ignition in the presence of hydrogen."

– Even the big promoter of hydrogen in transport, the International Energy Agency's working group (Hydrogen Implementing Agreement) wrote: "The lack of operating experience with hydrogen energy systems in consumer environments continues as a significant barrier to the widespread adoption of these systems and the development of the required infrastructure…. Although an understanding of hydrogen's physical properties is well established, and there have been many experimental efforts attempted to fully characterize risks and hazards related to hydrogen, the actual risks and hazards are best be determined within the context of real systems and real operating experience. Likewise, previous experience with hydrogen has not been with systems that will interface with consumers, but in controlled environments using trained personnel." – 2014.

What has happened since 2014 when IEA wrote that H_2 is not suitable for public application? For example: a tiny leakage which happened in a Norwegian fuel station in 2019, despite the fact that it was produced and operated by one of

the most experienced company, dealing with hydrogen globally, and that the station was not more than 2.5 years old. The leakage happened because of not properly torqued bolts around an O-ring. The blast wave that followed sent parts of the station which were found in a 200 m radius, just to mention one figure.

Figure 2. The pressure-wave lifted away the complete roof of the compartment
[photo: Heiko Junge / NTB scanpix]

6. Hazard related to the consumer environment
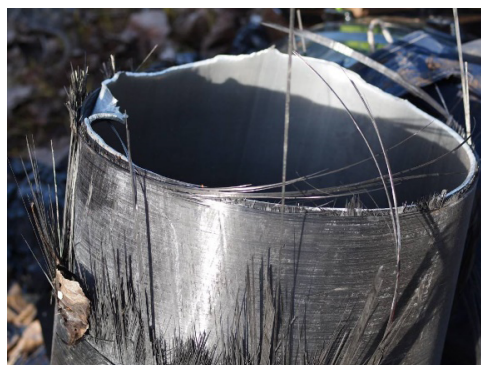
Figure 3. The overused composite tank ruptured way under design pressure
because of carbon fibre wrapping accumulated too much stress. [photo: Author]

As it must be clear from the words above that hydrogen constitutes a risk for society. While a very expensive part of the hydrogen system in the vehicle, -i.e. the tank-, has only a lifetime of 15 years as limited by the respective regulation, the vehicle fleet in Europe even in the wealthier EU member states is drastically ageing, while the poorer countries are reporting around or sometimes over 15 years as the average age of the current car stock. The European emission regulations have been forcing a rapid acceleration of the vehicle price, while the latest Euro 6d has effectively eliminated most of the small and mid-category entry priced new vehicles from the market. Consequently, the ageing of the

vehicle stock is speeding-up within the EU, and so it is in their used vehicle markets in the Balkans and in Africa.

To replace a hydrogen tank after 15 years costs more than an average used vehicle nowadays, which means vehicle owners will not ready to replace them. As it is stated, and as de facto accident have demonstrated if a tank is overused: it destroys everything in its surrounding.

The regulatory system cannot be so chaste to believe that an expensive system that it wants to be introduced – with less than half of the lifetime needed by society today (and even more so in the future) – will stay in a safe condition comparable to a brand new vehicle.

Just some of the reasons why this cannot happen:
  − no tracking on the tanks exist, means cannot avoid over usage;
  − no possibility to preventing repair or even making maintenance on hydrogen vehicles by not properly trained personal, or self-made tinkering;
  − no possibility to prevent using aftersales market parts, which pose risks because of the material uses and for other quality assurance reasons;
  − it is not feasible to ensure heavy industrial safety levels in a low budget operation environment even in the third world, and this applies to the fuelling network too.

Conclusion

Most certainly, even a brand new hydrogen vehicle's safety level is not high enough, due to the related "knowledge gaps" in quite a number of areas. Not to mention the cost reduction pressures associated with hydrogen technology, in every point from the fuel system through the fuel-cell system, closing it at the electric system components. These are the targets of 5-digits per vehicle cost saving try-outs today.

Meanwhile, H_2-refilling systems have no potential to demonstrate a return on investment, as long as safety is sacrificed.

If you still believe in hydrogen as safe fuel for future vehicles, just read the complete paper: *Rising safety hazard related to hydrogen on-road applications as leave the laboratory environment*.

References

[1] Bártfai, Z. et al. (2019): A gáz, mint alternatív hajtóanyag, Mezőgazdasági Technika, 60 : 11 pp. 2-6. , 5 p.
[2] Barth, R. R., Simmons, K. L., San Marchi, C. (2013): Polymers for Hydrogen Infrstructure and Vehicle Fuel Systems: Applications, Properties, and Gap Analysis, Sandia Reports, SAND2013-8904
[3] Devilliers, C. (2013): D2.4 Summary report for the WP2 with remarks and recommendations, HyCOMP Project – FCH-JU-2009-1-256671

[4] Domanovszky H. Could we fulfil the 2°C climate goal by G-mobility?, http://www.lng.hu/could-we-fulfil-the-2c-climate-goal-by-g-mobility/

[5] DomanovszkyH. (2018): Examination of the sustainability of global penetration growth targets for electric vehicle drive systems, XII IFFK 2018

[6] Furfari, S. (2020): The hydrogen illusion, Independently published, ISBN-13: 979-8693059931

[7] Camara, S., Bunsell, A.R., Thionnet, A., Allen D.H. (2011): Determination of lifetime probabilities of carbon fibre composite plates and pressure vessels for hydrogen storage, International Journal of Hydrogen Energy, V. 36, Issue 10, 2011, Pages 6031-6038

[8] Cirrone, D. M. C. (2018): Hazards from catastrophic failure of high-pressure hydrogen storage, PhD Thesis, Ulster University

[9] Cirrone, D. M. C. et al. (2019): FCH JU D1.2 Report on hydrogen hazards and risks in tunnels and similar confined spaces,

[10] Perrette, L., Wiedemann H. K. (2007): CNG buses fire safety: learnings from recent accidents in France and Germany, Society of automative engineer world Congress Detroit, United States. pp.NC. ffineris-00976180

[11] Simonovski, I., Baraldi, D., Melidio, D., Acosta-Iborra, B. (2015): Thermal simulations of hydrogen storage tank during fast filling, Joint Research Centre of the European Commission, Institute for Energy and Transport

[12] Weiner S. C. (2013): What Can We Learn from Hydrogen Safety Event Databases? Webinar. https://www.energy.gov/sites/prod/files/2014/03/f11/webinarslides_hydrogen_safety_events_databases_091013.pdf

[13] Zalosh, R. (2008): CNG and Hydrogen Vehicle Fuel Tank Failure Incidents, Testing, and Preventive Measures, Firexplo Wellesley, MA

[14] France Ministry of Ecology, Energy, Sustainable Development and Town and Country Planning, ARIA Database – Accidentology Involving Hydrogen, 2009

[15] France Ministry of Ecology, Energy, Sustainable Development and Town and Country Planning, FLASH ARIA – Hydrogen and transport: the risks should not be underestimated, 2020

[16] International Energy Agency's Hydrogen Implementing Agreement (IEA HIA), Tasks 19 and 31 on Hydrogen Safety – Final Technical Report, 2014